UNIVERSITÀ DEGLI STUDI DI MILANO

Scuola di Dottorato in Scienze Biologiche e Molecolari

XXVII Ciclo

Dual regulation of ERp44 activity in the early secretory compartment

Sara Sannino

PhD Thesis

Scientific tutor:

Prof. **Roberto Sitia**

Academic year: 2013-2014

SSD: BIO/10; BIO/11; BIO/13

Thesis performed at the Division of Genetics and Cell Biology, Protein Transport and Secretion Unit, IRCCS Ospedale San Raffaele, Milan, Italy.

Index

Abstract

Secretory proteins start their journey from the endoplasmic reticulum to the Golgi undergoing stringent quality control to guarantee the integrity of the secretory proteome. This fundamental process is mediated by the coordinated action of numerous resident chaperones and enzymes. Amongst these, ERp44 is rather unique in that it is a multifunctional chaperone involved in maintaining redox homeostasis and in controlling thiol-mediated quality control and calcium and KDEL-Rs signalling. The crystal structure of ERp44 reveals 3 domains, **a**, **b** and **b'**, and a C terminal tail that connects domain **a** with **b**. Here we demonstrate that ERp44 activity is regulated by the pH gradient existing between the ER and Golgi. The more acidic Golgi pH (about 6.5) induces conformational changes in the ERp44 C-terminal tail that simultaneously expose the substrate-binding site and RDEL motif. In this way, ERp44 and its client proteins can be retrieved to the ER, where the higher pH (about 7.1) likely induces complex dissociation. The region at the interface between the C-tail and the substrate binding site is crucial to sense the changes of pH from the ER to the Golgi, acting like a sensor, intrinsic in the amino acidic composition of the protein. Alteration of Golgi pH induces increased secretion of ERp44 clients, due to a lower retentive activity of the chaperone. Moreover, we found that the conserved histidines located at the border between the **b'** domain and the flexible C-tail are important for regulating ERp44 localization and function. Unlike wild type ERp44, mutants lacking key histidines are O-glycosylated in the Golgi and in part secreted. Interestingly, co-expression of client proteins restores retention of mutant ERp44, suggesting that conserved histidines regulate RDEL exposure in the absence of clients. Surprisingly, not all the clients bind ERp44 in the same compartment of the secretory pathway. Our data indicate that, depending on their affinity for ERp44 binding site and on the surrounding environment (different pH and/or variable cofactor concentration), ERp44-substrate complexes form before or downstream the site where O-linked glycosylation takes place. The client-induced retrieval mechanisms may allow the distinct and sequential localization of ERp44 interactors along the early secretory pathway. Remarkably, endogenous ERp44 can also undergo O-glycosylation in physiological conditions. A cyclic oscillation of the amount of O-glycosylated ERp44 is observed in stromal endometrial cells during the menstrual cycle, suggesting a pathophysiological role of this chaperone in these processes.

Part I

State of Art

1. Protein folding and quality control

After synthesis, proteins must rapidly fold to perform their biological activities. Folding takes place in three main subcellular compartments: cytosol, endoplasmic reticulum (ER) and mitochondria. Each cellular region is equipped with a specific set of chaperones and folding enzymes optimized to work in the local conditions. The final result of numerous reactions must be a native molecule ready to absolve properly its function. Moreover, structural maturation must be completed within a rather short time frame to assess all the cell necessities. In the crowded environment of the cell, unfolded proteins are a danger as they may aggregate and become toxic. Extensive aggregation is prevented by several proteolytic systems that rapidly dispose of aberrant or damaged polypeptides[1].

Analysis of the human genome reveals that approximately a third of all open reading frames code for proteins that enter the endoplasmic reticulum (ER), demonstrating the importance of this organelle for global protein maturation. A considerable fraction of the proteins that enter the ER are destined to the extracellular space[2]: these are either secreted by the cell or inserted in membranes, to act as ligands and receptors, respectively. Secretory proteins or enzymes and chaperons resident in the secretory pathway are synthesized on ER-bound ribosomes, and are co-translationally translocated into the ER lumen where they attain their native conformation, before being transported to the Golgi and downstream compartments. In a few cases, such as particularly small polypeptides or proteins with "weak" signal sequences, proteins can access the ER post-translationally[3,4]. Being physically segregated from the cytosol, the ER lumen has a distinct folding environment, crucial for specific protein modifications that cannot occur in the cytosol, such as glycosylation and extensive disulfide bond formation[5].

Secreted and membrane proteins are the main devices of intercellular communications. The fidelity of ligand–receptor interactions requires that both molecules attain the very conformations that allow signals to be properly transmitted and understood. Thus, in the early secretory compartment (ESC) the proper protein folding is subjected to a strict quality control (QC) scrutiny and only properly folded and assembled proteins can reach the Golgi, where they are further modified, to be transported to the extracellular space or to lysosomes (Figure1).

The logics of protein QC is: 1. Preventing the deployment of aberrant proteins; 2. Retaining precursor proteins in an environment suitable for their maturation; 3. Favoring correct assembly by

increasing subunit concentration; 4. Reducing the risks of proteotoxicity by inhibiting aggregation and degrading terminally misfolded proteins; 5. Maintaining homeostasis in ESC; 6. Developmental regulation of protein secretion (like IgM, adiponectin); 7. Storing proteins for regulated secretion (plants, adipocytes)[6-9]. ER misfolded proteins are thus recognized and retained by ER chaperones and enzymes and eventually routed to degradation by ERAD pathway or autophagy[10, 11].

Different studies highlighted the spatial subdivision of the ESC in suitable sub-compartment for the retention and biogenesis of different proteins. This division has evolved to cope with the myriads of polypeptides that a cell can produce. The entire ESC is equipped with stress sensors that are able to sense the amount of misfolded proteins or the increased load of protein folding machinery. 3 different sensors (Ire1α, PERK and ATF6) can sense the accumulation of misfolded proteins in the mammalian ER and selectively activate a 3 different signal cascades, generally called unfolded protein response (UPR). The UPR can selectively inhibit protein entry into the ER, increase the folding capacity of ESC machinery by over-expressing specific chaperones or induce faster and more efficient protein degradation. The balance between protein load and protein degradation is fundamental to prevent cell death.

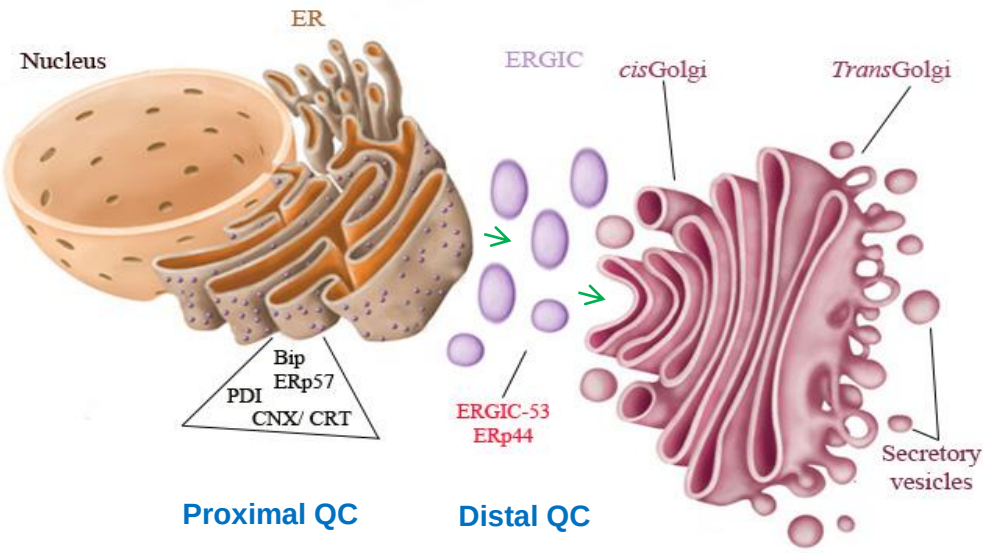

Fig.1 *Protein quality control in the early secretory compartment.* Proteins destined to the extracellular space or ESC resident ones are co-translationally translocate into the ER. Here they start their folding journey under strict quality control (QC). Chaperones can be grouped in two different classes according to their specificity and subcellular localization. Once entered into ER, nascent proteins can bind Bip or enter the calnexin/calreticulin cycle. The initial choice is dictated by N-glycan position. In addition, quality control can act in sequential steps. After the proximal QC, proteins (especially multimeric ones) can undergo distal check point in ERGIC-*cis*Golgi. This "second" quality control can mediate protein concentration and selective export of oligomerized species. While the proximal QC is based on protein retention, the distal QC can imply substrate retrieval to ER for another round of folding or for degradation.

2. Focus on protein folding in the early secretory compartment

In the ESC protein folding starts during synthesis, as a vectorial process. The journey of a protein entering the mammalian ER starts with the recognition of a signal sequence, typically but not exclusively found at the N terminus of the nascent protein[5]. Signal sequences are quite variable, but generally have 6 to 12 hydrophobic amino acids flanked by one or more positively charged residues. This amino acidic code is recognized by signal recognition particle (SRP)[12,13] with the resulting ribosome/nascent chain/SRP complex binding to the ER membrane via the SRP receptor. The ribosome/nascent chain complex is then directed toward a proteinaceous pore in the ER membrane called the Sec61 translocon: this allows the translocation of the growing polypeptide chain across the membrane and into the ER. Upon co-translational translocation, nascent secretory proteins enter the crowded environment of the ER lumen and soon begin to fold into more stable, lower energy, conformation(s)[14]. It is therefore important to realize that protein folding may well influence post-translational modification and the other way around.

The ER is unique in sustaining a set of covalent modifications, which include removal of the signal sequences, disulfide bond formation, N-glycosylation and GPI addition. A plethora of enzymes and assistants are found in the early secretory pathway (ESC), specific for catalyzing each step. The transport from a platform to another must follow the execution of a given step. The time allocated to the latter, however, must be precisely controlled in order to allow efficiency and prevent jams along the line. Glycoproteins have been analyzed in great detail as a prototypic example of labor organization in the ER protein factory. In fact, the sequential modifications of the oligosaccharides provide an elegant solution to dictate and time the manufacture of cargo glycoproteins. N-glycosylation involves binding of a preformed oligosaccharide (Glc3Man9GlcNAc2) to asparagine side chains in the sequence NXS/T, where X is any amino acid other than proline[15]. The sugar moieties are then progressively trimmed by resident enzymes of the secretory pathway. The so called proximal QC is thus composed of two well characterized ER folding pathways: the enzymes involved in the so called clareticulin - calnexin (CRT-CNX) cycle and Bip (also called GRP78) (Figure 1).

CNX and CRT retain substrates with immature glycans in the ER, prevent their aggregation, and promote oxidative folding via interactions with ERp57[16-19]. In particular, the UDP-glucose glycoprotein glucosyltrasferase (UGGT) acts as a folding sensor by producing mono-glucosylated proteins that can interact with CNX and CRT. The subsequent removal of the terminal glucose, glucosidase II dissociates the substrate from CNX/CRT for a novel round of inspection by UGGT[20].

Bip, on the other hand, is an abundant ER chaperone of the hsp70 family which recognizes exposed hydrophobic patches and is also involved in ER signalling (UPR)[21,22]. This chaperone is composed of an N-terminal ATPase domain and a C-terminal domain with affinity for hydrophobic patches[23,24]. The affinity for substrates depends on ATP binding at the N-terminal domain. When ATP is hydrolyzed to ADP, a conformational change occurs, which determines substrate release. Bip substrates can thus undergo cycles of BiP binding and release, depending on ATP hydrolysis[25]. Owing to the weak BiP ATPase activity, hsp40-like co-chaperones containing J domains (ERdj) can play a key regulatory role[1,26].

Very rarely glycoproteins are found to bind simultaneously to BiP and CNX or CRT. Therefore, it seems that a given glycoprotein has to choose between either BiP or the CNX/CRT cycle. The initial choice is dictated by the localization of the N-glycans: the closer these are to the N-terminus of the nascent protein, the higher the tendency to use CNX as a chaperone system[27].

Some proteins require assembly into complexes, and provision of lipids for ER membranes and the regulation of cholesterol content are also important considerations[5]. If the first attempts to fold fail, the protein can shift to the alternative pathway downstream the ER. To ensure orderly ER exit, proteins need the provision of sugars for glycoproteins, the availability of cofactors (particularly calcium), and the appropriate formation of disulfide bonds. The default pathway for ER exit to the Golgi is via COPII-coated vesicles[28]. COPII-coated vesicles subsequently fuse to form the ER-Golgi intermediate compartment (called ERGIC). Therefore, after a proximal QC, proteins can undergo distal QC checkpoints in ERGIC and Golgi (Figure 1). While many chaperones and enzymes reside stably in the ER, some particular proteins (like ERp44) may cycle through the earlier stacks of the Golgi or between ERGIC and *cis*Golgi via the KDEL receptor, either unbound or with client proteins[5,29,30]. This model could mediate cargo concentration in a specific compartment and selective binding of different protein species depending also from the surrounding environment.

While proximal QC can rely on simple retention, the distal checkpoints likely imply substrate retrieval to the ER, either for further attempts to fold, or for retro-translocation and degradation. In the ER-Golgi intermediate compartment, ERGIC 53, a protein with lectin activity is able to cycle between the ER and the ERGIC[31] and binds high-mannose cargoes, facilitating their forward transport. Further mannose trimming in the ER may favor degradation, possibly also because reducing the hydrodynamic volume of substrate glycoproteins could facilitate their retro-translocation[1]. ERGIC53 works together with MCFD2, a soluble calcium-dependent protein, to capture its cargo dynamically[32]. Various inactivating mutations in the ERGIC53 gene (LMAN1)

and in the MCDF2 gene lead to a multiple coagulation factor deficiency called MCFD1[33] because of a failure to package the heavily glycosylated Factor V and Factor VIII proteins[34].

2.1. Oxidative folding

One feature of the proteins folded in the ER is the oxidation of free thiols on cysteines to disulfide bonds. This is done by means of a process known as oxidative folding[35]. Disulfide bond formation is supported in the oxidizing environment of the ER, which has a relatively low ratio of reduced to oxidized glutathione (GSH:GSSG between 1:1 and 3:1)[36,37]. In fact, in terms of ionic composition and redox potential, the ER is similar to the extracellular space, providing an ideal folding test bench before exiting from the cell. The higher ratio between reduced and oxidized glutathione however is not sufficient to guarantee the efficient power to oxidative folding, which often implies both disulfide bond *de novo* formation and isomerization[38]. On the other hand, an hyper-oxidizing environment in the ER lumen might prevent the correct folding of proteins with multiple disulfide bonds and decrease protein stability, promoting misparing, which can induce protein misfolding[1].

The transition from free thiols to disulfides is based on the dynamic and concerted formation, reduction, and reshuffling of disulfide bonds that favor the introduction of native (and therefore functional) disulfide bonds. In addition, the free thiols on proteins can be exposed to a competing H_2O_2-mediated oxidative process that produces oxygenated thiol derivatives, like sulfenylated proteins[35]. This type of derivatives can be transient intermediates in the formation of more stable disulfides or precursors of higher oxidized sulfur oxides (sulfinic and sulfonic acids); they can also react with GSH to produce S-glutathionylated proteins[39]. It is thus clear that the intricate disulfide relay requires enzymatic assistance: a specialized class of enzymes of the protein disulfide isomerase (PDI) family in fact has evolved to promote the efficient formation of native disulfides in folding ER proteins. PDIs, through a redox-active thioredoxin-like catalytic domain (CXXC), directly introduce disulfide bonds into reduced client proteins being thus finally reduced themselves[40]. The endoplasmic oxidoreductins 1 (Ero1 α and β) re-oxidize and reactivate the thioredoxin-like (TRX) domain of PDI for a new cycle of oxidative protein folding, transferring electrons to molecular oxygen (the final electron acceptor in aerobic condition) thanks to their cofactor flavin adenine dinucleotide (FAD): as a consequence Ero1 activity produces H_2O_2[41-46]. In particular PDI consists of four TRX domains: the two lateral domains (**a** and $\mathbf{a_0}$) are endowed with oxidoreductase activity, while the two central ones, **b** and $\mathbf{b_0}$, provide a hydrophobic surface suited to bind and present nascent proteins to the active sites in **a** and $\mathbf{a_0}$. This overall structure is likely

important for the redox dependent chaperone function of PDI[47,48], particularly with terminally misfolded proteins, which must be reduced before dislocation to the cytosol for proteasomal degradation[49-52].

The final balance of oxidative folding is that one molecule of H_2O_2 is produced for every disulfide bond formed[53]. The efficient disposal of H_2O_2 is done by means of ER peroxidases which, as their name suggests, are dedicated to degrading H_2O_2. The mammalian ER is endowed with three known peroxidases Prx4, GPx7 and GPx8[54-56]. Peroxiredoxin 4 (Prx4) is the oldest of these in evolutionary terms and is more expressed in secretory tissues. Prx4 has the characteristic of coupling hydrogen peroxide catabolism with oxidative protein folding. This enzymatic arrangement involves the ingenious use of H_2O_2 as a substrate to streamline protein metabolism (Figure 2). Recent studies demonstrated that oxidized Prx4 clearly transfers disulfide bonds much more efficiently to PDI[57,58], ERp46[59] and possibly other ER oxidoreductases than to GSH[60].

Eight mammalian GPxs are known and among them only three are CysGPxs (GPx5,7 and 8). In particular GPx 7 and 8 are ER monomeric ER enzymes. Whereas GPx7 possesses a cleavable leader sequence at the N terminus, GPx8 is a transmembrane protein with a short N terminal cytoplasmic tail. Both Gpx7 and 8 are retained into the ESC thanks to REDL and KEDL motif which are recognized by KDEL-Rs in the distal compartments[61]. In analogy to Prx4, GPx7 and 8 can act as PDI peroxidases by using them as electron donor. In particular, it's clear that Prx4 preferentially oxidizes the domain $\mathbf{a_0}$ of PDI while GPx7 the domain **a** in the active site[57,62]. The model proposed for GPxs is based on their ability in coupling the reduction of Ero1α derived H_2O_2 to H_2O with the introduction of a second disulfide bond into a PDI family member[56]. Thus these enzymes protect nascent proteins from an alternative oxidative fate, and cells from the consequences of having misfolded proteins. Moreover, as Ero1 enzymes, also Prx4 lack a C-terminal ER retention signal and depends on ERp44 for its intracellular localization: when PDI is down-regulated, in fact, Ero1α and Prx4 are retained by ERp44 in the distal ESC[63].

Over the last years, many other ER-resident PDI-like oxidoreductases have been characterized in mammalian cells. There are about twenty proteins in the human PDI family containing up to five thioredoxin domains and from zero to four redox-active CXXC like motifs[40,6466]. The abundance of PDI family member in the ESC confirms that the proper disulfide bond formation is crucial for nascent protein folding and for protein complex composition (like IgM)[67,68]. The reactivity of thiol groups can favor the formation of mixed disulfides with PDI, ERp44 and other ER-Golgi resident proteins[69-71]. The thiol-dependent retention mechanisms, originally described in the developmental control of IgM[72], and HMW adiponectin secretion[73] is

extended to retention of ESC soluble molecules that lack retention motifs but that need rest inside the compartment to explain fundamental functions (like Ero1α, Prx4 and Sumf1).

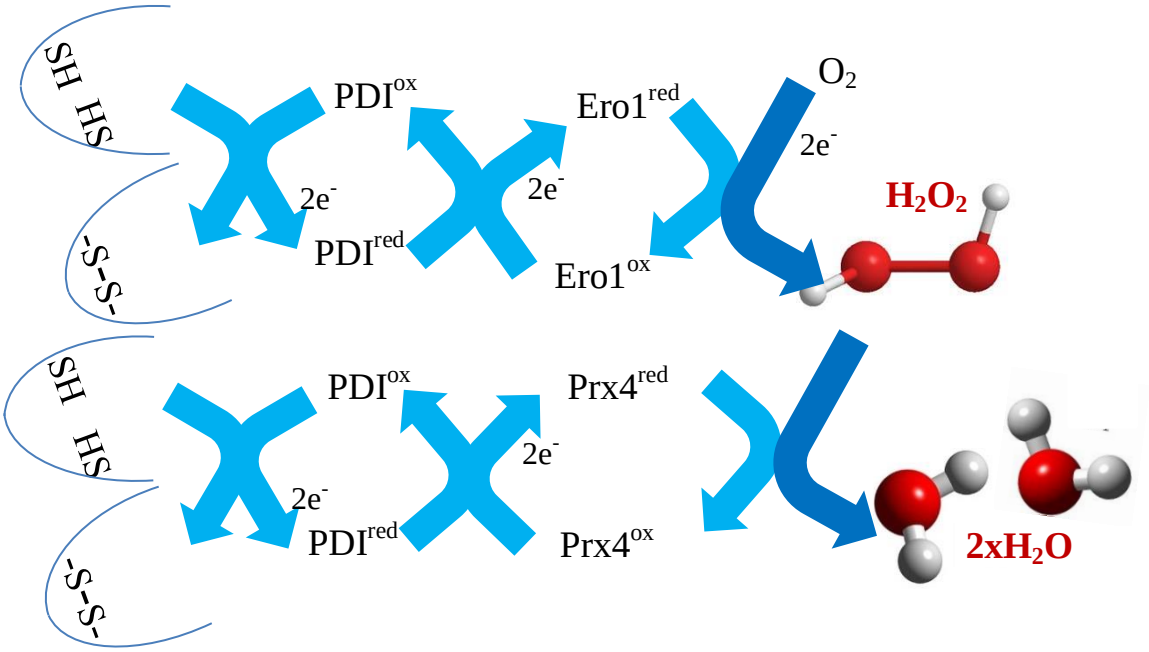

Fig.2 *Disulfide bond formation.* Disulfide bond formation leaves PDI in a reduced state (PDI^{red}). Ero1 can re-oxidaze the active site of PDI and renders the chaperone ready for another reaction. The two electrons received by PDI are then assed to molecular oxygen producing H_2O_2 . PRX4 can use the H_2O_2 produced by Ero1 mediated oxidative folding to catalyze another cycle of oxidative folding.

3. Zinc contribution to cellular processes

Zinc (Zn^{2+}) is the second most abundant trace element in living organisms[74] and is the most abundant trace element in cells. Interestingly, Zn^{2+} is clearly not a trace element from the perspective of the cell[75], as it is required for an immense number of catalytic, structural, and regulatory functions in specific subcellular compartments, including gene transcription in the nucleus[74], ATP production and apoptosis in the mitochondria[76], enzyme activation in the secretory pathway[77] and microtubule formation[78] and cell signaling in the cytoplasm[79]. The intracellular amount of zinc can be divided in different pools: the zinc bound to macromolecules, the zinc stored inside vesicles, exchangeable or mobile zinc and zinc bound to metallothionein (MT), that can be released in a redox dependent way[80]. Most of the intracellular zinc is bound with high affinity to proteins including GSH, via cysteine, histidine and diphosphate molecules. An excess of mobile zinc can be toxic for the cell, in part due to its ability to be easily coordinated by endogenous proteins and peptides. However, up to millimolar concentration of mobile zinc is stored in synaptic

vesicles in the mossy fibers of the hippocampus, which is proposed to play a role in learning and memory formation during neurotransmission[81,82]. Recently, zinc mobilization into and out the intracellular organelles, including ESC, has received great interest. Proteome analysis revealed that about 10% of the known proteins have a potential zinc-binding motif, which confirms the importance of this ion[83]. Alteration of the zinc homeostasis is crucial in several neurodegenerative pathologies including Alzheimer's and ischemia[82] and a decreased concentration of mobile zinc in prostate serves as an important marker for early diagnosis of prostate cancer[84]. In vertebrates two are the major family of transporters, Zip (*SLC39A*) and ZnT (*SLC30A*), which are involved in zinc transport and homeostasis. Zips transport zinc into the cytosol from extracellular or intracellular compartments, while ZnTs export cytosolic zinc to extracellular or intracellular compartments[85,86]. Structurally, Zips have eight transmembrane domains with N- and C-termini on the non-cytoplasmic face. In contrast, the majority of ZnTs consist of six transmembrane domains (ZnT5 is the exception with nine additional transmembrane domains) with N- and C-termini within the cytoplasm. Transmembrane domains 3 – 4 and 4 – 5 on Zips and ZnTs, respectively, contain a long loop with a histidine-rich domain that is thought to facilitate metal binding. Zinc transporters function by forming both homo and hetero dimers, like ZnT5-ZnT6[77]. Both Zips and ZnTs are expressed in cell and tissue-specific manners and are developmentally regulated and localized in different intracellular compartments, as clearly demonstrated for mammary gland[87]. In mammalians, about 24 Zip/ZnT transporters are known and half of them are localized in secretory and endosomal - lysosomal compartments, underlying the importance of this subcellular regions as zinc storage sites[87].

Among the Zips, Zip7, 11 and 13 are located in ESC: in particular Zip7 is present at the ER membrane and is involved in zinc mobilization from ER to cytosol. When Zip7 is phosphorylated by CK2, it can activate a cytosolic signaling cascade which induces phosphatase inhibition[88]. A to ZnT transporters, instead, ZnT4, 5, 6 and 7 are all suggested to maintain zinc secretory pathway homeostasis and regulate zinc-requiring enzyme activities[89,90]. Zinc has no direct redox activity but it can interact with sulfur in cysteine residues under reducing conditions and the nature of the sulfur-zinc binding allows a rapid association/dissociation of the metal in response to cell needs. In fact, zinc can be released by NO or H_2O_2, oxidized glutathione and other oxidant species. For these reasons, zinc is known to contribute to cell redox balance regulating oxidant production, glutathione metabolism and the overall protein thiol redox status and redox signaling[87].

4. Retention and selective secretion: role of chaperones and environment.

In a complex multicellular organism, different cell types engage in specialist functions, and as a result the secretory output of cells and tissues varies widely. Whereas some quiescent cell types secrete minor amounts of proteins, tissues like the pancreas, which produces insulin and other hormones, and mature B cells, which secrete antibodies, place a great demand on their ESC[37]. Unless retained by interactions with resident proteins, a folded protein could exit from the ER and be subjected to selection for transport to the plasma membrane[5,91]. Many proteins are actively transported out of the ER by interaction with specialized export machineries[92,93]. Export from the ER occurs at ER exit sites[94] (ERES), where budding of COPII-coated vesicle takes place.
The exit from the ER and the entry into ERGIC and then Golgi complex expose the nascent proteins to different environment with specific ions concentration (Ca^{2+}, Zn^{2+} and H^{+}) and different chaperones and enzymes.

4.1. Role of ESC pH gradient

The maintenance of an appropriate pH within the different compartment is a constant challenge for all the living cells[95]. Cells have evolved a variety of proton translocation devices (proton pumps) thus produce a proton gradient used to regulate protein degradation, activity and ATP production. The pH varies along the ESC compartment with acidification increasing progressively from ER to lysosomes (Figure 3). The pH of ER is in fact near the neutrality (7,0-7,1)[96,97] while acidification develops along ERCIG-Golgi complex and is maximal at the *trans*Golgi network (TGN, pH 6,0-5,8)[98,99]. The acidic pH of organelles is generated primary by vacuolar (V) H^{+}-ATPases, which actively pump protons in presence of Mg^{2+} and ATP. The proton gradient thus generated can then be used to drive a variety of second active transport processes. Due to its electrogenic nature, proton pumping can be limited by the generation of a transmembrane voltage. In order to avoid this phenomenon and to sustain the rapid acidification of certain compartment, Cl^{-} fluxes are used [98]. GPHR is one of the voltage-dependent anion channel present at Golgi complex level that acts as counterion to proton pumps and is involved in maintaining a lower pH with respect to the ER[100]. The correct acidification of distal ESC is known to be crucial for protein trafficking, processing, glycosylation and recycling[100-103].

In mammalian cells, one of the best characterized transporters is ERGIC-53, a hexameric transmembrane lectin[104] that derives its name from being particularly abundant in the ERGIC. ERGIC-53 is described to capture high-mannose glycoproteins in the ER, and release them in the

ERGIC in a Ca^{2+} and pH-dependent manner[105]. It has been suggested that another lectin, VIPL, binds de-glucosylated cargoes exiting the CNX/CRT cycle, protecting them from de-mannosylation. The cargo is then passed to ERGIC-53, perhaps owing to its hexameric structure, and exported toward the Golgi[105].

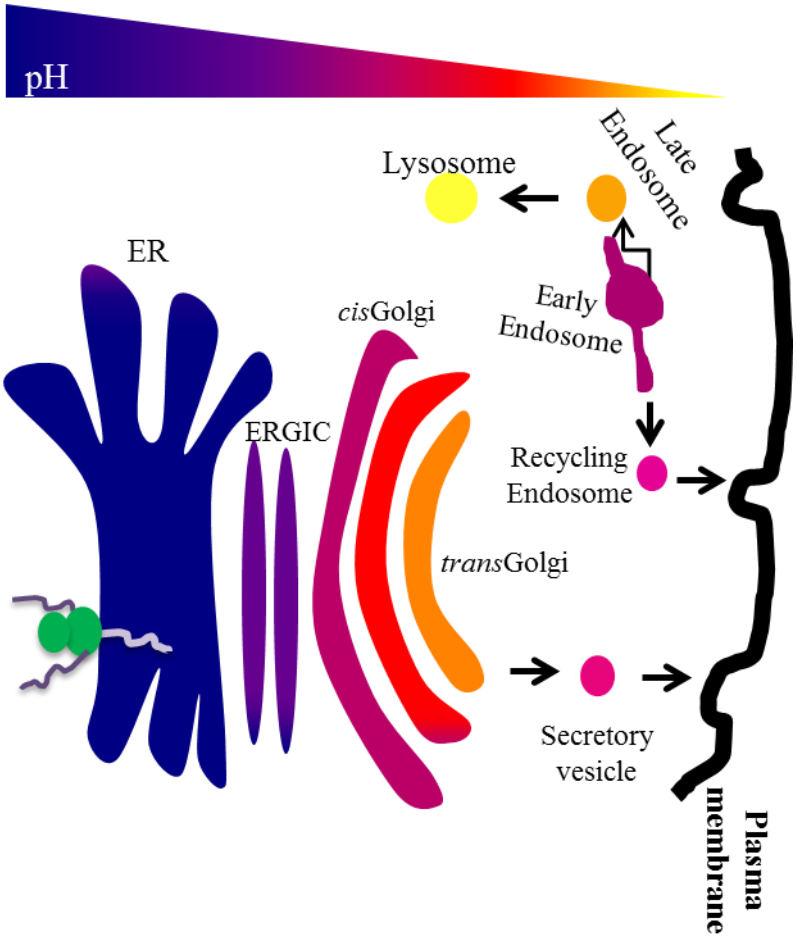

Fig.3 *pH of endocytic and secretory compartments.* Organelles rapidly acidify as they progress along the secretory and endocytic pathway. Here, the pH gradient is represented with a color scale from blue to yellow. The nascent protein (in light violet) is co-translationally translocated into the ER lumen at pH 7,0-7,1 (in blue) and continues its trip where can be transported to secretory vesicles (in purple, pH 5,5) or to lysosomes (in yellow, pH<5,5).

4.2. KDEL Receptor role in protein recycling and inter-organelle signaling

The flow of proteins leaving the ER has been estimated to be between 1-5% of the total ER volume per minute[106]. In this respect, the rates of traffic flow across the ESC must be precisely coordinated to avoid structural and functional disruption of the system. In order to control the protein flow within the ESC, different stations/organelles receptors and signaling components are used and take part of the so called "endomembrane" signaling pathway. Some signaling proteins could be in transit through the Golgi complex and then directed to the plasma membrane, others can

be retained in the ESC thanks to a recycling mechanism. The endomembrane signaling can be defined as a stimulus generated in a specific intracellular organelle that is targeted to a different compartment within the same cell[107]. This mean that protein traffic itself can initiate the endomembrane signaling, sustaining both an anterograde (*cis-trans*Golgi and Golgi-plasma membrane) and a retrograde (ERGIC/*cis*Golgi-ER) protein transport, depending on the cell needs.

In the late 90s it was discovered that the KDEL motif at the carboxyl terminus of many soluble and membrane proteins is a way to impair ESC resident protein secretion, retro-localizing them to the ER[108].

The KDEL-receptors (KDEL-Rs) are seven transmembrane proteins of 26kDa with a 3D structure that resembles that of G protein-couple receptors (GPCRs)[109]. They can recognize and bind proteins that contain KDEL like motifs at the ERGIC-Golgi level. Thanks to this interaction, KDEL-Rs are activated and can thus dimerize and recruit COPI-trafficking machinery to retro-transport and release the client into the ER. From this ESC station the KDEL-Rs can again shuttle between ER-Golgi complex[110]. Different experiments demonstrated that the binding to KDEL like motif by the receptors requires an acidic pH as the one encountered in the Golgi. The KDEL-Rs are thus able to bind KDEL sequences in the Golgi and retrieve their cargo back to the ER, where the higher pH favors their release. In this way the receptors can return to their original localization[111].

Recent studies uncover the role of KDEL-Rs in activating signaling by carriers arriving at the Golgi from the ER[109,112,113]. The triggering signal is provided by ER chaperones containing KDEL like motif. KDEL-bearing chaperones can be divided in 2 groups. Most of them bind the ER matrix and seldom reach the Golgi; some, instead, diffuse more easily and can exit the ER. It seems that ERp44, a chaperone active at ERGIC-Golgi level, is a member of the second (Luini's group, personal communication).

At the Golgi level, KDEL-Rs can activate a pool of Gq and Gs signaling proteins[109,112], adapting Golgi traffic to input from the ER. Thus, KDELRs act as traffic sensors and activate controllers that in turn elicit responses eventually adapting transport efficiency to load volume. Moreover, the Golgi complex hosts many molecules that are potentially involved in diverse cell functions like cell motility and growth and cell cycle. The read out of the KDEL-Rs activation has thus many implications in a wide range of cellular processes. The proposed model is the following: cargo vesicles leave the ER and reach the downstream compartments (ERGIC and Golgi complex) carrying also chaperones that have KDEL-like motif and that can be recognized by KDEL-R. This interaction triggers a specific response activating the PKA pathway (Gs pool) for the retrograde transport or Src signal cascade for the anterograde flow (Gq pool)[114] (Figure 4).

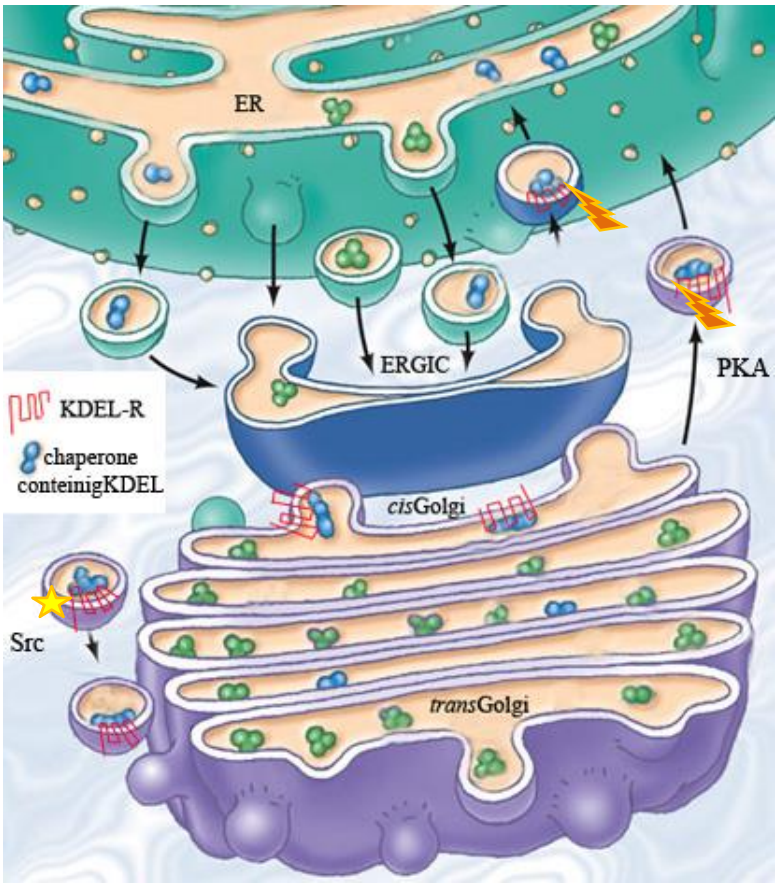

Fig.4 *Model of KDEL-R signaling in the ESC.* Chaperones containing KDEL like motif (blue molecules) leave the ER and on the arrival to ERGIC or Golgi complex, they bind KDEL-R (in red), triggering Src response (yellow star) for the anterograde transport to *trans*Golgi and plasma membrane or PKA (in orange) for the retrograde translocation to the ER.

5. ERp44: structure and function of a multifunctional chaperone in the ESC

ERp44 is a chaperone of the PDI family, highly expressed in many secretory tissues like pancreas, urinary bladder, salivary gland, stomach, duodenum, testis, prostate, seminal vesicles, ovary, placenta, and bone marrow (see www.proteinatlas.org for detailed information). Moreover, ERp44 protein levels can be modulated in cancer tissues as reported for liver cancer where this chaperone is over-expressed or for testis cancer, where ERp44 expression is down regulated compared to normal tissue (see www.proteinatlas.org for detailed information).

ERp44 was discovered in 2002 as a covalent partner of the oxidases Ero1α and β[115]. By using in silico modelling it was predicted that ERp44 structure can be largely superimposed on PDI active domains even if at amino acidic level there are important differences. In particular, there is a CFRS motif in the substrate binding site (SBS) of ERp44, so the second cysteine residue of the CXXC motif typical of PDI is absent. However, deep in the ERp44 SBS, there's an additional cysteine

(C63) that is not present in other PDI family members[115]. This residue is present on a loop juxtaposed to C29, suggesting its putative role as accessory binding residue.

Subsequently, the X-ray analysis of human ERp44[116] revealed a clover like structure composed of 3 thioredoxin-like domains **a**, **b** and **b'** and a C-terminal tail (C-tail) that connects **b'** and **a** domains (Figure 5). In the last part of the C-tail it is present a KDEL like motif that plays an important role in preventing ERp44 secretion by binding KDEL-Rs. For this reason ERp44 is also studied as a possible trigger of KDEL-R signaling. Even if the protein is retrieved by KDEL-Rs to ER, endogenous ERp44 accumulates in the distal ESC (ERGIC-*cis*Golgi), while its over-expression induces ER localization. This peculiar scheme of compartmentalization depends in part on interactions with ERGIC-53, and reflects a specific role of ERp44 in distal QC[71]. In particular cell types, like pre-adipocyte, the ERp44 localization can change from ERGIC-*cis*Golgi to ER depending on the state of differentiation and so reflecting the needs of preventing misfolded or unfolded protein secretion.

Thanks to the C29 present in the domain **a**, ERp44 binds and retains substrates of thiol-mediated retention (TMR)[72], including unassembled IgM subunits, SUMF1, adiponectin (APN)[117] but also soluble clients that must be retained into the ESC for maintaining the redox homeostasis like the oxidases Ero1α and β[45,115,118] and Prx4[119,120]. The C-tail movements are crucial for the simultaneous exposure of both the substrate binding site (containing C29) and the RDEL motif. In fact, the formation of a disulfide bond between C29 and C369 in T369C mutant hinders the accessibility of clients, like Ero1α, to the active site of ERp44 but also the impairs the KDEL-Rs binding to the final RDEL motif inducing both client and ERp44 secretion. Moreover, the amount of ERp44 T369C in the spent medium is similar to the one detected when the mutant lacking the final RDEL is over-expressed (ERp44ΔRDEL).

Substitution of C29 with alanine (C29A) renders ERp44 less active as a covalent binder but it is still able to retain clients with high affinity for the SBS of the chaperone (non-covalent binding). So ERp44 is able to bind covalently and non-covalently its clients and impair their secretion. Surprisingly, removal of the C-tail (ERp44 ΔTail) doesn't induce ERp44 secretion but enhances the binding capacity of the chaperone[116]. Therefore, the C-tail is fundamental not only for the retention but also for the specificity of binding (choosing the proper client in a specific compartment).

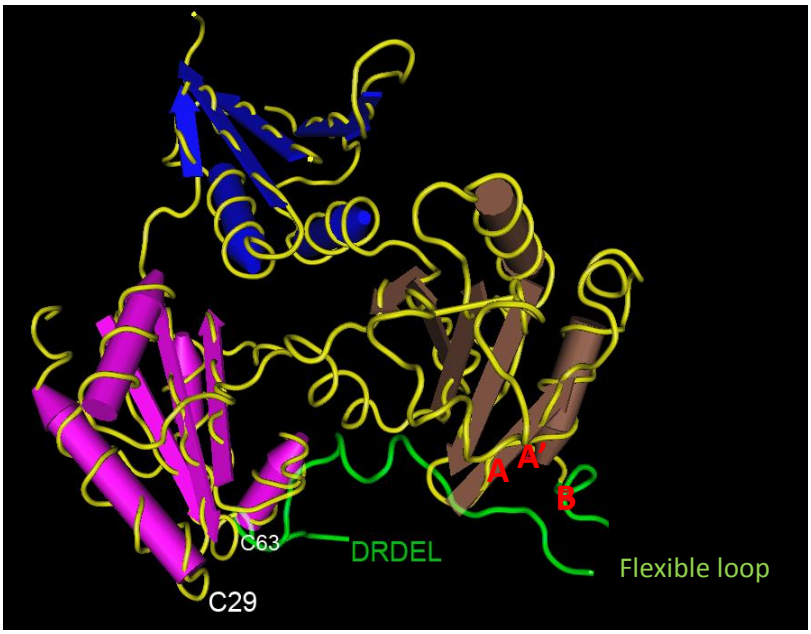

Fig.5 *3D model of ERp44 closed structure.* The picture highlights the different domain of ERp44 with different colors (domain **a** in light violet, domain **b** in blue and domain **b'** in light brown, respectively) and the C-tail in green. C29 and C63 in white are located in the substrate binding site present in the domain and covered by the tail in the closed structure. Red letters (A, A' and B) point at the position of the resolved histidine residues. From residue 332 to 350 the crystal structure is not resolved by x-ray probably due to the extreme flexibility of the loop (flexible loop) as the five last C –terminal DRDEL residues.

5.1. Role of ERp44 in IgM polymerization and secretion

IgM polymers are planar multimeric molecules assembled in the ESC and secreted by plasma cells. Each monomer must be correctly folded, bend and expose the complement binding sites to be fully functional. Secretion of non-polymerized subunits with not fix complement could inhibit lytic antibody activity and, moreover, misshaping polymers could activate antibody response in absence of a real antigen[117]. However, plasma cells have to produce and secrete thousands of functional Ig per second to face possible organism injury. Thus production of antibodies keeps the protein quality control machinery very busy. The biogenesis of IgM polymers starts from the folding of heavy chain (μ) and proceeds with the paring with the light chain (μL) and μ_2L_2. This first part of the process occurs rapidly in the proximal ESC thanks to the help of Bip that binds the first constant domain of heavy chain (CH1). The polymers formation is slower and it is peculiar of certain cell types like plasma cells. Once passed this first step of QC, μ_2L_2 can be bound by ERGIC-53, whose hexameric structure provides a planar platform for the IgM assembly. ERGIC-53 binds preferentially N-glycan located in the conserved C-terminal tailpiece of μ chain (μtp) upstream the C575 where ERp44 is able interact[121]. Previous studies showed that ERp44 and ERGIC-53 amount

increases during plasma cell differentiation in line with the pattern of polymerization of IgM and over-expression of ERp44 in Hela cells prevents un-polymerized subunit secretion in favor of polymer formation. In this scenario, ERp44 can help IgM polymerization by providing oxidative power via Ero1α recruitment, increasing concentration of subunits ready to polymerize in the right place and interacting directly with ERGIC-53[117].

5.2. ERp44 can regulate the calcium flux via IP3R1

Ca^{2+} signaling plays a fundamental role in a plethora of biological functions[122]. Two main sources of Ca^{2+} are the plasma membrane and the ER. Inositol 1, 4, 5-trisphosphate receptors (IP3R) are channels that upon binding to IP3 release Ca^{2+} and allow signal propagation[123]. Three IP3R isoforms are known, IP3R1, IP3R2 and IP3R3, with different tissue distributions. The activity of IP3Rs is regulated on both sides of the ER membrane. In particular, ERp44 was shown to bind specifically to the variable region of the 3rd luminal loop (L3V) of ER luminal side of IP3R1. The interaction inhibits the channel activity in a pH, redox and Ca^{2+} ER-dependent manner[124]. The interaction between ERp44 and IP3R1 is not related to the exposure of C29 but C160 and C212 present in the domain **b** of ERp44 seem to be crucial for the interaction[125]. Further studies from our laboratory indicated that Ero1α enhances IP3R1 activity in at least two ways: by favoring its oxidation and by competing with it for ERp44[126]. Both events inhibit the binding of ERp44 to IP3R1, and favor Ca^{2+} efflux from the ER. This is in line with the data showing that Ero1α is able to induce apoptosis in stressed macrophages[127]. Therefore, ERp44 is the link between thiol-mediated quality control, redox and calcium homeostasis.

5.3. ERp44 and the secretion of high molecular-weight adiponectin

Adipocytes are endocrine cells that are known to store lipids and secrete many molecules fundamental for the energy metabolism, like adiponectin (APN). This hormone stimulates fatty acid oxidation, suppresses hepatic gluconeogenesis, increases insulin sensitivity, has anti-atherogenic effects and acts to counter the effect of TNFα[128]. It is clear that the production of APN increases about 100 fold during adipocytes differentiation and this molecule seem to play a crucial role in type II diabetes, obesity and cardiovascular diseases[129,130]. Nascent adiponectin is a monomer of 30 kDa composed of a collagenous domain and a globular C-terminal domain. In the ER the protein is able to multimerize and form trimers (low molecular weight species). While trimers are held together by non-covalent interactions, hexamers and high molecular weight species (18-emers) are

formed thanks to disulfide bond formation via C39[131,132]. So APN undergoes sequential quality control in the ESC. In adipocytes ERp44 is over-expressed during differentiation and, moreover, it changes localization from distal ESC to ER, where it co-localizes with adiponectin. This suggests that ERp44 is crucial for the formation of high molecular weight adiponectin species. Over-expression of ERp44 impairs the secretion of low molecular weight APN in a dose dependent manner whereas depletion of this chaperone enhances their secretion. Equally important is also Ero1α contribution to the process. In fact, upon over-expression of Ero1α less ERp44 is associated with APN [73]. So these data confirm that Ero1α is a high affinity partner of ERp44 that can compete with other clients in binding. ERp44 is involved in different regulatory circuits important for metabolic homeostasis.

Aims of the project

In order to dissect the mechanisms underlying the multifunctional activity of ERp44, I have focused my attention on understanding how ERp44 is tightly regulated and associated with different clients in the early secretory compartment, using novel and innovative technology.

Aim I: ERp44 activity and regulation

A combination of crystallography, molecular dynamics, biochemical and cell biological assays reveal that ERp44 is able to cycle between ESC and perform different functions in each station. ERp44 is mainly localized at ERGIC-*cis*Golgi compartment at the steady state but it can be seen in the ER whenover-expressed. Moreover, the C-tail movements of ERp44 are crucial for retention of clients, selectivity in binding and retrieval of the chaperone itself. Preliminary data showed that C-tail movements can be regulated by the differential pH existing in each ER-Golgi complex stations (Figure 6). These finding indicated that the pH gradient along ESC coordinately regulates the activity of ERGIC-53, ERp44 and KDEL-Rs, coupling efficiency and fidelity of protein secretion.

Indeed, ERp44 binds much better its clients at pH 6.5 (as in the *cis*Golgi) than at 7.1 (as in the ER). It is hence tempting to speculate that the lower pH of the *cis*Golgi leads to C-tail opening thereby exposing both the active site and RDEL motif, allowing KDEL-Rs (that also shows pH dependency in vitro) [111] to retrieve ERp44-client complexes into the ER. In this organelle, the higher pH might favor substrate dissociation. Taking in account all the previous data, we decided to investigate how ERp44 is able to exploit the pH gradient existing in the ESC.

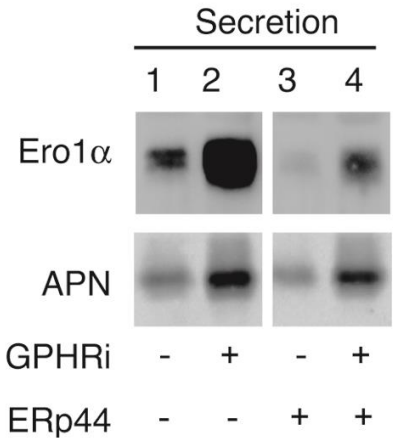

Fig.6 *ERp44 activity is pH dependent in vivo.* GPHR silencing induces Golgi pH basification and specifically inhibits retention of ERp44 clients. Aliquots from culture media (Secretion) were collected from HeLa transfectants expressing Ero1α (upper panel), adiponectin (APN, lower panel) and subjected (+) or not (-) to GPHRi. Co-expression of ERp44 and its partners impair their secretion (both Ero1α and APN; compare lanes 1 and 3), while Golgi pH basification induced client secretion (compare lanes 1-2 and 3-4).

Aim II: ERp44 association with partners and identification of novel ones

ERp44 cycles between ESC stations and mitochondrial associated ER membranes (MAM), binding -in addition to its clients- ERGIC-53, IP3R1 and KDEL-Rs. So during its "journeys" this chaperone has to be able to discriminate between different possible partners and bind the right one in a specific compartment. ERp44 mutants without the C-tail or with a partial deletion of it (Δβ16) are known to bind more covalent cargoes but with less specificity[116]; moreover, they are not secreted but blocked in the ER. On the other hand, mutation of C29 into alanine impairs covalent binding to clients but not the retention of high affinity partners like Ero1. Thanks to different ERp44 mutants we wanted understand where, along the secretory pathway, the interaction with known ERp44 partners (Ero1α, Sumf1, Prx4, Ig-μΔCH1 and APN) occur and the role of ERp44 domains in the differential binding. As ERp44 has multiple interactions in different cellular compartment, by using special tag we expect to learn more about the physiology of ERp44 cycling. With protein precipitation assays, we can isolate novel ERp44 substrates, activity regulators and MAM-ER-Golgi complex resident proteins that can dictate ERp44 localization.

Results

How ERp44 senses the pH

In silico and structural analysis predict C29 has a role in the pH sensing activity of ERp44. In particular, molecular modelling suggested that specific residues (S32, R98, T368) are crucial to contribute in maintaining lower the local pKa value of C29 in the active site and favors the closed conformation (Figure 7). At higher pH the differential protonation of C29 can induce the C-tail opening, favoring the client binding.

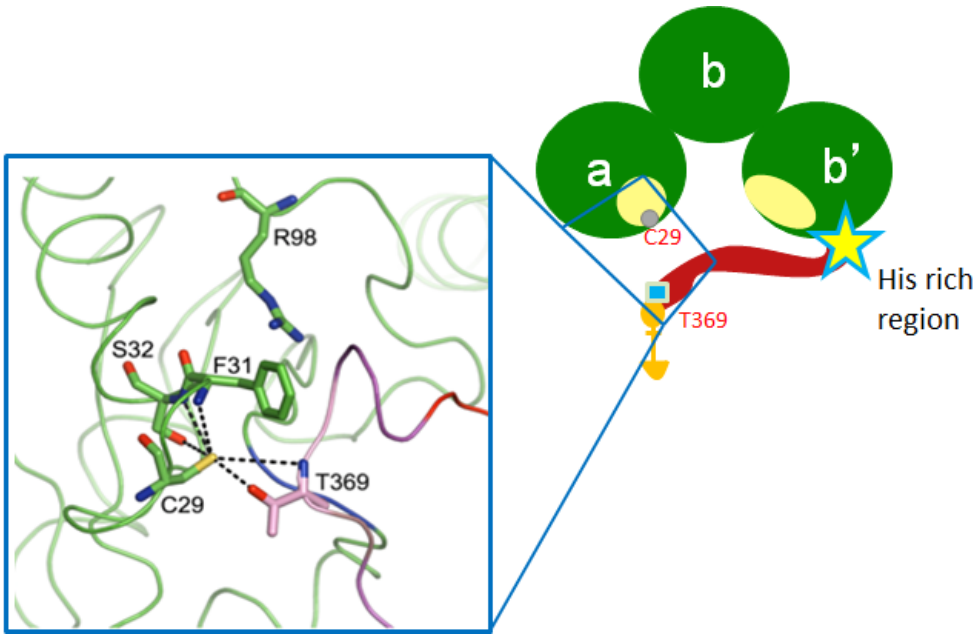

Fig.7 *Schematic representation of the amino acidic environment around C29.* The panel shows a closer view of the active site C29 and of the last part of the C-tail, highlighting interactions between C29 and neighboring residues shown as a stick models. Hydrogen bonds between polar atoms are shown as dashed lines. The β16 strand is colored in pink.

To test these prediction, both *in vitro* and *in vivo* assay were performed whit ERp44 mutants. *In vitro*, MalPEG binding assay demonstrated that:

a) ERp44 wt can covalently bind maleimide when the C-tail is open, so in a pH dependent manner;
b) the binding is mainly to C29 present in the active site;
c) altering the side chain of S32, R98, T369 renders ERp44 constitutively accessible to MalPEG and abolishes the pH sensitivity of the reaction;
d) partial deletion of the C-tail (β16 strand, represented in pink in Figure 7) give similar results to the one obtained with residues substitution, supporting S32A, R98Q and T369A mutants adopt the open C-tail conformation (Figure 8).

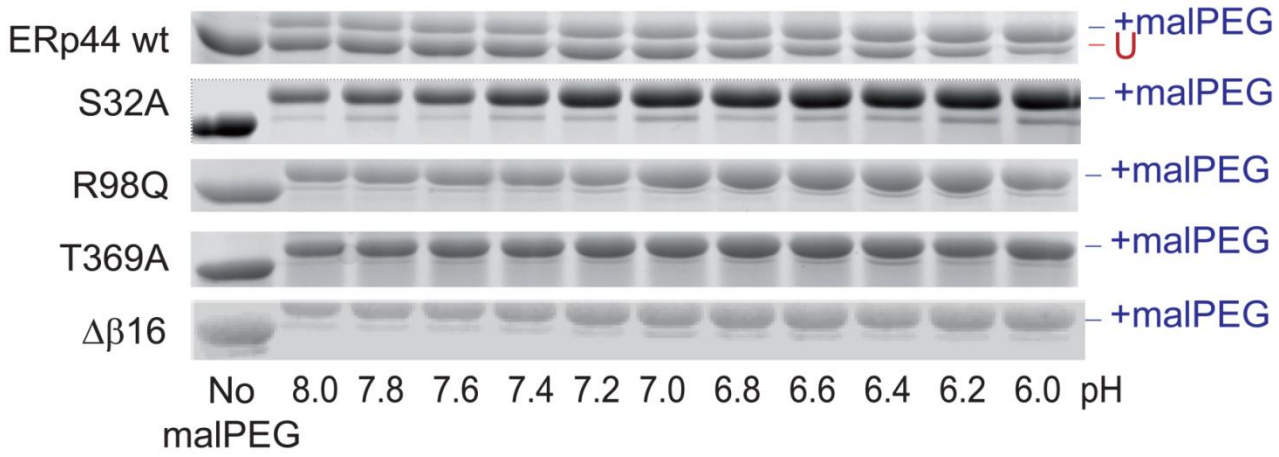

Fig.8 *pH dependent binding of maleimide to ERp44 variants. In vitro* MalPEG binding causes reduced ERp44 gel mobility (U stands for unbound ERp44) and was analyzed at various pH to determine changes in the accessibility to C29 in the active site. While more MalPEG is bound to the C29 at lower pH, the indicated mutants seem to show an increased pH independent MalPEG reactivity.

The phenotype of the above mutants was also investigated by using different in vivo assays. In line with the previous results, mutation of the residues expected to affect the protonation of C29 (S32, R98, and T369) dramatically increased the tendency of ERp44 to form covalent complexes with client and partner proteins, reaching levels comparable to a mutant lacking the whole β16 strand (ERp44 Δβ16) and the fraction of covalently bound partners doesn't change upon basification of Golgi pH (GPHR silencing) (Figure 9).

Not only the covalent binding but also the client retention ability of ERp44 is altered upon residue substitution. In particular, clients like APN are less retained by S32A, R98Q, T369A and C29A mutants and in a pH independent way.

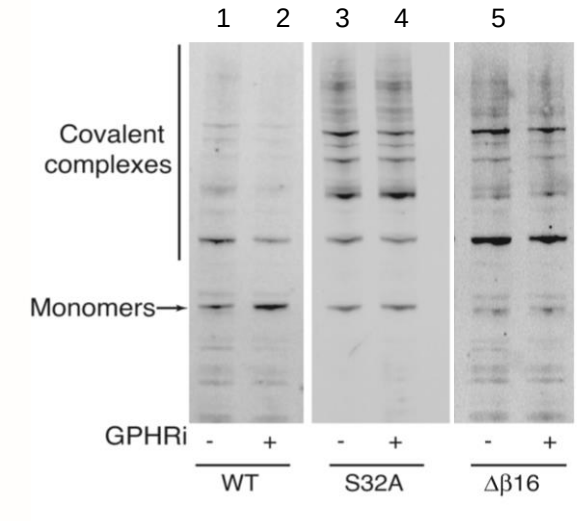

Fig.9 *In vivo analysis of pH sensor residues.* HeLa transfectants expressing the indicated ERp44 mutants were subjected (+) or not (-) to GPHR silencing (GPHRi). Aliquots of lysates were resolved under non-reducing conditions and decorated with anti-HA antibody that recognize only the over-expressed ERp44. The black arrow points to monomeric ERp44. While the amount of ERp44 wt engaged in covalent complexes goes down after Golgi pH basification (compare lanes 1-2), the mutants have higher binding capacity in a pH independent manner (lanes 3-4 and 5-6).

Role of conserved histidine residues in ERp44 activity

By looking at ERp44 amino acidic sequence an histidine rich region was found to be very conserved during evolution (Figure 10). This region is located at the border between the domain **b'** and the C-tail of the chaperone. Moreover, in the available ERp44 crystals, part of the C-tail (residues 332–350) is not resolved, suggesting an higher flexibility of the region[116]. In particular there are five histidine residues called here after A, A', B, C and D. C and D are present at the beginning of the unstructured region of the C-tail while A and A' are in the domain **b'**. In literature is known that histidine residues can change protonation near pH 6,5-6,0 and we previous described that ERp44 is a pH regulated chaperone[29]. The presence of two of the histidines in unstructured region reinforces the hypothesis that this region can play a fundamental role for co-factor binding to ERp44 (both regulators and ions). To investigate the role of the histidine rich region, a deletion mutant of ERp44 (ΔHis) was created by substituting residues 332-350 with a spacer (SGSG).

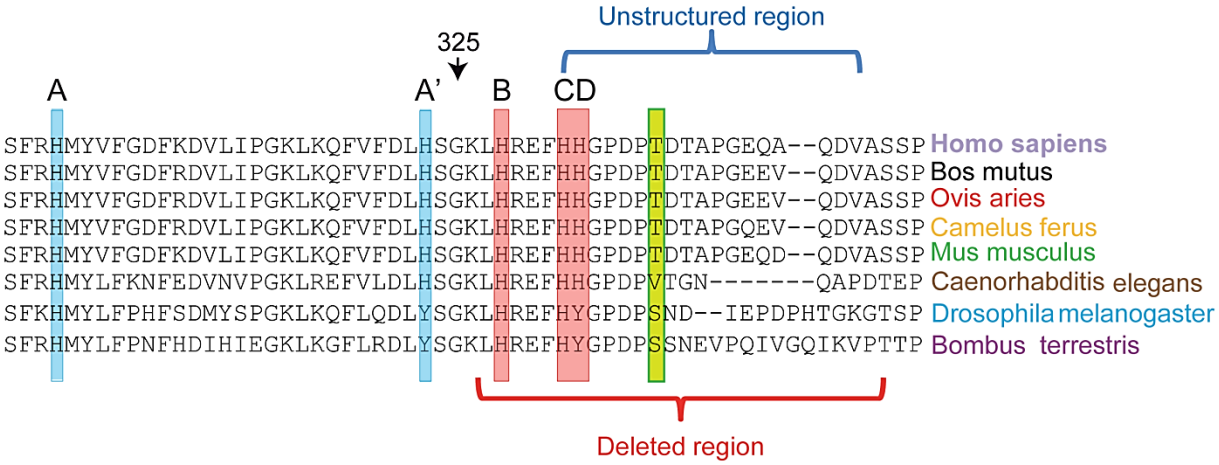

Fig.10 *Sequence alignment of the proximal part of the ERp44 C-tail.* The amino acidic sequence of the histidine rich region and of the first part of the C-terminal tail reveals high sequence conservation in different organisms. Three histidine residues reside in the tail (B, C and D, highlighted here in red) and two in the domain **b'** (A and A', in light blue). The unstructured region in the crystal and the region deleted in the ΔHis mutant are indicated by blue and red brackets.

Even if ERp44 ΔHis behaved similarly to the wt protein *in vitro*, the mutant did show evident phenotypes in vivo. In particular, secretion assays clearly demonstrated that:

a) ΔHis was in part secreted and the residual retention of the mutant is due to KDEL-Rs activity;

b) ΔHis was more efficient than wt protein in retaining Ero1α, a known partner of ERp44;

c) Ero1α retention is pH independent;

d) co-expression of ERp44 ΔHis and Ero1α impairs mutant secretion.

Thus, the deletion of histidine rich region allows ERp44 secretion unless a high affinity client is present. This also suggests that clients could favor RDEL motif exposure in ERp44 ΔHis like in a client induced retrieval mechanism. At the same time, deletion of the histidine rich region increases the ability of ERp44 to retain its partners (both Ero1α and Ig-μΔCH1) in a pH-independent way.

How could a partially secreted protein (ERp44 ΔHis) be hyperactive in retaining a soluble and potentially secretable partner (Ero1α)? By looking at the cellular localization of ERp44 ΔHis it was discovered that while over-expressed ERp44 wt is present at ER-ERGIC level[70,115], this mutant accumulates in more distal regions, a localization that could favor capture of clients destined to be retrieved. Taking in account the previous data on differential secretion of ERp44 ΔHis with and without its partners, the localization of the mutant was analyzed in presence of Ero1αGFP (a partner) or in co-expression with sGFP-RDEL (a non-partner). Clearly, the co-expression of Ero1αGFP, but not sGFP–RDEL, caused re-localization of ERp44 ΔHis into the ER (Figure 11). Thus, these data reinforce our previous hypothesis about the client induced retrieval of ERp44 which implies that interaction with high affinity clients keep the C-tail of ERp44 in an open conformation, favoring the exposure of RDEL motif and the KDEL-Rs dependent retrieval of the entire complex (ERp44-client) to the ER.

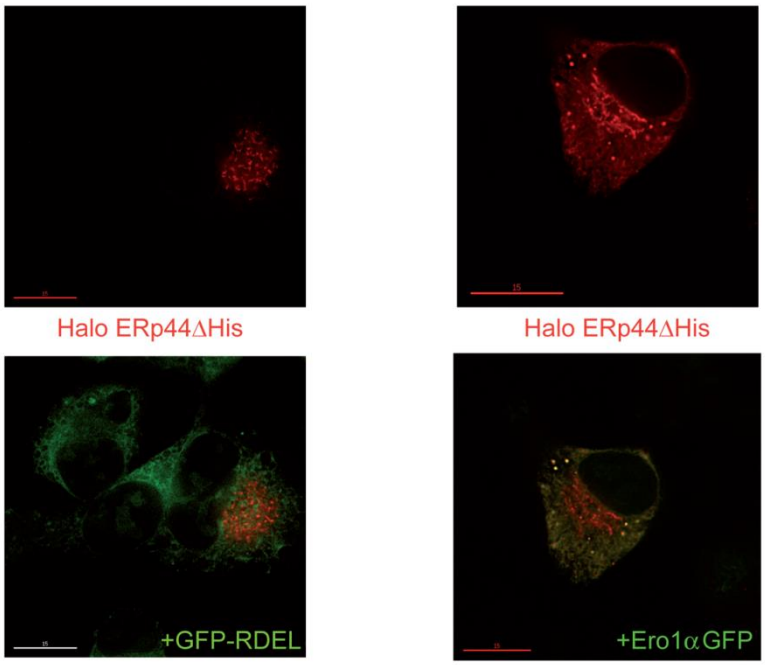

Fig.11 *Client-induced relocalisation of ΔHis to the ER.* Co-expressing Ero1α–GFP, but not sGFP–RDEL, causes the relocalization of ΔHis in the ER. HepG2 cells were co-transfected with Halo-tagged ERp44 ΔHis and sGFP–RDEL or Ero1α–GFP and then decorated with a Halo ligand (red signal). Clearly, no co-localization is detectable between sGFP–RDEL (green) and ERp44 ΔHis (red), whereas expression of Ero1α–GFP also causes ΔHis to localize in the ER, yielding a reticular yellow staining (bottom right panel).

Considering their conservation from *Homo sapiens* to *Caenorhabditis Elegans*, histidine residues were replaced singularly or in combination (Figure 10). The more histidines are replaced the more ERp44 is secreted and, as for the deletion mutant ERp44 ΔHis, the co-expression of Ero1α alters their secretion in favor of retention. In line with sequence conservation during evolution, histidine A, B, C appear to be the most important in regulating the C-tail movements, while A' and D seem to play an accessory role. Western blot analysis with anti-Ha revealed the presence of two bands in the histidine mutants lysates (In) and only the upper band is present in the outside medium (Sec) (Figure 12).

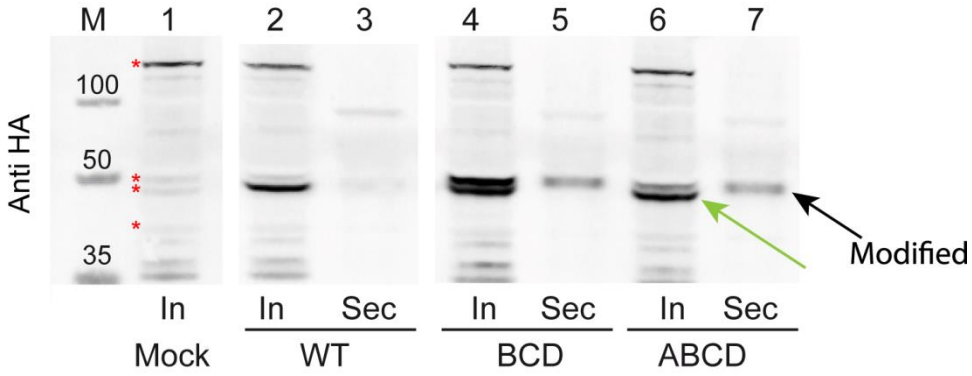

Fig.12 *Replacement of histidine residues causes ERp44 modification and secretion.* Aliquots from lysates (In) and culture medium of HeLa transfectants expressing the indicated ERp44 mutants were collected and blotted with anti-HA antibody. Note that anti HA detects two bands in the lysates of histidine mutants (BCD and ABCD) of which only the upper one is present in the secreted material (pointed with a black arrow). ERp44 wt is represented as a single band in intracellular material (pointed with green arrow).

Although ERp44 has no potential N-glycosylation sites, mutants that escaped KDEL-R dependent retrieval could undergo O-glycosylation in the Golgi.

To establish if this was the case, HeLa transfectants were treated with brefeldin A (BFA), a drug known to induce the retrograde transport of Golgi enzymes to the ER[133]. The electrophoretic mobility of ERp44 wt and BCD mutant was impaired after BFA treatment while the one of ERp44 ΔHis was not (Figure 13). Treatment of lysates with O-glycosidase restored the faster migration and abolished the doublet observed in the BCD intracellular material, demonstrating that ERp44 can be O-glycosylated before being secreted downstream the ER. In contrast, ERp44 ΔHis is not modified in presence of BFA indicating that either the target residue was deleted in this mutant or the replacement caused its inaccessibility to O-glycosyl transferases.

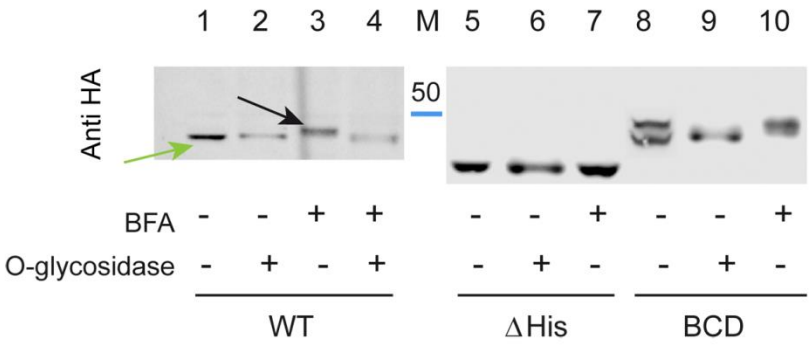

Fig.13 *Secreted ERp44 is O-glycosylated.* HeLa cells transfected as indicated were treated with (lanes 3, 4, 7, 10) or without brefeldin A (BFA) for 4 h to determine whether retrieval of Golgi enzymes to the ER caused processing of ERp44. Aliquots from the lysates were digested with (lanes 2, 4, 6, 9) or without O-glycosidase, resolved by gel electrophoresis and blots stained with anti-HA antibody.

The fact that most ERp44 wt was not modified in normal conditions implied its retrieval before the modification occurs. In silico prediction programs[134,135] pointed at threonine residues 338 and 340 as possible substrates of O-glycosylation. Both are located within the loop deleted in ΔHis, which would explain why this mutant is not O-glycosylated. Replacing the most conserved one, T338, with alanine in a mutant that was in part secreted and modified (ABCD) was sufficient to prevent the processing. To verify the physiological relevance of ERp44 processing, a wide panel of cells and tissues was screened and we find ERp44 as a double band in primary endometrial stromal cells obtained from healthy donors. Treatment with O-glycosidase of lysate aliquots collapsed the doublet into a single band, confirming that endogenous ERp44 can undergo O-glycosylation physiologically (Figure 14). Notably, the relative abundance of O-glycosylated ERp44 was higher in endometrial stromal cells in the secretory phase than in the proliferative phase[136]. Processed ERp44 was detected in the spent medium of secretory endometrial cells (Figure 15).

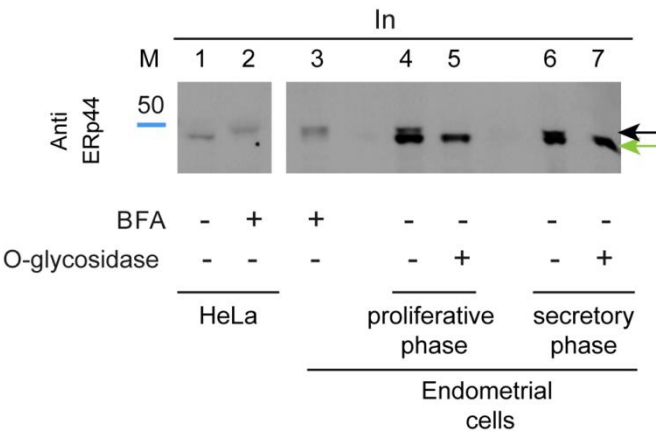

Fig.14 *Endogenous ERp44 is O-glycosylated in endometrial stromal cells.* Lysates obtained from endometrial stromal cells in their proliferative (lanes 4–5) or secretory (lanes 3, 6–7) phase were digested with (lanes 5, 7) or without (lanes 3, 4, 6) O-glycosidase and resolved by SDS page under reducing conditions. Note that upon digestion, the doublet visible in untreated samples collapses into a single higher mobility band, which comprises un-glycosylated and de-glycosylated ERp44 (green arrow). The black arrow points at the O-glycosylated species, the main form accumulating in HeLa (lane 2) or endometrial (lane 3) cells after treatment with BFA.

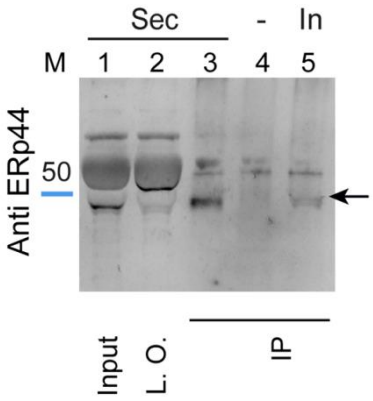

Fig.15 *Endogenous ERp44 is secreted by endometrial stromal cells.* Aliquots from the lysates or spent media (48 h) corresponding to $8x10^4$ and $7x10^5$ endometrial cells in their secretory phase were immunoprecipitated (IP) with the monoclonal anti-ERp44 antibody, resolved under reducing conditions and stained with rabbit anti-ERp44 antibody. Lanes 1 and 2 show one-third of the spent medium before (Input) or after (L.O., left over) immunoprecipitation.
The band migrating above the 50-kDa marker is BSA, which is highly abundant in fetal calf serum. Cross-linked beads were used as a negative control (lane 4). Endogenous ERp44 is clearly detectable in the culture medium and migrates with a molecular mass similar to the O-glycosylated ERp44 species present intracellularly (black arrow).

Exploring partner binding by ERp44 into ESC

Knowing that histidine mutants could be O-glycosylated in the distal ESC, these mutants were used as a marker of ERp44 complex formation with different partners. Thus, the binding before the O-glycosylation site would increase the amount of the un-glycosylated ERp44, while O-glycosylated ERp44 should increase if the binging occurs post O-site. Over-expression of Ero1α and Prx4 favors the accumulation of un-modified ERp44, while Sumf1 is able to bind ERp44 also after sugar attachment. These observations tell us that, depending on partner affinity for ERp44 binding site and on the surrounding environment (different pH and/or variable co-factor concentration), ERp44-client complexes form before or downstream the subregion where O-linked glycosylation takes place. The client-induced retrieval mechanism described before may allow the distinct and sequential localization of ERp44 interactors along the ESC (Figure 16).
To isolate novel ERp44 molecular partners, a special tag, called Halo tag, was added to ERp44. Since ERp44 has a mobile C-tail that regulates partner binding and ERp44 localization, Halo tag was inserted between the ERp44 leader sequence and the coding one, to not influence the C-tail movements and ERp44 localization. HaloERp44 constructs were generated and their expression, activity and localization were tested in different cell lines (HeLa and HepG2). Having confirmed that Halo-ERp44 recapitulates most of the properties of ERp44, we are proceeding with the interactome study. Moreover, to follow the dynamic processes engaged in protein folding and

secretion, Halotag technology was used to study the behavior of protein with different fates in ESC: a chaperone (ERp44), an ERAD substrate (Ig-μs) and an aggregation-prone molecule (Ig-μΔCH1) (see Mossuto et al., 2014 for more details). Exploiting the Halo property of binding covalently ligands labelled with different fluorochromes, we monitor protein secretion and degradation and we discriminate between old and newly made proteins without using radioactive labelling. We can also follow the biogenesis, growth, accumulation and movements of protein aggregates in the ESC.

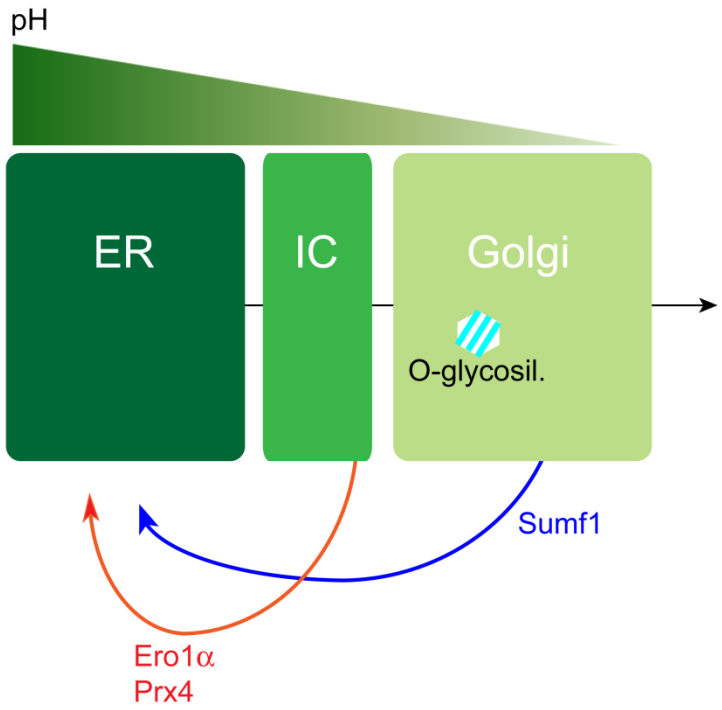

Fig.16 *Schematic representation of sequential client binding.* The lower pH encountered by ERp44 as it proceeds along the early secretory pathway, favors opening of the C-tail and KDEL-R binding regardless of the presence or absence of high-affinity client proteins. By contrast, mutants lacking key conserved histidine residues or a loop at the border between the domain **b'** and the C-tail bind poorly to KDEL-Rs, proceed towards the extracellular space and are O-glycosylated. Client binding induces KDEL-R dependent retrieval of histidine mutants before (Ero1α, Prx4) or after (Sumf1) O-glycosylation takes place.

Discussion and Future issues

Cells possess an extensive network of components to safeguard proteome integrity and maintain protein homeostasis, the so called cell proteostasis[137]. Mammalian cells must ensure that more than 10.000 different proteins fold, assemble efficiently and preserve their functionally active states in a wide range of environmental and metabolic conditions. This is a challenging task, because proteins are only marginally stable at physiological temperature and are constantly at risk of misfolding[137]. In addition, the concentration and subcellular localization of each individual protein species needs to be carefully controlled. That's why the subdivision of the early secretory pathway in distinct subcellular compartment and the dynamic expression of different chaperones and enzymes are crucial for maintaining the cell protein factory under control. When the proteostasis network declines in performance, as occurs during aging, newly synthesized proteins are no longer able to fold efficiently and metastable proteins lose their functionally active conformations, particularly under conditions of cell stress. Apart from "loss of function" effects, a critical consequence of these proteostasis defects is the accumulation of toxic protein aggregates in different cell compartments, which is associated with many age-dependent neurodegenerative diseases and other medical disorders (for example unfolded protein diseases)[137]. One of the fundamental questions in cell biology is how size and activity of the different ESC compartments are regulated in physiological as well as in stress conditions. For instance, the secretory route is traversed by intense membrane fluxes whose extent and composition must be tightly regulated to prevent dangerous events that could induce cell death. Recent studies demonstrated that the paring between KDEL-Rs and specific partners is crucial for regulating retrograde and anterograde traffic in ESC, adapting the subcellular compartment composition and extent to cell demands [109, 112, 113]. The study of ESC resident chaperones can be a good target to understand more about flux sensors and cell response.

One of the known partners of KDEL-Rs is ERp44, a multifunctional chaperone of ESC, involved in different cell functions such as distal quality control and calcium signaling. The data I obtained regarding the activity and localization of this protein has proven more information about how a chaperone of ESC is able to cycle and bind specific clients in different sub-compartments and is improving our knowledge about physiological and pathological processes.

ERp44 regulation by the pH gradient between the ER and the Golgi

The existence of a pH gradient between ER and Golgi complex is known from 1978 and is important for numerous processes like cell signaling, protein folding and trafficking and lectin activity [100-103]. The discovery of ERp44 as a pH regulated chaperone adds more information about the importance of H^+ concentration in regulating protein quality control and oxidative folding and in selective protein secretion[29]. In fact, the pH regulated opening of ERp44 C-tail determines both client capture and KDEL-Rs mediated retrieval and, as consequence, the activation of a signal cascade that alerts the ER about the incoming proteins and membrane fluxes. Owing to the fact that the two cysteine residues (C29 and C63) in SBS are progressively more exposed from ER to Golgi complex, different clients can bind proximally or distally along the secretory route. Moreover, the nature of these interactions can be covalent or not, also depending on the affinity of the client for the substrate binding site. Moreover, differences in the pH optimum for ERp44 interactions with partners may account for differences in the intracellular distribution of specific clients like Ero1α, which is also present at mitochondrial-associated ER membranes (MAM) and can regulate calcium signaling[126,138]. ERp44 can receive clients from, and associates with, ERGIC-53[71], a lectin that also embraces glycoproteins released by the calnexin/calreticulin quality control[8]. The ERp44-ERGIC53 tandem may thus integrate thiol-mediated and glycan-trimming-dependent ER quality control cycles. So ERp44 can act as a shuttle for soluble proteins that need to be in different ESC compartments depending on certain cellular demand and occasionally to be secreted. In line with the model of pH dependent retention, silencing of ERp44 causes the secretion of proteins with exposed reactive cysteine residues like IgM[71,139], adiponectin[73,140], SUMF1[119,120], and peroxiredoxin4[63]. Similarly upon Golgi pH basification ERp44 partners like Ero1α, adiponectin, and IgM are secreted presumably because the SBS of ERp44 remains less accessible. Interestingly, even if its clients are secreted, ERp44 is not found in the spent medium of cells with an altered ESC pH gradient. This led us to think that the kinetic of tail opening is not a two-step one: probably at ERGIC-Golgi pH, the C-tail flips rapidly and can then be stabilized in an open conformation by other co-factors, cargoes or regulatory proteins. In line with this hypothesis, mutation of conserved histidine residues at the border between domain **b'** and C-tail of ERp44 have notable consequences on its retention, likely decreasing the RDEL accessibility to KDEL-Rs in the ERGIC-Golgi. Accordingly, co-expression of clients that could bind to the SBS of ERp44 and force the C-tail in an open conformation and thus the RDEL exposure restored the histidine mutant retrieval (see result section).

A possible role for extracellular O-glycosylated ERp44: the endometrium and the menstrual cycle

The study of histidine mutants also shows that ERp44 can be O-glycosylated and that this modification can be used as a marker of ERp44 localization and secretion. In fact, the more ERp44 is accumulated in the distal ESC the more is abundant the O-glycosylated form of the chaperone and which can be also present in the spent medium. Accordingly with these observations, stromal endometrial primary cells secrete ERp44 in the secretory phase of the menstrual cycle[30]. In human beings, the menstrual cycle begins with the proliferative phase under the influence of estrogen levels, leading to epithelium and stroma proliferation and vasphase[141]. Analyzing different samples of primary endometrial stromal cells, we observed that the amount of O-glycosylated ERp44 changes during the menstrual cycle, with a peak when the cells are in the early secretory phase(Figure16): this suggests that the amount of intracellular O-glycosylated ERp44 could correlate to cell demand for secretion. After ovulation, in fact, the endometrium starts to be prepared to embryo implantation: this process is remarked by progesterone secretion, gland transition from quiescent to secretory state and stromal cells undergo differentiation for the predecidualization phase[141]. Thus also suggests possible role(s) for ERp44 in intercellular dialogues and as a marker of menstrual cycle phases.

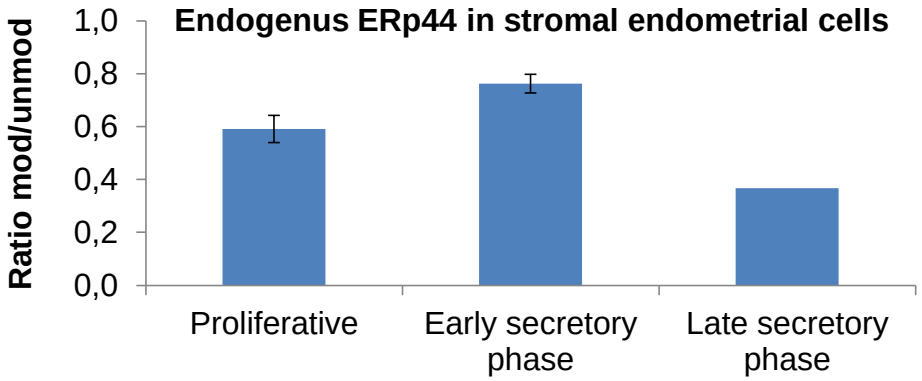

Fig.16 *Schematic quantification of O-glycosylated ERp44.* The histograms show the ratio between O-glycosylated and not O-linked endogenous ERp44 present in lysate of endometrial stromal cells taken from patients without endometrial pathologies. Data represent the mean of three different samples except in the case of cells in late secretory phase. The more the ratio is similar to 1 the more the amount of O-glycosylated ERp44 is increased.

Moreover, different genes are expressed at the blastocyst attachment to the uterus during decidualization process. One of them is Cox2 (cyclooxygenase derived prostaglandins 2) that seems to play a crucial role in embryo implantation. It acts by activating PPAR-γ (peroxisome-proliferator-activated receptor γ) and retinoidX receptor fundamental both form embryo and

maternal side for the implantation[142,143]. Interestingly, PPAR-γ has been described to be an essential regulatory factor for the transcription activity of ERp44 in adipocyte[128]. PPAR-γ has been implicated in the pathology of numerous diseases including obesity, diabetes, atherosclerosis, and cancer [144]. It acts as a master gene in metabolic regulation through stimulating insulin sensitivity, glucose lowering, and lipid uptake and storage in peripheral organs such as skeletal muscle, liver, and adipose tissue. Gene transcription is regulated by PPAR-γ in at least three mechanisms: ligand-dependent transactivation by forming heterodimers with retinoinX receptor, ligand-dependent trans-repression, and ligand-independent repression. It seems that PPAR-γ repressed ERp44 expression through the third mechanism, favoring adiponectin secretion[128]. Taking into account these data, we can speculate that ERp44 is a new target of transcript regulation by known transcription factors depending on the menstrual cycle phase and that it is expression and O-linked modification could be mis-modulated in certain pathologies like in diabetes type I that can let to spontaneous abortion.

Searching for novel ERp44 partners/cargoes

Some ERp44 clients are more effective than others in competing for SBS in the histidine mutants. In particular, Ero1α and Prx4 bind to ERp44 mainly before it undergoes O-glycosylation, whereas Sumf1 can also interact afterwards. These observations suggest that different proteins could be deposited sequentially in the exocytic pathway, depending on their affinity for ERp44 and on the pH dependency of the chaperone–client interactions. Along these lines, it is interesting that most ERp44 substrates and/or partners that are ER-resident enzymes (Ero1α, Prx4 and Sumf1) lack a C-terminal KDEL like sequence and rely on protein–protein interactions for their intracellular localization. Thus, the amount and activity of ERp44 is likely to regulate their localization and activity in and between different cells[145-147]. The different localization of ERp44 itself can also be due to interactions with sub-compartment specific resident proteins. In order to better understand the physiology of all these interactions, we have tried to isolate the interactome of ERp44 using a novel tagging technology, the Halo tag. the Halo tag, in fact, has many different applications[148] and can be used to precipitate chimeric proteins (together with their partners) in a higher amount compared to canonical co-immunoprecipitation. The preliminary data on the ERp44 interactome in HeLa cells, as a result of 3 independent experiments, are summarized in Table1. Proteins have been divided for their cellular localization and activity (in yellow ESC resident proteins, in blue putative substrates and in orange mitochondrial proteins) and subsequently organized in functional subcategories (highlighted with different colors). Numerous are the proteins present both at ER-Golgi complex and at mitochondrial level, indicating that ERp44 can not only cycle between proximal and distal ESC but it is also present at the mitochondrial membrane associated to ER

(MAM), as previously described[126,138]. Moreover, we detected a large group of proteins involved in redox homeostasis, suggesting that they can cooperate absolving their redox activity in specific compartments. As a control of the specificity of the experiments, known partners are present, like Ero1α, peroxiredoxin-4 and Sumf1. Analysing the isolated ERp44 partners, we noticed that 2 of them (Sec23A and DnaJ homolog subfamily A member 1) are able to bind zinc ions (indicated by *) and others binds calcium ions, indicating not only a role of ERp44 in regulating calcium signaling but also highlighting a possible novel role as a zinc folding protein regulator.

Table 1

ER-Golgi complex resident interactors	
Ac number	**Name**
Redox related proteins	
B5MCQ5	PDIA6 - ERp5
Q8NBK3	Sumf1
Q9H3N1	TMX1
P07237	PDI
E9PFN5	Glutathione S-transferase kappa 1
Q96HE7	Ero1α
P30101	ERp60 - ERp57
Q86UY0	ERp46
P13667	PDIA4 - ERp70 - ERp72
Q13162	Peroxiredoxin-4
P30040	ERp29
Proximal ER protein quality control	
P27797	Calreticulin
P11021	BIP (GRP-78)
B4DGP8	Calnexin
Vesicles transport	
Q86UP2	Kinectin
Q9BVK6	emp24
P55072	Transitional ER ATPase
Q9Y678	COPG1
P53621	COPA
F5H365	Sec23A*
P51153	Rab13
Q00610	Clathrin heavy chain 1
N-glycan metabolism	
P04843	Ribophorin I
Q14697	Neutral alpha-glucosidase AB
Calcium binding proteins	
K7ELL7	Glucosidase 2 subunit beta
P14625	Endoplasmin - GRP94
P51571	TRAP delta
P16615	SERCA2
Others	
Q92896	Golgi apparatus protein 1
Q9NQC3	Reticulon-4
P50454	Serpin H1

Putative substrates	
Ac number	**Name**
P02786	Transferrin receptor protein 1
P05556	Integrin beta-1
Q9HDC9	Adipocyte PM associated protein
P30086	Tubulin beta-4B chain
Mithocondrial interactors	
Redox related proteins	
P30041	PRX6
Q99497	Protein DJ-1
E9PH29	Peroxiredoxin-3
P54886	Delta-1-pyrroline-5-carboxylate synthase
B4DHG0	Dihydrolipoyl dehydrogenase
P30044	Peroxiredoxin-5
Energy metabolism	
P25705	ATP synthase subunit alpha
O75489	NADH dehydrogenase iron-sulfur protein 3
P48047	ATP synthase subunit O
P05141	ADP/ATP translocase 2
O95831	Apoptosis-inducing factor 1
Q9NVI7	Isoform 2 ATPase family containing protein
D6RFM5	Succinate dehydrogenase subunit
P56381	ATP synthase subunit epsilon
P00403	Cytochrome c oxidase subunit 2
P38117	Electron transfer flavoprotein β
Lipid metabolism	
P40939	Trifunctional enzyme subunit alpha
P30084	Enoyl-CoA hydratase
P00505	Aspartate aminotransferase
P49748	acyl-CoA dehydrogenase
Protein folding	
P31689	DnaJ homolog subfamily A member 1*
F5H897	Heat shock protein 75 kDa - TRAP1
Others	
Q15691	Mitochondrial dicarboxylate carrier
Q00325	Phosphate carrier protein

ERp44 as a zinc binding protein

Whereas the C29-based tail regulation is intrinsic to ERp44 and can be revealed *in vitro*, the histidine-dependent mechanisms are evident only *in vivo* as they require additional regulatory elements. In fact, deletion or mutation of the conserved histidine residues had only marginal effects *in vitro* [30], indicating that additional 'histidine-region-binding factors' regulate ERp44 *in vivo*. Searching for protein sequences similar to the histidine rich region of ERp44 by Blastp tool (query sequence used: DXHXXXXHRXXHH), we found few proteins with high similarity, highlighting the great conservation of this specific sequence in different organisms. Indeed, it is possible to identify an high score of similarity between the ERp44 histidine loop and 4 different zinc binding proteins:

- Solute carrier family 39 and cation channel sperm-associated protein 1 in homo sapiens;
- Dystrophin isoform X1 in *canis lupus familiaris*;
- Zinc finger protein 488 in *Eptesicus fuscus*.

By analyzing the available closed 3D structure of ERp44 and keeping in mind that histidine residues can coordinate zinc ions, we are now investigating the role of conserved histidines in binding Zn^{2+} and/or other putative regulatory molecules both *in vivo* and *in vitro*. Moreover, comparative proteomic analysis between ERp44 wt and ΔHis mutant is ongoing and will increase our knowledge on novel client and regulatory proteins.

Pathophysiological role of ERp44 and its partners: platelets activation and endothelial cells

It is described in literature that upon activation platelets can secrete ERp44 (Holbrook et al., 2010). This chaperone is not the only one secreted upon platelets activation together with different PDI family isomerases (for example PDI, ERp57, ERp5, ERp72, ERp29), which are known to be present in platelets secretory granules and in the outer medium or at the outer side of the platelets plasma membrane[149,150]. These PDI like proteins seem to play a role in thrombus formation and in integrin activation. In line with the platelets secretion, several experiments demonstrated that PDI is also present on the surface of endothelial cells. Thus, after vascular injury, PDI and other family members (like ERp5, ERp46 and ERp57) can be first secreted by endothelial cells to line the area of injury and then secreted from bound platelets[151,152]. Numerous studies try to dissect the role of secreted PDI from endothelium and platelets and, even if it is the same molecule, this chaperone is useful for different functions (Kim K. et al., 2013). In fact, platelets PDI is crucial for the thrombus growth but it is not essential for platelets adhesion, function that is supported by endothelial PDI.

These different roles of PDI could reflect the exit from the cell together with different co-partners like Ero1α, ERp46 or ERp44.The majority of the PDI like isomerases secreted by platelets and endothelial cells are also present in our preliminary interactome of ERp44 wt, confirming a possible cooperation between them depending on a specific cell demand (Table1 proteins in light yellow subgroup). Platelet aggregation is enhanced by serotonin (5-hydroxytryptamine), a molecule secreted by intestinal enterochromaffin cells into the blood. The binding of serotonin to its cognate receptor on platelets membrane induces a modification of N-glycan content that favor aggregation [153]. In particular, activation of serotonin receptor initiates a G-protein dependent signaling in platelets, which triggers the release of pro-coagulant molecules including serotonin and other molecules present at the α granules levels[154,155]. According to these finding ERp44 can be secreted to favor platelets aggregation (thrombus growth) in collaboration with other PDI family members.

As described for PDI related enzymes, also proteins belonging to the redox related QSOX family other redox ESC enzymes (belonging to the QSOX family) can be secreted under specific conditions. QSOXs are able to directly oxidize unfolded reduced peptides and proteins without significant collateral oxidation of PDI_{red}[156-159]. In particular, QSOX1 is an atypical disulfide catalyst localized at Golgi complex and it is secreted from confluent fibroblasts. It was shown that QSOX1 can play a role in laminin incorporation into extracellular matrix favoring cell-matrix adhesion[160]. It's reasonable to hypothesize a possible interaction and extracellular communication between ERp44-Ero1α couple and QSOX1.

It has been recently demonstrated that the level of expression of ERp44 are six fold higher in preeclampic placental cells if compared to normal controls. In pre-eclampic placentas, also the expression of miR-101(-3p) is decreased, highlighting a possible role of miR-101(-3p) and ERp44 in this kind of pathologic pregnancy[161]. Moreover, over-expression of miR-101(-3p) inhibits trophoblast apoptosis and decreases the protein level of ERp44 in culture.

Concluding remarks and future issues:

It is clear, from all these new emerging data, that the complex role of ERp44 in different tissues still needs many effort to be fully evaluated, and that it will surely give new information both on human pathologies and on physiological processes. Moreover, from a molecular point of view, how C29 of ERp44 reacts with clients to form mixed disulfides and in which state the cysteine residues of clients should stay to be bound by ERp44 require further investigation.

Many more general questions regarding protein folding in the ESC still need an answer:

- Does co-translational folding limit the number of folding pathways a protein can take?
- Which folding factors remain to be identified?
- What limits disulfide bond formation in different physiological contexts?

In this context, better understanding the mechanisms of activity of ERp44 will be important:

- Which is the status of the cysteines in ERp44 client proteins? Is the mixed disulfide introduced between two free thiols by an oxidase, or are the client proteins in a mixed disulfide with another protein and ERp44 has only to mediate reshuffle?
- Can the histidine rich region coordinate a zinc ion? Can ERp44 act as a zinc storage in the ER-Golgi complex?
- How ERp44 can escape the control of KDEL-Rs being thus secreted?
- Which is the role of secreted ERp44 in a physiological contest? Could it be a DAMP (damage-associated protein) or an anti-inflammatory signal?

Further experiments are ongoing to try to answer these questions.

References

1. Anelli, T. & Sitia, R. Protein quality control in the early secretory pathway. *EMBO J.* **27**, 315-327 (2008).

2. Chen, Y. *et al*. SPD - A web-based secreted protein database. *Nucleic Acids Res.* **33**, D169-D173 (2005).

3. Ng, D. T. W., Brown, J. D. & Walter, P. Signal sequences specify the targeting route to the endoplasmic reticulum membrane. *J. Cell Biol.* **134**, 269-278 (1996).

4. Shao, S. & Hegde, R. S. Membrane protein insertion at the endoplasmic reticulum. *Annual Review of Cell and Developmental Biology* **27**, 25-56 (2011).

5. Braakman, I. & Bulleid, N. J. Protein folding and modification in the mammalian endoplasmic reticulum. *Annual Review of Biochemistry* **80**, 71-99 (2011).

6. Larkins, B. A., Lending, C. R. & Wallace, J. C. Modification of maize-seed-protein quality. *Am. J. Clin. Nutr.* **58**, 264S-269S (1993).

7. Jolliffe, N. A., Craddock, C. P. & Frigerio, L. Pathways for protein transport to seed storage vacuoles. *Biochem. Soc. Trans.* **33**, 1016-1018 (2005).

8. Ellgaard, L. & Helenius, A. Quality control in the endoplasmic reticulum. *Nature Reviews Molecular Cell Biology* **4**, 181-191 (2003).

9. Sitia, R. & Braakman, I. Quality control in the endoplasmic reticulum protein factory. *Nature* **426**, 891-894 (2003).

10. Klausner, R. D. & Sitia, R. Protein degradation in the endoplasmic reticulum. *Cell* **62**, 611-614 (1990).

11. Yoshida, H. ER stress and diseases. *FEBS Journal* **274**, 630-658 (2007).

12. High, S. Protein translocation at the membrane of the endoplasmic reticulum. *Prog. Biophys. Mol. Biol.* **63**, 233-250 (1995).

13. Saraogi, I. & Shan, S. -. Molecular Mechanism of Co-translational Protein Targeting by the Signal Recognition Particle. *Traffic* **12**, 535-542 (2011).

14. Dobson, C. M. Principles of protein folding, misfolding and aggregation. *Seminars in Cell and Developmental Biology* **15**, 3-16 (2004).

15. Khalkhali, Z. & Marshall, R. D. Glycosylation of ribonuclease A catalysed by rabbit liver extracts. *Biochem. J.* **146**, 299-307 (1975).

16. Ellgaard, L. *et al*. NMR structure of the calreticulin P-domain. *Proc. Natl. Acad. Sci. U. S. A.* **98**, 3133-3138 (2001).

17. Schrag, J. D. *et al*. The structure of calnexin, an ER chaperone involved in quality control of protein folding. *Mol. Cell* **8**, 633-644 (2001).

18. Frickel, E. -. *et al*. TROSY-NMR reveals interaction between ERp57 and the tip of the calreticulin P-domain. *Proc. Natl. Acad. Sci. U. S. A.* **99**, 1954-1959 (2002).

19. Russell, S. J. *et al*. The Primary Substrate Binding Site in the b' Domain of ERp57 Is Adapted for Endoplasmic Reticulum Lectin Association. *J. Biol. Chem.* **279**, 18861-18869 (2004).

20. Williams, D. B. Beyond lectins: The calnexin/calreticulin chaperone system of the endoplasmic reticulum. *J. Cell. Sci.* **119**, 615-623 (2006).

21. Bertolotti, A., Zhang, Y., Hendershot, L. M., Harding, H. P. & Ron, D. Dynamic interaction of BiP and ER stress transducers in the unfolded-protein response. *Nat. Cell Biol.* **2**, 326-332 (2000).

22. Ron, D. & Walter, P. Signal integration in the endoplasmic reticulum unfolded protein response. *Nature Reviews Molecular Cell Biology* **8**, 519-529 (2007).

23. Flynn, G. C., Pohl, J., Flocco, M. T. & Rothman, J. E. Peptide-binding specificity of the molecular chaperone BiP. *Nature* **353**, 726-730 (1991).

24. Blond-Elguindi, S. *et al*. Affinity panning of a library of peptides displayed on bacteriophages reveals the binding specificity of BiP. *Cell* **75**, 717-728 (1993).

25. Gething, M. -. Role and regulation of the ER chaperone BiP. *Seminars in Cell and Developmental Biology* **10**, 465-472 (1999).

26. Guo, F. & Snapp, E. L. ERdj3 regulates BiP occupancy in living cells. *J. Cell. Sci.* **126**, 1429-1439 (2013).

27. Molinari, M. & Helenius, A. Chaperone selection during glycoprotein translocation into the endoplasmic reticulum. *Science* **288**, 331-333 (2000).

28. Dancourt, J. & Barlowe, C. Protein sorting receptors in the early secretory pathway. *Annual Review of Biochemistry* **79**, 777-802 (2010).

29. Vavassori, S. *et al*. A pH-Regulated Quality Control Cycle for Surveillance of Secretory Protein Assembly. *Mol. Cell* **50**, 783-792 (2013).

30. Sannino, S. *et al*. Progressive quality control of secretory proteins in the early secretory compartment by ERp44. *J. Cell. Sci.* (2014).

31. Kamiya, Y. *et al*. Molecular basis of sugar recognition by the human L-type lectins ERGIC-53, VIPL, and VIP36. *J. Biol. Chem.* **283**, 1857-1861 (2008).

32. Nishio, M. *et al*. Structural basis for the cooperative interplay between the two causative gene products of combined factor V and factor VIII deficiency. *Proc. Natl. Acad. Sci. U. S. A.* **107**, 4034-4039 (2010).

33. Nichols, W. C. *et al*. Mutations in the ER-Golgi intermediate compartment protein ERGIC-53 cause combined deficiency of coagulation factors V and VIII. *Cell* **93**, 61-70 (1998).

34. Zhang, B. *et al*. Bleeding due to disruption of a cargo-specific ER-to-Golgi transport complex. *Nat. Genet.* **34**, 220-225 (2003).

35. Zito, E. PRDX4, an endoplasmic reticulum-localized peroxiredoxin at the crossroads between enzymatic oxidative protein folding and nonenzymatic protein oxidation. *Antioxidants and Redox Signaling* **18**, 1666-1674 (2013).

36. Hwang, C., Sinskey, A. J. & Lodish, H. F. Oxidized redox state of glutathione in the endoplasmic reticulum. *Science* **257**, 1496-1502 (1992).

37. Benham, A. M., van Lith, M., Sitia, R. & Braakman, I. Ero1-PDI interactions, the response to redox flux and the implications for disulfide bond formation in the mammalian endoplasmic reticulum. *Philos. Trans. R. Soc. Lond. B. Biol. Sci.* **368**, 20110403 (2013).

38. Jansens, A., Van Duijn, E. & Braakman, I. Coordinated nonvectorial folding in a newly synthesized multidomain protein. *Science* **298**, 2401-2403 (2002).

39. Kettenhofen, N. J. & Wood, M. J. Formation, reactivity, and detection of protein sulfenic acids. *Chem. Res. Toxicol.* **23**, 1633-1646 (2010).

40. Ellgaard, L. & Ruddock, L. W. The human protein disulphide isomerase family: Substrate interactions and functional properties. *EMBO Rep.* **6**, 28-32 (2005).

41. Frand, A. R. & Kaiser, C. A. The ERO1 gene of yeast is required for oxidation of protein dithiols in the endoplasmic reticulum. *Mol. Cell* **1**, 161-170 (1998).

42. Pollard, M. G., Travers, K. J. & Weissman, J. S. Ero1p: A novel and ubiquitous protein with an essential role in oxidative protein folding in the endoplasmic reticulum. *Mol. Cell* **1**, 171-182 (1998).

43. Cabibbo, A. *et al*. ERO1-L, a human protein that favors disulfide bond formation in the endoplasmic reticulum. *J. Biol. Chem.* **275**, 4827-4833 (2000).

44. Pagani, M. *et al*. Endoplasmic reticulum oxidoreductin 1-Lß (ERO1-Lß), a human gene induced in the course of the unfolded protein response. *J. Biol. Chem.* **275**, 23685-23692 (2000).

45. Mezghrani, A. *et al*. Manipulation of oxidative protein folding and PDI redox state in mammalian cells. *EMBO J.* **20**, 6288-6296 (2001).

46. Tu, B. P. & Weissman, J. S. The FAD- and O2-dependent reaction cycle of Ero1-mediated oxidative protein folding in the endoplasmic reticulum. *Mol. Cell* **10**, 983-994 (2002).

47. Wilkinson, B. & Gilbert, H. F. Protein disulfide isomerase. *Biochimica et Biophysica Acta - Proteins and Proteomics* **1699**, 35-44 (2004).

48. Forster, R. *et al*. Secretory cargo regulates the turnover of COPII subunits at single ER exit sites. *Current Biology* **16**, 173-179 (2006).

49. Gillece, P., Luz, J. M., Lennarz, W. J., De La Cruz, F. J. & Römisch, K. Export of a cysteine-free misfolded secretory protein from the endoplasmic reticulum for degradation requires interaction with protein disulfide isomerase. *J. Cell Biol.* **147**, 1443-1456 (1999).

50. Fagioli, C. & Sitia, R. Glycoprotein quality control in the endoplasmic reticulum. Mannose trimming by endoplasmic reticulum mannosidase I times the proteasomal degradation of unassembled immunoglobulin subunits. *J. Biol. Chem.* **276**, 12885-12892 (2001).

51. Tsai, B., Rodighiero, C., Lencer, W. I. & Rapoport, T. A. Protein disulfide isomerase acts as a redox-dependent chaperone to unfold cholera toxin. *Cell* **104**, 937-948 (2001).

52. Molinari, M., Galli, C., Piccaluga, V., Pieren, M. & Paganetti, P. Sequential assistance of molecular chaperones and transient formation of covalent complexes during protein degradation from the ER. *J. Cell Biol.* **158**, 247-257 (2002).

53. Tu, B. P. & Weissman, J. S. Oxidative protein folding in eukaryotes: Mechanisms and consequences. *J. Cell Biol.* **164**, 341-346 (2004).

54. Tavender, T. J., Sheppard, A. M. & Bulleid, N. J. Peroxiredoxin IV is an endoplasmic reticulum-localized enzyme forming oligomeric complexes in human cells. *Biochem. J.* **411**, 191-199 (2008).

55. Nguyen, V. D. *et al*. Two endoplasmic reticulum PDI peroxidases increase the efficiency of the use of peroxide during disulfide bond formation. *J. Mol. Biol.* **406**, 503-515 (2011).

56. Ramming, T. & Appenzeller-Herzog, C. Destroy and exploit: Catalyzed removal of hydroperoxides from the endoplasmic reticulum. *International Journal of Cell Biology* (2013).

57. Tavender, T. J., Springate, J. J. & Bulleid, N. J. Recycling of peroxiredoxin IV provides a novel pathway for disulphide formation in the endoplasmic reticulum. *EMBO J.* **29**, 4185-4197 (2010).

58. Zito, E. *et al*. Oxidative Protein Folding by an Endoplasmic Reticulum-Localized Peroxiredoxin. *Mol. Cell* **40**, 787-797 (2010).

59. Cao, Z., Tavender, T. J., Roszak, A. W., Cogdell, R. J. & Bulleid, N. J. Crystal structure of reduced and of oxidized peroxiredoxin IV enzyme reveals a stable oxidized decamer and a non-disulfide-bonded intermediate in the catalytic cycle. *J. Biol. Chem.* **286**, 42257-42266 (2011).

60. Kakihana, T., Nagata, K. & Sitia, R. Peroxides and peroxidases in the endoplasmic reticulum: Integrating redox homeostasis and oxidative folding. *Antioxidants and Redox Signaling* **16**, 763-771 (2012).

61. Raykhel, I. *et al*. A molecular specificity code for the three mammalian KDEL receptors. *J. Cell Biol.* **179**, 1193-1204 (2007).

62. Wang, L., Zhang, L., Niu, Y., Sitia, R. & Wang, C. -. Glutathione peroxidase 7 utilizes hydrogen peroxide generated by Ero1a to promote oxidative protein folding. *Antioxidants and Redox Signaling* **20**, 545-556 (2014).

63. Kakihana, T. *et al*. Dynamic regulation of Ero1a and peroxiredoxin 4 localization in the secretory pathway. *J. Biol. Chem.* **288**, 29586-29594 (2013).

64. Hatahet, F. & Ruddock, L. W. Substrate recognition by the protein disulfide isomerases. *FEBS Journal* **274**, 5223-5234 (2007).

65. Galligan, J. J. & Petersen, D. R. The human protein disulfide isomerase gene family. *Human Genomics* **6** (2012).

66. Hudson, D. A., Gannon, S. A. & Thorpe, C. Oxidative protein folding: From thiol-disulfide exchange reactions to the redox poise of the endoplasmic reticulum. *Free Radical Biology and Medicine* (2014).

67. Fra, A. & Sitia, R. The endoplasmic reticulum as a site of protein degradation. *Subcell. Biochem.* **21**, 143-168 (1993).

68. Guenzi, S. *et al*. The efficiency of cysteine-mediated intracellular retention determines the differential fate of secretory IgA and IgM in B and plasma cells. *Eur. J. Immunol.* **24**, 2477-2482 (1994).

69. Reddy, P., Sparvoli, A., Fagioli, C., Fassina, G. & Sitia, R. Formation of reversible disulfide bonds with the protein matrix of the endoplasmic reticulum correlates with the retention of unassembled Ig light chains. *EMBO J.* **15**, 2077-2085 (1996).

70. Anelli, T. *et al*. Thiol-mediated protein retention in the endoplasmic reticulum: The role of ERp44. *EMBO J.* **22**, 5015-5022 (2003).

71. Anelli, T. *et al*. Sequential steps and checkpoints in the early exocytic compartment during secretory IgM biogenesis. *EMBO J.* **26**, 4177-4188 (2007).

72. Sitia, R. *et al*. Developmental regulation of IgM secretion: The role of the carboxy-terminal cysteine. *Cell* **60**, 781-790 (1990).

73. Wang, Z. V. *et al*. Secretion of the adipocyte-specific secretory protein adiponectin critically depends on thiol-mediated protein retention. *Mol. Cell. Biol.* **27**, 3716-3731 (2007).

74. Vallee, B. L. & Falchuk, K. H. The biochemical basis of zinc physiology. *Physiol. Rev.* **73**, 79-118 (1993).

75. Eide, D. J. Zinc transporters and the cellular trafficking of zinc. *Biochimica et Biophysica Acta - Molecular Cell Research* **1763**, 711-722 (2006).

76. Costello, L. C., Franklin, R. B. & Feng, P. Mitochondrial function, zinc, and intermediary metabolism relationships in normal prostate and prostate cancer. *Mitochondrion* **5**, 143-153 (2005).

77. Fukunaka, A. *et al*. Demonstration and characterization of the heterodimerization of ZnT5 and ZnT6 in the early secretory pathway. *J. Biol. Chem.* **284**, 30798-30806 (2009).

78. Oteiza, P. I., Hurley, L. S., Lönnerdal, B. & Keen, C. L. Effects of marginal zinc deficiency on microtubule polymerization in the developing rat brain. *Biol. Trace Elem. Res.* **24**, 13-23 (1990).

79. Yamasaki, S. *et al*. Zinc is a novel intracellular second messenger. *J. Cell Biol.* **177**, 637-645 (2007).

80. Fukada, T., Yamasaki, S., Nishida, K., Murakami, M. & Hirano, T. Zinc homeostasis and signaling in health and diseases. *Journal of Biological Inorganic Chemistry* **16**, 1123-1134 (2011).

81. Li, Y., Hough, C. J., Suh, S. W., Sarvey, J. M. & Frederickson, C. J. Rapid translocation of Zn(2+) from presynaptic terminals into postsynaptic hippocampal neurons after physiological stimulation. *J. Neurophysiol.* **86**, 2597-2604 (2001).

82. Sensi, S. L., Paoletti, P., Bush, A. I. & Sekler, I. Zinc in the physiology and pathology of the CNS. *Nature Reviews Neuroscience* **10**, 780-791 (2009).

83. Andreini, C., Banci, L., Bertini, I. & Rosato, A. Zinc through the three domains of life. *Journal of Proteome Research* **5**, 3173-3178 (2006).

84. Ghosh, S. K. *et al*. A novel imaging approach for early detection of prostate cancer based on endogenous zinc sensing. *Cancer Res.* **70**, 6119-6127 (2010).

85. Liuzzi, J. P. & Cousins, R. J. Mammalian zinc transporters. *Annual Review of Nutrition* **24**, 151-172 (2004).

86. Fukada, T. & Kambe, T. Molecular and genetic features of zinc transporters in physiology and pathogenesis. *Metallomics* **3**, 662-674 (2011).

87. Hennigar, S. R. & Kelleher, S. L. Zinc networks: The cell-specific compartmentalization of zinc for specialized functions. *Biol. Chem.* **393**, 565-578 (2012).

88. Taylor, K. M., Kille, P. & Hogstrand, C. Protein kinase CK2 opens the gate for zinc signaling. *Cell Cycle* **11**, 1863-1864 (2012).

89. McCormick, N. H. & Kelleher, S. L. ZnT4 provides zinc to zinc-dependent proteins in the trans-Golgi network critical for cell function and Zn export in mammary epithelial cells. *American Journal of Physiology - Cell Physiology* **303**, C291-C297 (2012).

90. Fukunaka, A. *et al*. Tissue nonspecific alkaline phosphatase is activated via a two-step mechanism by zinc transport complexes in the early secretory pathway. *J. Biol. Chem.* **286**, 16363-16373 (2011).

91. Wieland, F. T., Gleason, M. L., Serafini, T. A. & Rothman, J. E. The rate of bulk flow from the endoplasmic reticulum to the cell surface. *Cell* **50**, 289-300 (1987).

92. Hauri, H. -., Nufer, O., Breuza, L., Tekaya, H. B. & Liang, L. Lectins and protein traffic early in the secretory pathway. *Biochemical Society Symposium* **69**, 73-82 (2002).

93. Gürkan, C., Stagg, S. M., LaPointe, P. & Balch, W. E. The COPII cage: Unifying principles of vesicle coat assembly. *Nature Reviews Molecular Cell Biology* **7**, 727-738 (2006).

94. Mezzacasa, A. & Helenius, A. The transitional ER defines a boundary for quality control in the secretion of tsO45 VSV glycoprotein. *Traffic* **3**, 833-849 (2002).

95. Demaurex, N. pH homeostasis of cellular organelles. *News in Physiological Sciences* **17**, 1-5 (2002).

96. Kim, J. H. *et al*. Noninvasive measurement of the pH of the endoplasmic reticulum at rest and during calcium release. *Proc. Natl. Acad. Sci. U. S. A.* **95**, 2997-3002 (1998).

97. Kneen, M., Farinas, J., Li, Y. & Verkman, A. S. Green fluorescent protein as a noninvasive intracellular pH indicator. *Biophys. J.* **74**, 1591-1599 (1998).

98. Llopis, J., McCaffery, J. M., Miyawaki, A., Farquhar, M. G. & Tsien, R. Y. Measurement of cytosolic, mitochondrial, and Golgi pH in single living cells with green fluorescent proteins. *Proc. Natl. Acad. Sci. U. S. A.* **95**, 6803-6808 (1998).

99. Miesenböck, G., De Angelis, D. A. & Rothman, J. E. Visualizing secretion and synaptic transmission with pH-sensitive green fluorescent proteins. *Nature* **394**, 192-195 (1998).

100. Maeda, Y., Ide, T., Koike, M., Uchiyama, Y. & Kinoshita, T. GPHR is a novel anion channel critical for acidification and functions of the Golgi apparatus. *Nat. Cell Biol.* **10**, 1135-1145 (2008).

101. Tartakoff, A. & Vassalli, P. Comparative studies of intracellular transport of secretory proteins. *J. Cell Biol.* **79**, 694-707 (1978).

102. Presley, J. F., Mayor, S., McGraw, T. E., Dunn, K. W. & Maxfield, F. R. Bafilomycin A1 treatment retards transferrin receptor recycling more than bulk membrane recycling. *J. Biol. Chem.* **272**, 13929-13936 (1997).

103. Paroutis, P., Touret, N. & Grinstein, S. The pH of the secretory pathway: measurement, determinants, and regulation. *Physiology (Bethesda)* **19**, 207-215 (2004).

104. Schindler, R., Itin, C., Zerial, M., Lottspeich, F. & Hauri, H. -. ERGIC-53, a membrane protein of the ER-Golgi intermediate compartment, carries an ER retention motif. *Eur. J. Cell Biol.* **61**, 1-9 (1993).

105. Appenzeller-Herzog, C., Roche, A. -., Nufer, O. & Hauri, H. -. pH-induced Conversion of the Transport Lectin ERGIC-53 Triggers Glycoprotein Release. *J. Biol. Chem.* **279**, 12943-12950 (2004).

106. Thor, F., Gautschi, M., Geiger, R. & Helenius, A. Bulk flow revisited: Transport of a soluble protein in the secretory pathway. *Traffic* **10**, 1819-1830 (2009).

107. Sallese, M., Giannotta, M. & Luini, A. Coordination of the secretory compartments via inter-organelle signalling. *Seminars in Cell and Developmental Biology* **20**, 801-809 (2009).

108. Munro, S. & Pelham, H. R. B. A C-terminal signal prevents secretion of luminal ER proteins. *Cell* **48**, 899-907 (1987).

109. Giannotta, M. *et al*. The KDEL receptor couples to Gaq/11 to activate Src kinases and regulate transport through the Golgi. *EMBO J.* **31**, 2869-2881 (2012).

110. Semenza, J. C., Hardwick, K. G., Dean, N. & Pelham, H. R. B. ERD2, a yeast gene required for the receptor-mediated retrieval of luminal ER proteins from the secretory pathway. *Cell* **61**, 1349-1357 (1990).

111. Wilson, D. W., Lewis, M. J. & Pelham, H. R. B. pH-dependent binding of KDEL to its receptor in vitro. *J. Biol. Chem.* **268**, 7465-7468 (1993).

112. Pulvirenti, T. *et al*. A traffic-activated Golgi-based signalling circuit coordinates the secretory pathway. *Nat. Cell Biol.* **10**, 912-922 (2008).

113. Cancino, J., Capalbo, A. & Luini, A. Golgi-dependent signaling: Self-coordination of membrane trafficking. *Methods in Cell Biology* **118**, 359-382 (2013).

114. Cancino, J., Jung, J. E. & Luini, A. Regulation of Golgi signaling and trafficking by the KDEL receptor. *Histochem. Cell Biol.* **140**, 395-405 (2013).

115. Anelli, T. *et al*. ERp44, a novel endoplasmic reticulum folding assistant of the thioredoxin family. *EMBO J.* **21**, 835-844 (2002).

116. Wang, L. *et al*. Crystal structure of human ERp44 shows a dynamic functional modulation by its carboxy-terminal tail. *EMBO Rep.* **9**, 642-647 (2008).

117. Cortini, M. & Sitia, R. From antibodies to adiponectin: Role of ERp44 in sizing and timing protein secretion. *Diabetes, Obesity and Metabolism* **12**, 39-47 (2010).

118. Otsu, M. *et al*. Dynamic retention of Ero1a and Ero1ß in the endoplasmic reticulum by interactions with PDI and ERp44. *Antioxidants and Redox Signaling* **8**, 274-282 (2006).

119. Fraldi, A. *et al*. Multistep, sequential control of the trafficking and function of the multiple sulfatase deficiency gene product, SUMF1 by PDI, ERGIC-53 and ERp44. *Hum. Mol. Genet.* **17**, 2610-2621 (2008).

120. Mariappan, M., Radhakrishnan, K., Dierks, T., Schmidt, B. & Von Figura, K. ERp44 mediates a thiol-independent retention of formylglycine-generating enzyme in the endoplasmic reticulum. *J. Biol. Chem.* **283**, 6375-6383 (2008).

121. Cortini, M. & Sitia, R. ERp44 and ERGIC-53 synergize in coupling efficiency and fidelity of IgM polymerization and secretion. *Traffic* **11**, 651-659 (2010).

122. Berridge, M. J., Bootman, M. D. & Roderick, H. L. Calcium signalling: Dynamics, homeostasis and remodelling. *Nature Reviews Molecular Cell Biology* **4**, 517-529 (2003).

123. Patterson, R. L., Boehning, D. & Snyder, S. H. Inositol 1,4,5-trisphosphate receptors as signal integrators. *Annual Review of Biochemistry* **73**, 437-465 (2004).

124. Higo, T. *et al*. Subtype-specific and ER lumenal environment-dependent regulation of inositol 1,4,5-trisphosphate receptor type 1 by ERp44. *Cell* **120**, 85-98 (2005).

125. Pan, C. *et al*. ERp44 C160S/C212S mutants regulate IP3R1 channel activity. *Protein and Cell* **2**, 990-996 (2011).

126. Anelli, T. *et al*. Ero1a regulates Ca 2+ fluxes at the endoplasmic reticulum-mitochondria interface (MAM). *Antioxidants and Redox Signaling* **16**, 1077-1087 (2012).

127. Li, G. *et al*. Role of ERO1-a-mediated stimulation of inositol 1,4,5-triphosphate receptor activity in endoplasmic reticulum stress-induced apoptosis. *J. Cell Biol.* **186**, 783-792 (2009).

128. Long, Q. *et al*. Peroxisome proliferator-activated receptor-γ increases adiponectin secretion via transcriptional repression of endoplasmic reticulum chaperone protein ERp44. *Endocrinology* **151**, 3195-3203 (2010).

129. Hada, Y. *et al*. Selective purification and characterization of adiponectin multimer species from human plasma. *Biochem. Biophys. Res. Commun.* **356**, 487-493 (2007).

130. Basu, R. *et al*. Comparison of the effects of pioglitazone and metformin on hepatic and extra-hepatic insulin action in people with type 2 diabetes. *Diabetes* **57**, 24-31 (2008).

131. Shapiro, L. & Scherer, P. E. The crystal structure of a complement-1q family protein suggests an evolutionary link to tumor necrosis factor. *Current Biology* **8**, 335-338 (1998).

132. Schraw, T., Wang, Z. V., Halberg, N., Hawkins, M. & Scherer, P. E. Plasma adiponectin complexes have distinct biochemical characteristics. *Endocrinology* **149**, 2270-2282 (2008).

133. Lippincott-Schwartz, J., Yuan, L. C., Bonifacino, J. S. & Klausner, R. D. Rapid redistribution of Golgi proteins into the ER in cells treated with brefeldin A: evidence for membrane cycling from Golgi to ER. *Cell* **56**, 801-813 (1989).

134. Hamby, S. E. & Hirst, J. D. Prediction of glycosylation sites using random forests. *BMC Bioinformatics* **9** (2008).

135. Steentoft, C. *et al*. Precision mapping of the human O-GalNAc glycoproteome through SimpleCell technology. *EMBO J.* **32**, 1478-1488 (2013).

136. Di Blasio, A. M. *et al*. Basic fibroblast growth factor messenger ribonucleic acid levels in eutopic and ectopic human endometrial stromal cells as assessed by competitive polymerase chain reaction amplification. *Mol. Cell. Endocrinol.* **115**, 169-175 (1995).

137. Hipp, M. S., Park, S. -. & Hartl, F. U. Proteostasis impairment in protein-misfolding and -aggregation diseases. *Trends Cell Biol.* **24**, 506-514 (2014).

138. Simmen, T., Lynes, E. M., Gesson, K. & Thomas, G. Oxidative protein folding in the endoplasmic reticulum: tight links to the mitochondria-associated membrane (MAM). *Biochim. Biophys. Acta* **1798**, 1465-1473 (2010).

139. Ronzoni, R. *et al*. Pathogenesis of ER storage disorders: Modulating russell body biogenesis by altering proximal and distal quality control. *Traffic* **11**, 947-957 (2010).

140. Qiang, L., Wang, H. & Farmer, S. R. Adiponectin secretion is regulated by SIRT1 and the endoplasmic reticulum oxidoreductase Ero1-La. *Mol. Cell. Biol.* **27**, 4698-4707 (2007).

141. Cha, J., Sun, X. & Dey, S. K. Mechanisms of implantation: Strategies for successful pregnancy. *Nat. Med.* **18**, 1754-1767 (2012).

142. Lim, H. *et al*. Cyclo-oxygenase-2-derived prostacyclin mediates embryo implantation in the mouse via PPARd. *Genes and Development* **13**, 1561-1574 (1999).

143. Wang, H. *et al*. Stage-specific integration of maternal and embryonic peroxisome proliferator-activated receptor d signaling is critical to pregnancy success. *J. Biol. Chem.* **282**, 37770-37782 (2007).

144. Li, Y. *et al*. Molecular recognition of nitrated fatty acids by PPARγ. *Nature Structural and Molecular Biology* **15**, 865-867 (2008).

145. Pagani, M., Pilati, S., Bertoli, G., Valsasina, B. & Sitia, R. The C-terminal domain of yeast Ero1p mediates membrane localization and is essential for function. *FEBS Lett.* **508**, 117-120 (2001).

146. Swiatkowska, M. *et al*. Ero1a is expressed on blood platelets in association with protein-disulfide isomerase and contributes to redox-controlled remodeling of aIIbß3. *J. Biol. Chem.* **285**, 29874-29883 (2010).

147. Zito, E. *et al*. Sulfatase modifying factor 1 trafficking through the cells: From endoplasmic reticulum to the endoplasmic reticulum. *EMBO J.* **26**, 2443-2453 (2007).

148. Mossuto, M. F. *et al*. A dynamic study of protein secretion and aggregation in the secretory pathway. *PLoS One* **9**, e108496 (2014).

149. Holbrook, L. -. *et al*. Platelets release novel thiol isomerase enzymes which are recruited to the cell surface following activation. *Br. J. Haematol.* **148**, 627-637 (2010).

150. Furie, B. & Flaumenhaft, R. Thiol isomerases in thrombus formation. *Circ. Res.* **114**, 1162-1173 (2014).

151. Cho, J., Furie, B. C., Coughlin, S. R. & Furie, B. A critical role for extracellular protein disulfide isomerase during thrombus formation in mice. *J. Clin. Invest.* **118**, 1123-1131 (2008).

152. Jasuja, R., Furie, B. & Furie, B. C. Endothelium-derived but not platelet-derived protein disulfide isomerase is required for thrombus formation in vivo. *Blood* **116**, 4665-4674 (2010).

153. Mercado, C. P. *et al*. A serotonin-induced N-glycan switch regulates platelet aggregation. *Scientific Reports* **3** (2013).

154. Dale, G. L. *et al*. Stimulated platelets use serotonin to enhance their retention of procoagulant proteins on the cell surface. *Nature* **415**, 175-179 (2002).

155. Dale, G. L. Coated-platelets: An emerging component of the procoagulant response. *Journal of Thrombosis and Haemostasis* **3**, 2185-2192 (2005).

156. Kodali, V. K. & Thorpe, C. Quiescin sulfhydryl oxidase from trypanosoma brucei: Catalytic activity and mechanism of a QSOX family member with a single thioredoxin domain. *Biochemistry* **49**, 2075-2085 (2010).

157. Codding, J. A., Israel, B. A. & Thorpe, C. Protein substrate discrimination in the quiescin sulfhydryl oxidase (QSOX) Family. *Biochemistry* **51**, 4226-4235 (2012).

158. Thorpe, C. *et al*. Sulfhydryl oxidases: Emerging catalysts of protein disulfide bond formation in eukaryotes. *Arch. Biochem. Biophys.* **405**, 1-12 (2002).

159. Rancy, P. C. & Thorpe, C. Oxidative protein folding in vitro: A study of the cooperation between quiescin-sulfhydryl oxidase and protein disulfide isomerase. *Biochemistry* **47**, 12047-12056 (2008).

160. Ilani, T. *et al*. A secreted disulfide catalyst controls extracellular matrix composition and function. *Science* **341**, 74-76 (2013).

161. Zou, Y. *et al*. MiR-101 regulates apoptosis of trophoblast HTR-8/SVneo cells by targeting endoplasmic reticulum (ER) protein 44 during preeclampsia. *J. Hum. Hypertens.* (2014).

Part II:

- A pH-Regulated Quality Control Cycle for Surveillance of Secretory Protein Assembly
- Progressive quality control of secretory proteins in the early secretory compartment by ERp44
- A dynamic study of protein secretion and aggregation in the secretory pathway

Please cite this article in press as: Vavassori et al., A pH-Regulated Quality Control Cycle for Surveillance of Secretory Protein Assembly, Molecular Cell (2013), http://dx.doi.org/10.1016/j.molcel.2013.04.016

Molecular Cell
Article

A pH-Regulated Quality Control Cycle for Surveillance of Secretory Protein Assembly

Stefano Vavassori,[1,2,4,5] Margherita Cortini,[1,2,4,6] Shoji Masui,[3,4,7] Sara Sannino,[1,2,4] Tiziana Anelli,[1,2] Imma R. Caserta,[1] Claudio Fagioli,[1] Maria F. Mossuto,[1] Arianna Fornili,[1,8] Eelco van Anken,[1,2] Massimo Degano,[1] Kenji Inaba,[3,7] and Roberto Sitia[1,2,*]

[1]Divisions of Genetics and Cell Biology and Immunology, Transplantation and Infectious Diseases, San Raffaele Scientific Institute, 20132 Milan, Italy
[2]Università Vita-Salute San Raffaele, 20132 Milan, Italy
[3]Division of Protein Chemistry, Medical Institute of Bioregulation, Kyushu University, Fukuoka 812-8581, Japan
[4]These authors contributed equally to this work
[5]Present address: Département de Biochimie, Université de Lausanne, Epalinges CH-1015, Switzerland
[6]Present address: Department of Life Science, Università of Modena and Reggio Emilia, 42121 Modena, Italy
[7]Present address: Institute of Multidisciplinary Research for Advanced Materials, Tohoku University, Katahira 2-1-1, Aoba-ku, Sendai 980-8577, Japan
[8]Present address: Randall Division of Cell and Molecular Biophysics, King's College, New Hunt's House, London SE1 1UL, UK
*Correspondence: r.sitia@hsr.it
http://dx.doi.org/10.1016/j.molcel.2013.04.016

SUMMARY

To warrant the quality of the secretory proteome, stringent control systems operate at the endoplasmic reticulum (ER)-Golgi interface, preventing the release of nonnative products. Incompletely assembled oligomeric proteins that are deemed correctly folded must rely on additional quality control mechanisms dedicated to proper assembly. Here we unveil how ERp44 cycles between cisGolgi and ER in a pH-regulated manner, patrolling assembly of disulfide-linked oligomers such as IgM and adiponectin. At neutral, ER-equivalent pH, the ERp44 carboxy-terminal tail occludes the substrate-binding site. At the lower pH of the cisGolgi, conformational rearrangements of this peptide, likely involving protonation of ERp44's active cysteine, simultaneously unmask the substrate binding site and −RDEL motif, allowing capture of orphan secretory protein subunits and ER retrieval via KDEL receptors. The ERp44 assembly control cycle couples secretion fidelity and efficiency downstream of the calnexin/calreticulin and BiP-dependent quality control cycles.

INTRODUCTION

Protein folding in the endoplasmic reticulum (ER) is monitored by stringent quality control mechanisms that prevent release of immature or misfolded ER client proteins to travel further along the secretory pathway. Notable examples include the binding-and-release cycles of BiP, recognizing exposed hydrophobic stretches at the surface of nonnative conformers, and of calnexin/calreticulin, which exploit glucosylation status of N-linked glycans on ER client proteins to exert quality control (Ellgaard and Helenius, 2003). ER client proteins are rich in intra- and intermolecular disulfide bonds that are generally essential for their function. Numerous oxidoreductases reside in the ER to catalyze oxidative protein folding (Ellgaard and Ruddock, 2005). Also the process of disulfide bond formation is intimately linked to the quality control systems that prevent nonnative conformers to exit from the ER (Anelli and Sitia, 2008).

The same mechanisms that exert ER quality control on the folding of subunits also monitor certain steps in their oligomeric assembly. For instance, in the case of antibodies, BiP binds the first constant domain (CH1) of Ig heavy chain (H) and thereby retains it in the ER until it is displaced by the Ig light chain (L) to assemble into H_2L_2 structures, called "monomers" in the immunological jargon (Feige et al., 2009; Haas and Wabl, 1983; Hendershot and Sitia, 2005). The assembly process of μ_2L_2 monomers into IgM pentamers—$(\mu_2L_2)_5$J—and hexamers—$(\mu_2L_2)_6$—is favored by ERGIC-53 (Anelli et al., 2007), which resides preferentially in the ER-to-Golgi intermediate compartment (ERGIC) (Schindler et al., 1993).

Interaction of μ_2L_2 monomers with ERGIC-53 occurs upon release by BiP (Anelli et al., 2007), suggesting that these assemblies escape from the grasp of ER quality control and travel to more distal compartments of the early secretory pathway (Cortini and Sitia, 2010). This notion is perhaps not so surprising, as the μ_2L_2 monomers, even if not polymerized, are correctly folded and partially assembled and therefore no longer substrate to the ER chaperoning machinery. The only sign that betrays their unpolymerized state is the free tail-piece cysteine, which in mature IgM polymers is disulfide linked to corresponding cysteine residues in other μ_2L_2 monomers (Sitia et al., 1990). Members of the PDI family of oxidoreductases associate with free cysteines of orphan assembly subunits and thereby facilitate their so-called thiol-mediated retention (Fra et al., 1993; Reddy et al., 1996; Sitia et al., 1990).

We previously identified ERp44 as a PDI family member that covalently binds Ero1 oxidases and facilitates their intracellular localization (Anelli et al., 2002, 2003; Otsu et al., 2006). ERp44

Please cite this article in press as: Vavassori et al., A pH-Regulated Quality Control Cycle for Surveillance of Secretory Protein Assembly, Molecular Cell (2013), http://dx.doi.org/10.1016/j.molcel.2013.04.016

is special for having a single cysteine (C29) in its conserved active site (CRFS), consistent with a dedicated role in thiol-mediated retention not only of Ero1 oxidases but also of orphan subunits of otherwise disulfide-linked oligomers, including IgM (Anelli et al., 2003, 2007) and adiponectin (Qiang et al., 2007; Wang et al., 2007). Moreover, ERp44 localizes predominantly to the ERGIC (Anelli et al., 2007; Gilchrist et al., 2006), unlike other PDI family members, which reside in the ER (Ellgaard and Ruddock, 2005). Still, the C-terminal −RDEL motif of ERp44 allows its capture by KDEL receptors (KDEL-R) in distal stations of the early secretory compartment, presumably for retrieval to the ER (Anelli et al., 2003). It is yet unclear how ERp44 cycles between its predominant localizations in the distal early secretory pathway and the ER, and how such cycling would relate to thiol-mediated retention.

Here we show that the pH gradient between cisGolgi and ER controls association of ERp44 both with its clients and with the KDEL-R. Our results suggest a model in which the simultaneous unmasking of the client and KDEL-R binding interfaces is facilitated by dislocation of the ERp44 C-terminal tail (C-tail), which in turn likely involves protonation state of the active site cysteine (C29) at cisGolgi-equivalent pH. As such, both ERp44 activity and its shuttling between the ER and cisGolgi are pH regulated to drive a quality control cycle dedicated to the surveillance of secretory protein assembly.

RESULTS

pH-Dependent Regulation of ERp44 Activity

ERp44 associates with its client proteins via disulfide linkages to residue C29 in the active site and noncovalent interactions with the surrounding hydrophobic patches at the substrate-binding site (Anelli et al., 2003; Wang et al., 2008). In the ERp44 crystal structure (Wang et al., 2008), however, the substrate binding site is shielded from the solvent by the C-tail that submerges into a groove delimited by the a and b′ domains (see also Figure 4A).

The pH gradient existing in the early secretory pathway (Figure 1A, top panel) regulates ERGIC-53 (Appenzeller-Herzog et al., 2004), a glycoprotein transporter lectin that shares several clients with ERp44, including IgM (Anelli et al., 2007). pH also regulates the in vitro binding of peptides to KDEL-R (Wilson et al., 1993), which prevent ERp44 secretion (Anelli et al., 2003). We thus surmised that the ERp44 structure, obtained from crystals grown at pH 7.5, most likely corresponds to an *off* conformation of the protein, found in the pH-neutral ER. Arrival into the distal, more acidic stations of the early secretory pathway, namely ERGIC and cisGolgi, could entail exposure of the substrate binding site (Figure 1A). We therefore assessed pH-dependent ERp44 C-tail rearrangements in vitro by 1-anilinonaphthalene-8-sulfonate (ANS) binding fluorescence spectroscopy (Serve et al., 2010). Consistent with the exposure of hydrophobic surfaces in ERp44, the ANS fluorescence peak was blue-shifted and enhanced when the pH was lowered from 7.5 to 6.5 (Figure 1B, top panel). This hypsochromic effect was largely abolished for a mutant in which we had engineered a disulfide bond between C29 and the C-tail (T369C, lower panel) to restrict its movements (Wang et al., 2008), unless the engineered disulfide bond was disrupted with the reducing agent DTT (Figure 1B). We concluded that accessibility of ERp44's substrate binding site involves pH-dependent dislocation of the C-tail.

Next, we monitored reactivity of the active site C29 as a function of pH and found that ERp44 bound more polyethylene glycol 2000-modified maleimide (MalPEG) as the pH was lowered from 8.0 to 6.0 (Figure 1C), with 50% MalPEG binding at pH 6.6 (Figure 1C, right panel, red dots). MalPEG binding faithfully reported on C29 reactivity, since its substitution with serine almost abolished binding. The residual binding observed in C29S involved residue C63 (Figure 1C, right panel, turquoise dots), as indicated by the absence of mobility shifts in the double mutant C29S-C63A (Figure 1C). Importantly, MalPEG binding to C29S was not influenced by pH. This finding excludes the possibility that the results obtained with ERp44 WT reflected pH dependence of MalPEG reactivity (Makmura et al., 2001). The T369C mutant did not bind MalPEG, reflecting the constitutive engagement of C29 in a disulfide bond with C369 (Figure 1C; Wang et al., 2008). Taken together, these results indicate that both C29 and the surrounding hydrophobic substrate binding site become more exposed at pH values similar to those encountered downstream of the ER.

C-Tail Rearrangements Determine Accessibility of the –RDEL ER Retrieval Motif

Although the −RDEL motif was not resolved in the crystal structure (Wang et al., 2008), we reasoned that its accessibility would be limited by the adjacent domain a when the C-tail is in a closed conformation, in turn hindering its availability to KDEL-R. Indeed, the "tail-locked" T369C mutant was secreted at levels comparable to a mutant lacking the −RDEL motif (ΔRDEL) (Figure 2, upper panels). Insertion of a spacer peptide (FLAG) immediately upstream of the RDEL tetrapeptide—to let it protrude from the protein—increased retention of the T369C mutant to levels similar to those for ERp44 WT with the FLAG insert (Figure 2 lower panels). The finding that FLAG-tagged ERp44 (whether WT or T369C mutant) was less well retained than "FLAG-less" ERp44 WT may reflect that RDEL recognition by KDEL-R depends in part on its context. Indeed, in ERp44 the sequence upstream of RDEL is remarkably conserved in metazoans (data not shown). In all, these data support the notion that an "open and flexible conformation" of the C-tail increases accessibility of the −RDEL retrieval motif to its cognate receptors.

ERp44 Retains Clients in the Early Secretory Compartment in a pH-Regulated Manner and Thereby Patrols Oligomeric Assembly of Disulfide-Linked Secretory Proteins

Having demonstrated in vitro that accessibility of the ERp44 active site is pH regulated, we set out to analyze pH dependency of ERp44 activity in vivo. To this end, we silenced expression of the Golgi pH regulator (GPHR) (Maeda et al., 2008), which specifically raised the pH in the cisGolgi by $\geq$0.4 units (Figure 3A). In line with our in vitro findings, neutralizing the ER-cisGolgi pH gradient inhibited ERp44 reactivity with its partners/substrates, as is evident from the GPHR silencing-induced decrease of ERp44 being engaged in disulfide-linked complexes (Figure 3B).

Please cite this article in press as: Vavassori et al., A pH-Regulated Quality Control Cycle for Surveillance of Secretory Protein Assembly, Molecular Cell (2013), http://dx.doi.org/10.1016/j.molcel.2013.04.016

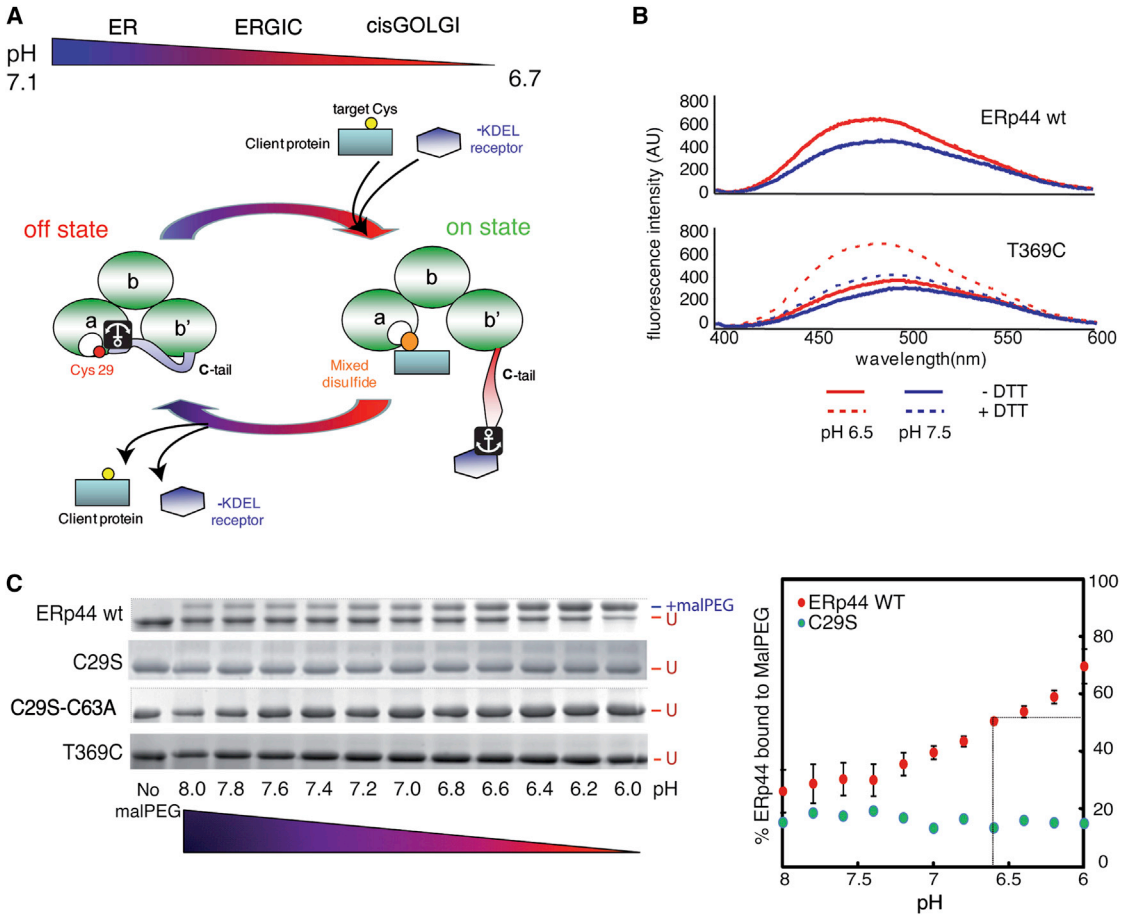

Figure 1. ERp44 Reactivity In Vitro Is pH Dependent

(A) Model for pH-dependent ERp44 quality control cycling. At neutral, ER-equivalent pH, ERp44 is mainly in an *off* conformation, corresponding to the structure resolved in crystals (Wang et al., 2008) with the C-tail closed. The lower pH in the cisGolgi provokes rearrangements of the C-tail that expose the substrate binding site (C29 in yellow and surrounding hydrophobic stretches in white) and −RDEL motif (depicted as an anchor), thus favoring client and KDEL-R binding, respectively. Capture by the KDEL-R engenders retrograde transport to the ER, where ERp44 may release both KDEL-R and client proteins to engage in further rounds of quality control, cycling through the early secretory pathway.

(B) pH-dependent conformational changes of ERp44. ANS fluorescence spectra were measured in the presence of recombinant ERp44 WT or the "tail-locked" T369C mutant in the presence or absence of DTT, at the indicated pH values. Exposure of hydrophobic surfaces correlates with increased and blue-shifted ANS fluorescence.

(C) pH-dependent accessibility of C29 in the substrate binding site. In vitro MalPEG binding causes reduced ERp44 gel mobility and was analyzed at various pH (U = unbound to MalPEG) to determine changes in the accessibility and reactivity of C29. The faint MalPEG-modified band in the C29S mutant is probably due to alkylation of C63, as it is absent in the C29S-C63A double mutant. Also the T369C mutant, in which C29 is bound covalently to C369 in the tail, did not bind MalPEG. At pH 6.6, about 50% of ERp44 WT is bound to MalPEG (see quantification on the right, red dots). Note that MalPEG binding C29S (tourquoise dots) does not change as a function of pH. Data are represented as average of three experiments ±SEM.

Consistently, thiol-mediated retention of ERp44 client proteins was inhibited upon GPHR silencing, as indicated by increased secretion of overexpressed Ero1α (Figures 3C and 3F and see Figure S2 online), adiponectin (APN, Figures 3C and 3F), and IgM assembly intermediates (Figures 3D and 3F).

Intracellular retention of Ero1α is a task that ERp44 shares with PDI, and overexpression of either ERp44 or PDI enhances Ero1α retention (Anelli et al., 2003; Otsu et al., 2006) (Figure 3C and Figure S2B). GPHR silencing strongly subdued this enhanced Ero1α retention when ERp44 was overexpressed, but much less so in the case of PDI overexpression (Figure 3C). Secretion of proteins that are not ERp44 clients, like α1-antitrypsin (α1AT) or a soluble GFP engineered for entry into the secretory pathway (sGFP), was also unaffected by raising the cisGolgi pH (Figures 3E and 3F). We concluded that ERp44-mediated retention in particular relies on the ER-cisGolgi pH gradient. Accordingly, retention of unassembled monomeric Ig-μ chains, which is mediated not by ERp44 but by the chaperone BiP, was pH insensitive (Figures 3D and 3F). Only when the CH1 domain, which is important for BiP binding (Haas and Wabl, 1983; Lee et al., 1999), is deleted (μΔCH1) or engaged in interactions with Ig-L chains (as in $\mu_2\lambda_2$ complexes) does ERp44 become the primary retainer of the Ig-μ chains, and hence their retention becomes pH dependent (Figures 3D and 3F).

Please cite this article in press as: Vavassori et al., A pH-Regulated Quality Control Cycle for Surveillance of Secretory Protein Assembly, Molecular Cell (2013), http://dx.doi.org/10.1016/j.molcel.2013.04.016

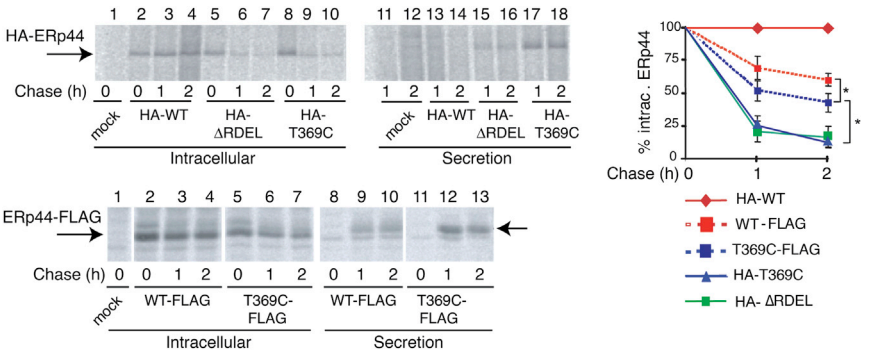

Figure 2. Rearrangements of the C-Tail Expose the –RDEL Motif

HeLa transfectants were pulsed with radiolabeled amino acids and chased in cold medium. At the indicated times, aliquots from the lysates (Intracellular) and supernatants (Secretion) were immunoprecipitated and analyzed by gel electrophoresis. Radiographs of a representative experiment are shown on the left; arrows indicate bands corresponding to overexpressed ERp44; the higher molecular weight of secreted ERp44 reflects posttranslational modifications (see also Anelli et al., 2003, 2007). Intracellular ERp44 levels were quantified from four to six experiments. Mean values and SEM are depicted in the graph shown on the right. Statistical significance was calculated by ANOVA one-way with Bonferroni's post test and indicated by brackets (T369C-FLAG-WT-FLAG, p = 0,041; T369C-T369C-FLAG, p = 0,006). In T369C, formation of a C29-C369 intrachain disulfide limits C-tail movements, likely impeding –RDEL binding to its receptors. Inserting a spacer peptide FLAG tag upstream –RDEL partially restores retrieval. The partial secretion of ERp44 WT upon insertion of a FLAG tag could depend on the acidity of the inserted peptide and/or its binding to the substrate binding site and hence reduced reactivity/accessibility of the –RDEL tetrapeptide.

Retention of sGFP-RDEL was pH insensitive (Figure 3E), as expected for a protein that lacks free cysteines and hence is not an ERp44 client. This finding implies at the same time that KDEL-R function, which is crucial for sGFP-RDEL retention, is not corrupted despite the rise in cisGolgi pH. Likewise, ERp44 was retrieved by KDEL-R despite GPHR silencing (Figure S2B), whereas this treatment allowed secretion of ERp44 client proteins (Figure 3F). Perhaps a partial C-tail opening in distal stations of the secretory pathway, which are less affected by GPHR silencing (Maeda et al., 2008), is sufficient for KDEL-R recognition but not for client binding.

The Reactive Site Cysteine 29 Is a Key Element in pH Regulation of C-Tail Opening and ERp44 Activity

Considering that the conformational changes that facilitate C-tail dislocation are induced by lowering the pH as ERp44 travels to the cisGolgi, we surmised that a protonation event may lie at the basis of the switch between the *on* and *off* conformations of ERp44. To explore this notion, we analyzed the crystal structure of ERp44 with the C-tail in the closed conformation using the program PROPKA3, a state-of-the-art semiempirical method that evaluates pKa values of ionizable residues starting from protein structures (Li et al., 2005; Olsson, 2011; Olsson et al., 2011). The most striking feature that emerged from the PROPKA3 analysis was the downward shift of the pKa of C29. Its predicted value of 7.7 units (Table 1) is significantly lower than the reference value for free cysteine in solution (9.0). This shift is mainly ascribed to the propensity of the neighboring side-chain hydroxyls of S32 and T369 and the main-chain amides of residues F31, S32, and T369 (Table 1 and Figure 4B) to form hydrogen bonds with C29 when in the thiolate form. Likewise, electrostatic interactions with the R98 side chain stabilize the thiolate form of C29 (Table 1). Based on this pKa value, a significant percentage of C29 would be in the thiolate form (41%) at pH 7.5 (Figure 4B and Table 1). Conversely, only 6.5% of C29 was predicted to be in the thiolate form at pH 6.5 (Table 1).

When we removed the β16 strand from the crystal structure in silico, simulating an "open" C-tail conformation of ERp44, the calculated pKa of C29 raised to 7.8 (Table 1). The effect was even more pronounced in sample structures at the end of molecular dynamics simulations of this Δβ16 model. As a consequence of a greater solvent exposure, loss of hydrogen bonding to T369, and an increased distance to the side chains of both S32 and R98, C29 had a calculated pKa of 8.7, implying that only a small percentage (6%) of C29 is in the thiolate form at pH 7.5 (Table 1 and Figure 4C).

Based on our in silico analyses, we mutated the residues predicted to affect the pKa of C29 in ERp44. Altering the side-chain groups such that they could no longer contribute to the stabilization of the thiolate form of C29 through hydrogen bonds or electrostatic interactions (S32A, R98Q, or T369A) indeed rendered ERp44 constitutively accessible to MalPEG and abolished the pH sensitivity of the reaction (Figure 4D). Deletion of strand β16 gave similar results (Figure 4D), supporting the notion that the S32A, R98Q, and T369A substitutions similarly led ERp44 to adopt the "open" C-tail conformation.

We then analyzed whether the enhanced accessibility of the ERp44 active site in the various mutants correlated with its affinity toward substrates. In surface plasmon resonance (SPR) assays (Masui et al., 2011), ERp44 WT showed a pH-dependent reactivity toward Ero1α, having a higher affinity for its partner at pH 6.5 than at pH 7.5 (Figure 4E). All the mutations that resulted in constitutive and pH-independent MalPEG binding of ERp44 made it also less pH dependent in SPR assays and increased its affinity for Ero1α (Figure 4E). The effect was weakest for the R98Q mutant, in agreement with the modest contribution of this arginine in stabilizing the thiolate form of C29 (Figure 4C).

In summary, our data indicate that C29, S32, R98, and T369 are components of the ERp44 pH-sensing mechanisms. The predicted pKa of C29 approaches neutral pH due to the interaction of its side chain with the surrounding residues, suggesting that its protonation, when ERp44 encounters the lower pH in the cisGolgi, is a key event for C-tail opening, and, hence, exposure of the substrate binding site.

pH Sensing by ERp44 In Vivo

We then further substantiated our findings on the mechanisms mediating ERp44 pH sensitivity by analyzing the phenotype of

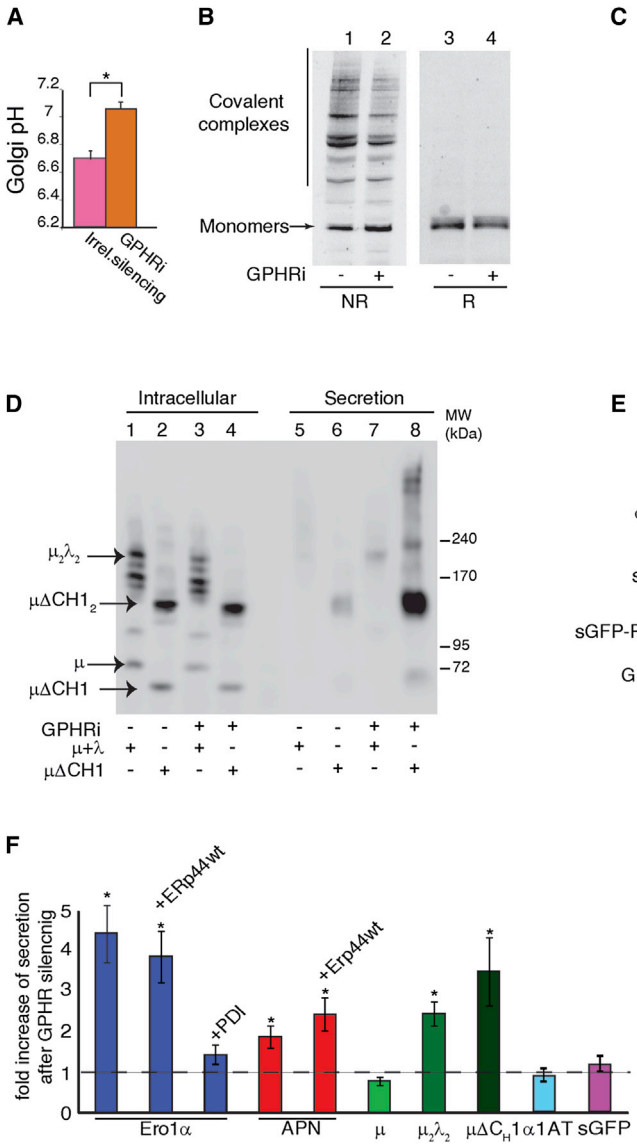

Figure 3. ERp44 Activity In Vivo Depends on the pH Gradient between ER and cisGolgi

(A) GPHR silencing ablates cisGolgi acidification. The pH in the cisGolgi was measured by organelle-targeted GPP130-pHluorins (Miesenböck et al., 1998), in HeLa cells expressing GPHR-specific or irrelevant siRNA, as indicated. Histograms display mean pH values ± SEM. *p = 0.001.

(B) GPHR silencing inhibits the accumulation of covalent complexes at steady state. Lysates of HeLa cells exposed to GPHR-specific (+) or irrelevant (–) siRNA were resolved under nonreducing (NR) or reducing (R) conditions in a 3%–8% acrylamide precasted gradient gel or in a 10% acrylamide gel, respectively. Nitrocellulose was decorated with monoclonal anti-ERp44 antibodies (36C9). As calculated by densitometric quantifications of two similar gels, the amount of ERp44 engaged in covalent complexes decreases by 40% after GPHRi.

(C and D) GPHR silencing specifically inhibits retention of ERp44 clients. Aliquots from lysates (Intracellular) and culture media (Secretion) were collected from HeLa transfectants expressing Ero1α (C, upper and lower panels), adiponectin (APN; C, midpanel), or Ig-μ, μΔCH1, Ig-λ (D), and subjected (+) or not (–) to GPHRi. ERp44 or PDI was coexpressed with Ero1α or adiponectin as indicated (C). (See also Figure S2.) Samples were analyzed under reducing or nonreducing conditions (C and D, respectively) and analyzed by immunoblotting with relevant antibodies. Bands corresponding to μ, μΔCH1, $\mu_2\lambda_2$, and $\mu\Delta CH1_2$ are indicated by arrows in (C).

(E) GPHR silencing does not affect transport of non-ERp44 clients, such as α1-AT or secretory green fluorescent protein extended a C-terminal RDEL peptide (sGFP-RDEL) or not (sGFP). Aliquots of cell lysates (Intracellular) and supernatants (Secretion) were collected and analyzed under reducing conditions.

(F) To compare the effects of GPHR silencing on the transport of the indicated proteins, the levels of intracellular and secreted proteins were quantified by densitometric analyses of four to ten experiments like the ones shown in (C)–(E) and Figure S2B. The percentage of secretion was then calculated relative to the intracellular pools. Histograms show the mean fold of induction upon GPHR silencing relative to cells treated with irrelevant siRNA ± SEM. Statistical significance was calculated using the paired Student's t test for parametric data. Ero1α, p = 0.038; Ero1α + ERp44 WT, p = 0.001; APN, p = 0.033; APN + ERp44 WT, p = 0.012; $\mu_2\lambda_2$, p = 0.004; μΔCH1, p = 0.040.

the above mutants in vivo. In line with the in vitro results, mutation of the residues expected to affect the pKa of C29 (S32, R98, and T369) dramatically increased the tendency of ERp44 to form covalent complexes with client and partner proteins, reaching levels comparable to a mutant lacking the whole β16 strand (see Figure 5A and Figure S3A). This was particularly evident when anti-HA antibodies were used to selectively analyze the behavior of the overexpressed transgenes (Figure S3A). We concluded that the S32A, R98Q, and T369A mutations increased the accessibility of C29 also in vivo, likely reflecting a more "open" conformation of the C-tail. In further support of our model, pH sensitivity of ERp44 activity was lost in all these mutants, since the fraction of molecules covalently bound to client and partner proteins did not decrease upon GPHR silencing in these mutants, as it did instead in ERp44 WT (Figure 5A). In addition, the activity of these mutants in retaining adiponectin was no longer sensitive to basification of the cisGolgi (Figure 5B and Figure S3B). Similar results were obtained also on Ero1α secretion (data not shown). Therefore, pH sensitivity is severely reduced when the critical residues S32, R98, and T369 are mutated and, consequently, the predicted C29 pKa is raised over neutral values.

DISCUSSION

The pH gradient between ER and Golgi may serve multiple roles in the cell, such as calibrating activity of lectins and Golgi

Please cite this article in press as: Vavassori et al., A pH-Regulated Quality Control Cycle for Surveillance of Secretory Protein Assembly, Molecular Cell (2013), http://dx.doi.org/10.1016/j.molcel.2013.04.016

Table 1. Modulation of the pKa of C29 in ERp44 as Predicted by PROPKA3

Structure	pKa	Percentage Thiolate at pH 7.5	Percentage Thiolate at pH 6.5	Desolvation	Side-Chain HB		Backbone HB			Coulombic			
					S32	T369	F31	S32	T369	R30	R98	D64	K77
WT ERp44 Closed	7.66	40.9	6.5	2.09	−0.85	−0.85	−0.46	−0.83	−0.33	–	−0.12	0.01	–
Δβ16	7.84	31.4	4.4	1.06	−0.85	–	−0.46	−0.83	–	–	−0.09	–	–
Δβ16 MD Snapshot	8.7	5.9	0.6	0.71	−0.33	–	−0.04	−0.57	–	−0.03	−0.02	–	−0.02

Deconvolution of the contribution of C29 neighboring residues to the pKa shifts in ERp44. The pKa of residue C29 of the different ERp44 models was predicted using PROPKA3. The percentage of thiolate at a given pH was calculated using the equation $\%[\text{thiolate}] = K_A/([H^+]+K_A)$. The values reported in the Desolvation, Side-Chain HB, Backbone HB, and Coulombic columns are the pKa shifts from the model value in water (9.0) due to the different interactions listed. HB, hydrogen bond.

glycan-modifying enzymes (Paroutis et al., 2004). We have shown here that the pH gradient is exploited also for regulating quality control and secretion of a selection of key proteins. pH-regulated opening of ERp44's tail determines both client capture and KDEL-R-mediated retrieval. Thus, ERp44 governs a pH-regulated protein quality control cycle shuttling between cisGolgi, where ERp44 engages its clients, and the ER, where they must be released and where ERp44's C-tail presumably closes to occlude the client binding active site. Our in vitro MalPEG binding studies reveal a midpoint transition for ERp44 at a pH of approximately 6.6, a value similar to that found in the cisGolgi (Figure 3A). In all likelihood, however, additional mechanisms contribute to the regulation of ERp44 activity in living cells. For instance, interactions with KDEL-R may prevent closing of the C-tail and perhaps provide interaction with additional proteins.

Owing to the fact that the opening of the C-tail is pH dependent, the substrate binding site of ERp44 becomes more accessible progressively from ER to cisGolgi. Client proteins may thus engage ERp44 more proximally or distally along the early secretory pathway, according to their affinity toward the substrate binding site at a given pH. Differences in the pH optimum for ERp44 association may thus account for differences in the intracellular distribution of Ero1α, which is enriched at mitochondrial-associated ER membranes (Anelli et al., 2012; Simmen et al., 2010) and resides overall more distally in the early secretory pathway, as compared to another ERp44 client, SUMF1, which localizes to the more proximal stations (Fraldi et al., 2008).

In the crystal structure of ERp44, the active site C29 is buried at the interface between domain a and the C-tail (Wang et al., 2008). The environment in which C29 resides induces a downward pKa shift of this residue toward neutral values, de facto stabilizing the thiolate form of the amino acid. The negative charge of the deprotonated C29 restrains the C-tail movements via hydrogen bonds to S32 and T369 and electrostatic interactions with R98, which also interacts with the tail backbone. Upon entry of ERp44 into the cisGolgi compartment, C29 protonation likely occurs. This event, in turn, weakens C29 interactions with surrounding residues, as a cysteine with a side-chain thiol is less effective in forming the same hydrogen-bonding and long-range Coulombic interactions that the thiolate can maintain. How C29 of ERp44 reacts with clients to form mixed disulfides and whether ERp44 can act alone or requires assistance for this process deserves further investigation.

In line with our model, silencing of ERp44 causes more abundant secretion of many proteins with one or more exposed reactive cysteine, including Ig-μ (Anelli et al., 2007; Ronzoni et al., 2010), adiponectin (Wang et al., 2007; Qiang et al., 2007), SUMF1 (Fraldi et al., 2008; Mariappan et al., 2008), and peroxiredoxin 4 (T. Kakihana, K. Araki, S.V., I. Shun-ichiro, M.C., C.F., T. Natsume, R.S., and K. Nagata, unpublished data). Similarly, upon neutralization of the Golgi pH, ERp44 substrates like Ero1α, adiponectin, and IgM subunits are secreted more abundantly, presumably because the active site of ERp44 remains largely inaccessible. However, ERp44 itself is efficiently retained intracellularly. This observation suggests that ERp44 could partially open the C-tail, exposing its −RDEL, and interact with KDEL receptors without binding client proteins through an as-yet-unknown mechanism.

ERp44 receives substrates from, and associates with, ERGIC-53 (Anelli et al., 2007), a lectin that also embraces glycoproteins released by the calnexin/calreticulin quality control (Ellgaard and Helenius, 2003). The ERp44-ERGIC-53 tandem may thus integrate thiol-mediated and glycan-trimming-dependent ER quality control cycles. Similarly, we have shown that upon displacement by Ig-L, BiP no longer warrants retention of orphan Ig-H chains but leaves this role to ERp44 instead. ERp44 indeed is strongly upregulated in the course of B cell differentiation (van Anken et al., 2003; Anelli et al., 2007) to help avoid release of incompletely assembled IgM, which would jeopardize the efficiency of the humoral immune response. The ERp44 assembly control cycle thus embodies the last-resort quality control mechanism to prevent the untimely exit from the early secretory compartment of orphan subunits of otherwise disulfide-linked oligomeric secretory proteins.

EXPERIMENTAL PROCEDURES

Constructs

The cDNA encoding human ERp44 without the signal sequence was amplified by PCR and cloned into pET28 vector (from Novagen) at NheI and XhoI sites. The recombinant form of ERp44, which was overproduced in *E. coli*, lacks the −RDEL motif at the C terminus. Vectors for expression of HA-ERp44 in mammalian cells were previously described (Anelli et al., 2002). Mutants were obtained by polymerase chain reaction (PCR) or site-directed mutagenesis (SDM) (Table S1). Human ERp44-FLAG-RDEL was a kind gift of Professor K. Nagata (Kyoto-Sangyo University). The construct encoding the GPP130 pHluorin probe was a kind gift of Dr. J.E. Rothman (Center for High Throughput Cell Biology, Yale University). Plasmids encoding α1AT and adiponectin were kindly provided by Drs. R.N. Sifers (Baylor College of Medicine) and P. Scherer, respectively. pcDNA3.1-sGFP was obtained by appending the signal peptide

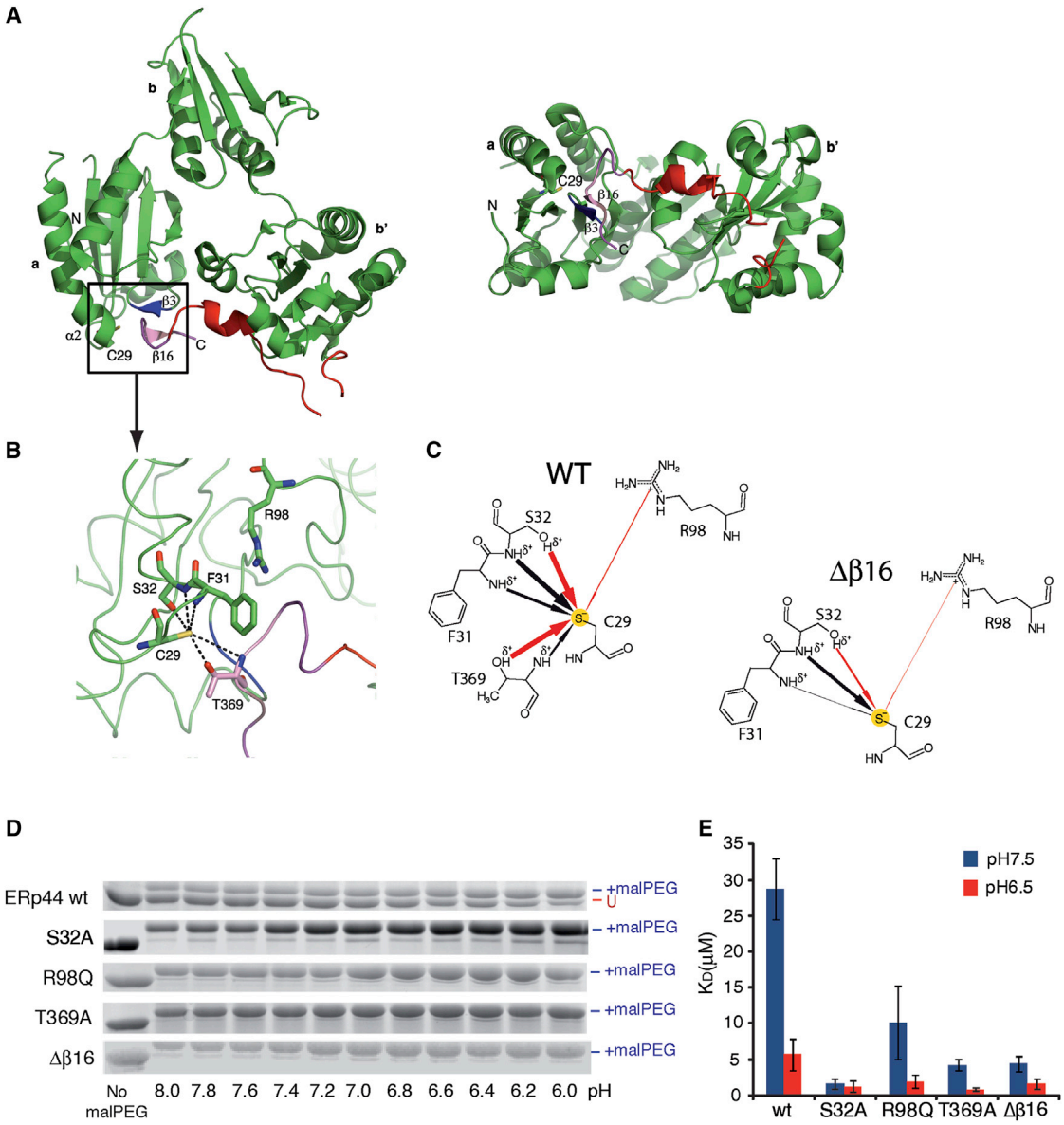

Figure 4. The Environment around C29 of ERp44 Modulates its pH-Dependent Reactivity at Physiological Values

(A) Overall structure of ERp44 (Wang et al., 2008), presented in two views related by a 90° rotation around the horizontal axis. The polypeptide folds into three thioredoxin-like domains (a, b, and b′); β strands are shown as arrows and α helices as ribbons. The C-terminal tail is colored in red, and strands β3 and β16 are colored blue and magenta, respectively. In the ERp44 crystal structure, residues of the β3 strand in domain a establish noncovalent interactions with the β16 strand in the C-tail, acting as a "molecular glue" that keeps the C-tail in the closed conformation.

(B) The panel shows a closer view of the active site C29, at the N-terminal portion of helix α2, highlighting interactions between C29 and neighboring residues shown as a stick models. Hydrogen bonds between polar atoms are shown as dashed lines. The positively charged guanidinium group in the side chain of residue R98 is 7.3 Å from the S_γ of C29.

(C) Two-dimensional diagrams showing the effect of the different interaction between C29 and amino acid residues on the thiol pKa in the crystal structure of ERp44 (top left panel) and in a representative snapshot from molecular dynamics simulations of the Δβ16 mutant (bottom right panel). The arrows represent interactions that decrease the pKa of C29, and their thickness is proportional to the magnitude of the reduction of C29 pKa by each residue shown (see also Table 1). The structural rearrangements following β16 removal greatly reduce the effect of the polar interactions on the thiol acidity. Red arrows indicate the interactions between side chains of each residue with C29 (which we could abolish through mutagenesis), while black arrows indicate interactions of C29 with the protein backbone.

(D) Increased accessibility of C29 in mutants with lower tendency to thiolate formation. The indicated mutants were reacted with MalPEG at different pH and resolved electrophoretically as described in Figure 1C. All the mutants show increased and pH-independent MalPEG reactivity.

(E) pH-dependent binding of ERp44to Ero1α. The K_D of association between recombinant Ero1α and WT or mutant ERp44 was determined by SPR at pH 6.5 and pH 7.5, as indicated. Histograms display the mean of at least four independent experiments ± SEM.

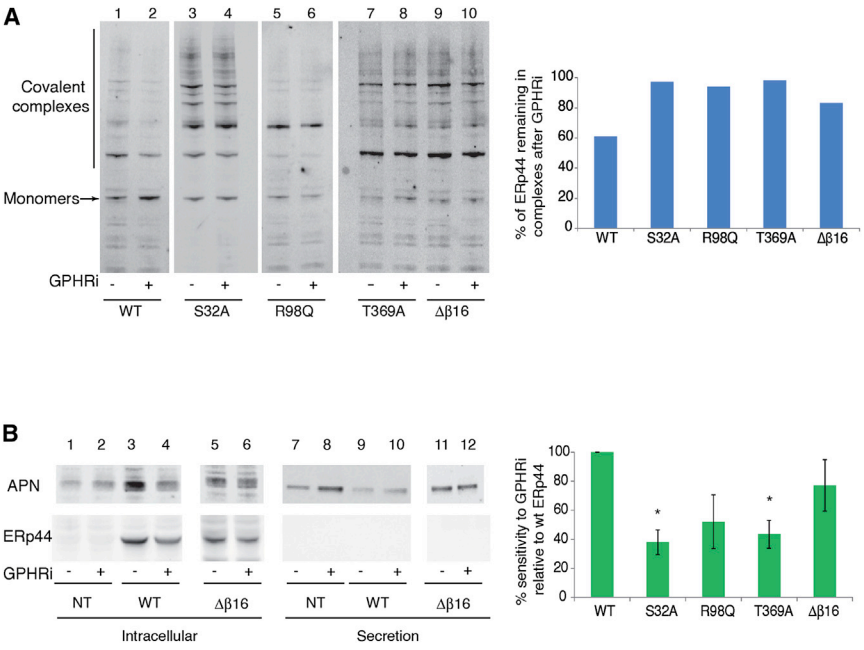

Figure 5. In Vivo Analysis of pH Sensor Mutants

(A) HeLa transfectants expressing the indicated ERp44 mutants were exposed to GPHR-specific (+) or irrelevant (−) oligonucleotides as described in Figure 3. Aliquots were resolved under nonreducing conditions and decorated with anti-ERp44 antibodies (36C9) that recognize also endogenous ERp44 (see also Figure S3A). Sensitivity to pH was calculated according to the formula (complexed ERp44/monomeric ERp44 under GPHRi) / (complexed ERp44/monomeric ERp44 under control conditions) * 100.

(B) HeLa transfectants expressing the indicated ERp44 mutants and adiponectin under GPHRi or control conditions were washed and cultured for 4 hr in fresh medium as also described in Figure S2. Aliquots of the lysates (Intracellular) and supernatants (Secretion) were resolved under reducing conditions and decorated with anti-adiponectin (APN) or anti-HA antibodies, which recognizes only transfected ERp44. One out of three independent experiments is shown for ERp44 WT and mutant Δβ16. Similar experiments were performed with other mutants (see also Figure S3). The graph shows the pH sensitivity of adiponectin retention [(secreted APN / intracellular APN under GPHRi) / (secreted APN / intracellular APN under control conditions) * 100 relative to the value obtained with ERp44 WT]. Data are represented as average of greater than or equal to three experiments ± SEM, and statistical significance was calculated using the Student's t test for parametric data. S32A, p = 0.041; T369A, p = 0.052.

of uromodulin to EGFP. Constructs were fully sequenced before utilization. Plasmids encoding WT and mutated secretory Ig-μ chains (μ_s and μΔCH1) were described in detail previously (Cenci et al., 2006; Mattioli et al., 2006).

Biochemical Techniques

The purification of wild-type and mutant ERp44 and Ero1α was performed as described (Inaba et al., 2010). The association and dissociation rate constants (k_{ON} or k_{OFF}) for the direct binding of ERp44 to immobilized Ero1α were determined by SPR measurements on a BIACORE2000 system (GE, Healthcare), in the presence of 1 mM GSH and 0.25 mM GSSG as described (Inaba et al., 2010). Experiments were replicated at least three times. Hyperactive Ero1α (with cysteines 104, 131, and 166 replaced by Ala) was used in SPR assays to limit variations caused by the autoregulatory mechanisms controlling Ero1α activity (Inaba et al., 2010). ANS fluorescence spectra were recorded in 1 cm cuvettes on a Hitachi F-4500 spectrofluorometer. ERp44 and mutants (5 μM) were mixed with 100 μM ANS in 20 mM Tris-HCl (pH 7.5) or MES (pH 6.5) containing 150 mM NaCl with or without 10 mM DTT and incubated at 293 K for 10 min.

Pulse-Chase, Immunoprecipitation, Western Blotting, and Densitometric Quantification

Cells were starved for 5 min in cysteine and methionine-free DMEM (GIBCO, Invitrogen), pulsed for 10 min with (^{35}S) cysteine and methionine (Easy Tag, Perkin-Elmer), washed twice, and chased for the indicated periods in complete medium. Cell lysates and supernatants were immunoprecipitated with anti-HA or anti-FLAG antibodies and resolved by SDS-PAGE. Fluorograms or western blot images were acquired with the Chemidoc-it Imaging System (UVP, Upland, CA) or with FLA-900 Starion (Fujifilm Life Science, USA) and quantified with Image Quant 5.2 as described (Anelli et al., 2007).

Cell Culture and Reagents

Tissue culture, transfection, and silencing were performed as described previously (Anelli et al., 2007). Fetal calf serum and cell culture medium were from GIBCO, Invitrogen. Unless otherwise indicated, chemicals were from Sigma. Polyclonal anti-mouse μ and anti-ERp44 (B68) antibodies were purchased from PRIMM srl (Milano, Italy). Rabbit polyclonal anti-adiponectin antibody was a kind gift of Dr. P. Scherer (University of Texas Southwestern Medical Center). Monoclonal anti-GFP (clones 7.1 and 13.1) was purchased from Roche (USA) and polyclonal anti-α1 antitrypsin (NCL A1Ap) from Novocastra. Monoclonal anti-ERp44 antibody (36C9) was previously described (Anelli et al., 2007). Goat anti-mouse μ and λ were from Southern Biotechnology Associates, Inc. Goat anti-mouse Ig and anti-rabbit Ig horse-radish peroxidase (HRP) were from Jackson ImmunoResearch Laboratories, Inc. Mouse monoclonal antibodies specific for Myc (9E10), HA (12CA5), and FLAG (M2) were immobilized by crosslinking to protein G and protein A beads, respectively. HRP rabbit anti-mouse IgG (H^+L) was from Dako Cytomation (Glostrup, CO).

Maleimidyl PEG-2K Modification of rERp44 Cys29

Each ERp44 derivative (5 μM) was incubated on ice for 30 min in various pH buffers containing 100 mM sodium phosphate and 150 mM NaCl, followed by incubation with maleimidyl PEG2K (300 μM) for 10 min at room temperature. The reaction was stopped by the addition of 5% trichloroacetic acid, and the protein pellet was washed with acetone and dissolved in buffer containing 50 mM Tris-HCl (pH 7.0) and 1% SDS before loading onto a reducing SDS gel (10%).

Measurement of Golgi pH by pHluorin Probes

HeLa cells expressing pME-Zeo-GPP130-pHluorin (Miesenböck et al., 1998) were cultured on glass-bottomed dishes and analyzed under a TCS SP2 Laser Scanning Confocal (Leica Confocal) equipped with an LD laser 405 (405 nm) and a multiline Ar laser (457, 488, and 515 nm) at room temperature. Data acquisition and analysis of intensity ratios (405 nm; 457 nm) were performed as described (Miesenböck et al., 1998). At least 120 regions of interest were analyzed by fluorescence microscopy. Statistical significance was calculated, comparing between conditions indicated by brackets using the two-tailed Student's t test.

RNAi

Oligonucleotides for RNA interference (Silencer Select predesigned siRNA products) were purchased from Ambion (siRNA ID #s56768). A final

concentration of 20 nM of each oligonucleotide was transfected. Lipofectamine RNAi MAX was from Invitrogen (Carlsbad, USA) and used for silencing in HeLa cells, according to the suppliers' instructions.

In Silico Calculations

We used the PROPKA 3.0 software (http://propka.ki.ku.dk) to predict the pKa value of ERp44 C29 and the role of surrounding amino acids starting from the crystal structure of the entire molecule (Wang et al., 2008; PDB ID code 2R2J) and from in silico models of the Δβ16 mutant. A description of the molecular dynamics simulations is presented in the Supplemental Information.

SUPPLEMENTAL INFORMATION

Supplemental Information includes three figures, one table, Supplemental Experimental Procedures, and Supplemental References and can be found with this article at http://dx.doi.org/10.1016/j.molcel.2013.04.016.

ACKNOWLEDGMENTS

We thank members of our labs for helpful suggestions, Jose Garcia-Manteiga and Alessandro Ambrosi for advice on statistical analyses, and the ALEMBIC Facility and Elena Pasqualetto for technical assistance. This work was supported by grants from Telethon (GGP11077), Associazione Italiana Ricerca Cancro (AIRC, IG10721, and 5 × 1000 SP9965), Fondazione Cariplo (NOBEL), Ministero della Salute, Regione Lombardia (ASTIL) to M.D. and R.S., and the Funding Program for Next Generation World-Leading Researchers from MEXT (to K.I.). S.M. is a research fellow of Japan Society for the Promotion of Science (JSPS). E.v.A. is supported through an Armenise Harvard Career Development Award and AIRC (MFAG13584 AIRC). M.F.M. is supported by a FEBS Fellowship. S.V., M.C., M.D., K.I., and R.S. designed the study and planned most of the experiments. S.V., S.M., and C.F. performed the in vitro experiments. M.C., S.S., T.A., and I.R.C. performed the in vivo experiments. A.F. and M.D. carried out the structural analysis and in silico studies. E.v.A., M.F.M., M.D., K.I., and R.S. helped in interpreting the results and with M.C. and S.V. played a major role in writing the manuscript.

Received: November 19, 2012
Revised: March 2, 2013
Accepted: April 10, 2013
Published: May 16, 2013

REFERENCES

Anelli, T., and Sitia, R. (2008). Protein quality control in the early secretory pathway. EMBO J. *27*, 315–327.

Anelli, T., Alessio, M., Mezghrani, A., Simmen, T., Talamo, F., Bachi, A., and Sitia, R. (2002). ERp44, a novel endoplasmic reticulum folding assistant of the thioredoxin family. EMBO J. *21*, 835–844.

Anelli, T., Alessio, M., Bachi, A., Bergamelli, L., Bertoli, G., Camerini, S., Mezghrani, A., Ruffato, E., Simmen, T., and Sitia, R. (2003). Thiol-mediated protein retention in the endoplasmic reticulum: the role of ERp44. EMBO J. *22*, 5015–5022.

Anelli, T., Ceppi, S., Bergamelli, L., Cortini, M., Masciarelli, S., Valetti, C., and Sitia, R. (2007). Sequential steps and checkpoints in the early exocytic compartment during secretory IgM biogenesis. EMBO J. *26*, 4177–4188.

Anelli, T., Bergamelli, L., Margittai, E., Rimessi, A., Fagioli, C., Malgaroli, A., Pinton, P., Ripamonti, M., Rizzuto, R., and Sitia, R. (2012). Ero1α regulates Ca(2+) fluxes at the endoplasmic reticulum-mitochondria interface (MAM). Antioxid. Redox Signal. *16*, 1077–1087.

Appenzeller-Herzog, C., Roche, A.C., Nufer, O., and Hauri, H.P. (2004). pH-induced conversion of the transport lectin ERGIC-53 triggers glycoprotein release. J. Biol. Chem. *279*, 12943–12950.

Cenci, S., Mezghrani, A., Cascio, P., Bianchi, G., Cerruti, F., Fra, A., Lelouard, H., Masciarelli, S., Mattioli, L., Oliva, L., et al. (2006). Progressively impaired proteasomal capacity during terminal plasma cell differentiation. EMBO J. *25*, 1104–1113.

Cortini, M., and Sitia, R. (2010). From antibodies to adiponectin: role of ERp44 in sizing and timing protein secretion. Diabetes Obes. Metab. *12*(*Suppl 2*), 39–47.

Ellgaard, L., and Helenius, A. (2003). Quality control in the endoplasmic reticulum. Nat. Rev. Mol. Cell Biol. *4*, 181–191.

Ellgaard, L., and Ruddock, L.W. (2005). The human protein disulphide isomerase family: substrate interactions and functional properties. EMBO Rep. *6*, 28–32.

Feige, M.J., Groscurth, S., Marcinowski, M., Shimizu, Y., Kessler, H., Hendershot, L.M., and Buchner, J. (2009). An unfolded CH1 domain controls the assembly and secretion of IgG antibodies. Mol. Cell *34*, 569–579.

Fra, A.M., Fagioli, C., Finazzi, D., Sitia, R., and Alberini, C.M. (1993). Quality control of ER synthesized proteins: an exposed thiol group as a three-way switch mediating assembly, retention and degradation. EMBO J. *12*, 4755–4761.

Fraldi, A., Zito, E., Annunziata, F., Lombardi, A., Cozzolino, M., Monti, M., Spampanato, C., Ballabio, A., Pucci, P., Sitia, R., and Cosma, M.P. (2008). Multistep, sequential control of the trafficking and function of the multiple sulfatase deficiency gene product, SUMF1 by PDI, ERGIC-53 and ERp44. Hum. Mol. Genet. *17*, 2610–2621.

Gilchrist, A., Au, C.E., Hiding, J., Bell, A.W., Fernandez-Rodriguez, J., Lesimple, S., Nagaya, H., Roy, L., Gosline, S.J., Hallett, M., et al. (2006). Quantitative proteomics analysis of the secretory pathway. Cell *127*, 1265–1281.

Haas, I.G., and Wabl, M. (1983). Immunoglobulin heavy chain binding protein. Nature *306*, 387–389.

Hendershot, L.M., and Sitia, R. (2005). Immunoglobulin assembly and secretion. In Molecular Biology of B Cells, T.A.F. Honjo and M.S. Neuberger, eds. (Amsterdam: Elsevier Acad Press), pp. 261–273.

Inaba, K., Masui, S., Iida, H., Vavassori, S., Sitia, R., and Suzuki, M. (2010). Crystal structures of human Ero1α reveal the mechanisms of regulated and targeted oxidation of PDI. EMBO J. *29*, 3330–3343.

Lee, Y.K., Brewer, J.W., Hellman, R., and Hendershot, L.M. (1999). BiP and immunoglobulin light chain cooperate to control the folding of heavy chain and ensure the fidelity of immunoglobulin assembly. Mol. Biol. Cell *10*, 2209–2219.

Li, H., Robertson, A.D., and Jensen, J.H. (2005). Very fast empirical prediction and rationalization of protein pKa values. Proteins *61*, 704–721.

Maeda, Y., Ide, T., Koike, M., Uchiyama, Y., and Kinoshita, T. (2008). GPHR is a novel anion channel critical for acidification and functions of the Golgi apparatus. Nat. Cell Biol. *10*, 1135–1145.

Makmura, L., Hamann, M., Areopagita, A., Furuta, S., Muñoz, A., and Momand, J. (2001). Development of a sensitive assay to detect reversibly oxidized protein cysteine sulfhydryl groups. Antioxid. Redox Signal. *3*, 1105–1118.

Mariappan, M., Radhakrishnan, K., Dierks, T., Schmidt, B., and von Figura, K. (2008). ERp44 mediates a thiol-independent retention of formylglycine-generating enzyme in the endoplasmic reticulum. J. Biol. Chem. *283*, 6375–6383.

Masui, S., Vavassori, S., Fagioli, C., Sitia, R., and Inaba, K. (2011). Molecular bases of cyclic and specific disulfide interchange between human ERO1alpha protein and protein-disulfide isomerase (PDI). J. Biol. Chem. *286*, 16261–16271.

Mattioli, L., Anelli, T., Fagioli, C., Tacchetti, C., Sitia, R., and Valetti, C. (2006). ER storage diseases: a role for ERGIC-53 in controlling the formation and shape of Russell bodies. J. Cell Sci. *119*, 2532–2541.

Miesenböck, G., De Angelis, D.A., and Rothman, J.E. (1998). Visualizing secretion and synaptic transmission with pH-sensitive green fluorescent proteins. Nature *394*, 192–195.

Olsson, M.H. (2011). Protein electrostatics and pKa blind predictions; contribution from empirical predictions of internal ionizable residues. Proteins *79*, 3333–3345.

Olsson, M.H., Chresten, R., Søndergaard, M., and Jensen, J.H. (2011). PROPKA3: consistent treatment of internal and surface residues in empirical pKa predictions. J. Chem. Theory Comput. *7*, 525–537.

Otsu, M., Bertoli, G., Fagioli, C., Guerini-Rocco, E., Nerini-Molteni, S., Ruffato, E., and Sitia, R. (2006). Dynamic retention of Ero1alpha and Ero1beta in the endoplasmic reticulum by interactions with PDI and ERp44. Antioxid. Redox Signal. *8*, 274–282.

Paroutis, P., Touret, N., and Grinstein, S. (2004). The pH of the secretory pathway: measurement, determinants, and regulation. Physiology (Bethesda) *19*, 207–215.

Qiang, L., Wang, H., and Farmer, S.R. (2007). Adiponectin secretion is regulated by SIRT1 and the endoplasmic reticulum oxidoreductase Ero1-L alpha. Mol. Cell. Biol. *27*, 4698–4707.

Reddy, P., Sparvoli, A., Fagioli, C., Fassina, G., and Sitia, R. (1996). Formation of reversible disulfide bonds with the protein matrix of the endoplasmic reticulum correlates with the retention of unassembled Ig light chains. EMBO J. *15*, 2077–2085.

Ronzoni, R., Anelli, T., Brunati, M., Cortini, M., Fagioli, C., and Sitia, R. (2010). Pathogenesis of ER storage disorders: modulating Russell body biogenesis by altering proximal and distal quality control. Traffic *11*, 947–957.

Schindler, R., Itin, C., Zerial, M., Lottspeich, F., and Hauri, H.P. (1993). ERGIC-53, a membrane protein of the ER-Golgi intermediate compartment, carries an ER retention motif. Eur. J. Cell Biol. *61*, 1–9.

Serve, O., Kamiya, Y., Maeno, A., Nakano, M., Murakami, C., Sasakawa, H., Yamaguchi, Y., Harada, T., Kurimoto, E., Yagi-Utsumi, M., et al. (2010). Redox-dependent domain rearrangement of protein disulfide isomerase coupled with exposure of its substrate-binding hydrophobic surface. J. Mol. Biol. *396*, 361–374.

Simmen, T., Lynes, E.M., Gesson, K., and Thomas, G. (2010). Oxidative protein folding in the endoplasmic reticulum: tight links to the mitochondria-associated membrane (MAM). Biochim. Biophys. Acta *1798*, 1465–1473.

Sitia, R., Neuberger, M., Alberini, C., Bet, P., Fra, A., Valetti, C., Williams, G., and Milstein, C. (1990). Developmental regulation of IgM secretion: the role of the carboxy-terminal cysteine. Cell *60*, 781–790.

van Anken, E., Romijn, E.P., Maggioni, C., Mezghrani, A., Sitia, R., Braakman, I., and Heck, A.J. (2003). Sequential waves of functionally related proteins are expressed when B cells prepare for antibody secretion. Immunity *18*, 243–253.

Wang, Z.V., Schraw, T.D., Kim, J.Y., Khan, T., Rajala, M.W., Follenzi, A., and Scherer, P.E. (2007). Secretion of the adipocyte-specific secretory protein adiponectin critically depends on thiol-mediated protein retention. Mol. Cell. Biol. *27*, 3716–3731.

Wang, L., Wang, L., Vavassori, S., Li, S., Ke, H., Anelli, T., Degano, M., Ronzoni, R., Sitia, R., Sun, F., and Wang, C.C. (2008). Crystal structure of human ERp44 shows a dynamic functional modulation by its carboxy-terminal tail. EMBO Rep. *9*, 642–647.

Wilson, D.W., Lewis, M.J., and Pelham, H.R. (1993). pH-dependent binding of KDEL to its receptor in vitro. J. Biol. Chem. *268*, 7465–7468.

Molecular Cell, Volume *50*

Supplemental Information

A pH-Regulated Quality Control Cycle for Surveillance of Secretory Protein Assembly

Stefano Vavassori, Margherita Cortini, Shoji Masui, Sara Sannino, Tiziana Anelli, Imma R. Caserta, Claudio Fagioli, Maria F. Mossuto, Arianna Fornili, Eelco van Anken, Massimo Degano, Kenji Inaba, and Roberto Sitia

Inventory of Supplemental Information

Supplemental Information provides 3 Supplemental Figures, 1 Supplemental Table, Supplemental Experimental Procedures, and Supplemental References; a brief description is given below.

- Supplemental Figure 1 (S1) provides a schematic representation of all ERp44 mutants used throughout the study.
- Supplemental Figure 2 (S2) shows a schematic representation of the transfection protocol used for the *in vivo* studies and an extended version of Figure 3B.
- Supplemental Figure 3 (S3) provides *in vivo* analysis of pH sensor mutants related to Figure 5. Non reducing gels for ERp44 mutants are shown in panel A while a comparative analysis of adiponectin secretion in the presence of the indicated mutants is shown in panel B.
- Supplemental Table 1 (S1) shows a list of all the primers employed throughout the study to generate ERp44 mutants.
- Supplemental Experimental Procedures provide details on the molecular dynamics simulation described in the main text in the paragraph entitled *"pH-regulation of C-tail opening accounts for ERp44 activity and involves protonation of the active site C29"*.
- Supplemental References are related to the Supplementary Experimental Procedures.

Supplemental Figures and Legends

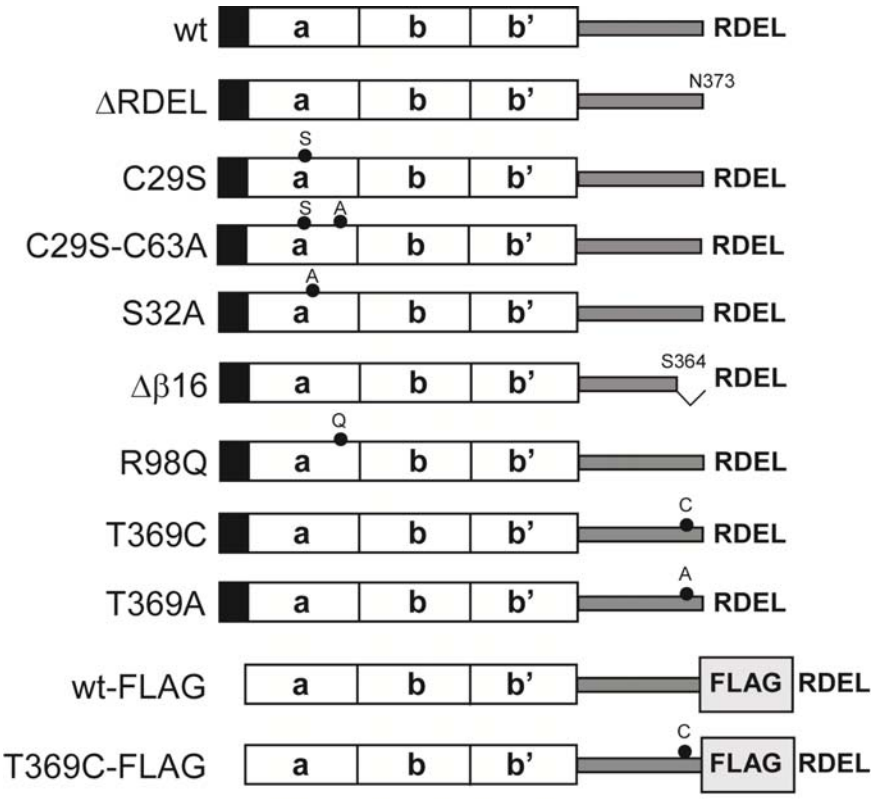

Supplemental Figure 1 (S1): Schematic representation of ERp44 mutants used in this study and related to all main text figures.

The three thioredoxin-like domains **a**, **b**, and **b'** are depicted as white rectangles. The C-tail is shown in grey. The FLAG is boxed in light grey. The C-terminal RDEL retention motif is indicated. The black square at N-terminus represents the HA tag, placed immediately downstream of the signal sequence. All constructs expressed in *E. coli* that were used in *in vitro* studies lack the tag, the N-terminal hydrophobic signal sequence and the C-terminal –RDEL motif. The latter is not resolved in the published crystal structure (PDB code: 2R2J, Wang et al., 2008) suggesting its high flexibility.

Black circles denote residues that were modified to the indicated residues by site directed mutagenesis. The coding sequence was severed at the indicated residues in deletion mutants (not in scale).

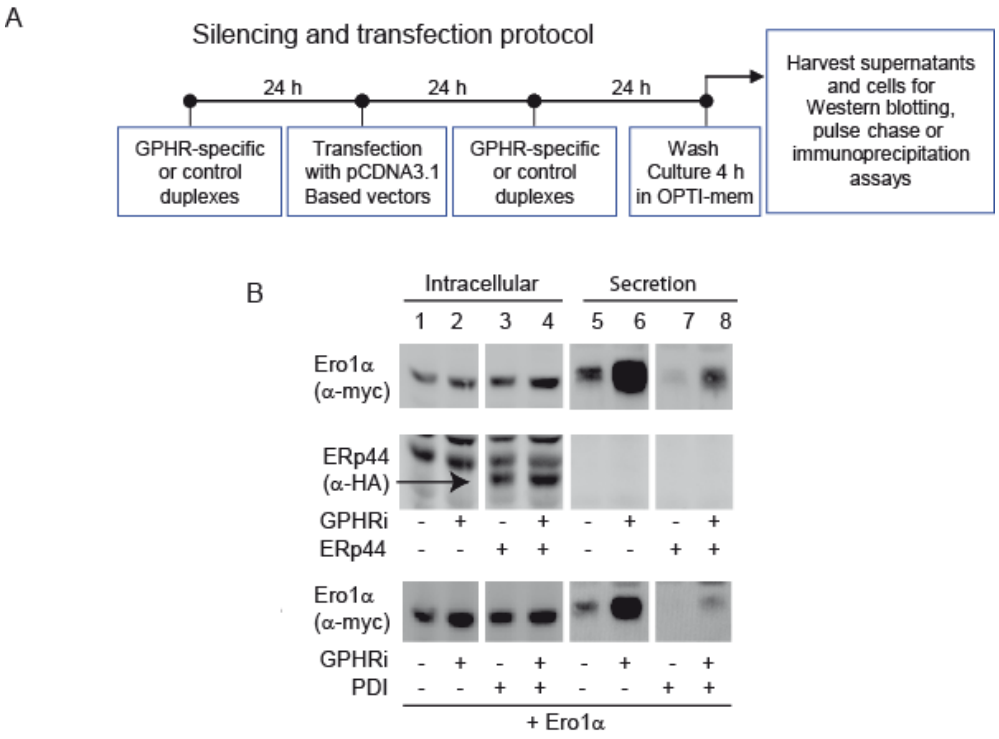

Supplemental Figure 2 (S2): The pH gradient along the early secretory compartment specifically regulates ERp44-mediated protein quality control (see also Figure 3).

A) Scheme of the transfection and silencing experiments shown in panel B and Fig. 3B-E. HeLa cells were silenced with specific or control oligonucleotides 72 and 24 h before analysis. Transfections were performed 48 h before analysis. Efficiency of GPHR silencing routinely exceeded 75%, as determined by mRNA quantification (not shown).

B) ERp44- but not PDI-mediated Ero1α retention is pH sensitive. HeLa transfectants expressing Ero1α alone or in conjunction with ERp44 or PDI were silenced with GPHR-specific or irrelevant siRNA. Lysates (Intracellular) and culture media (Secretion) were analyzed as in Fig. 3. The arrow points at over-expressed HA-tagged ERp44. Upper right panels for Ero1α secretion are identical to those in Fig. 3B. The slight increase in Ero1α secretion in PDI overexpressing cells (lane 8 of lower panel in part B of the Figure) likely reflects a residual role of ERp44 in Ero1α retention (Otsu et al., 2006).

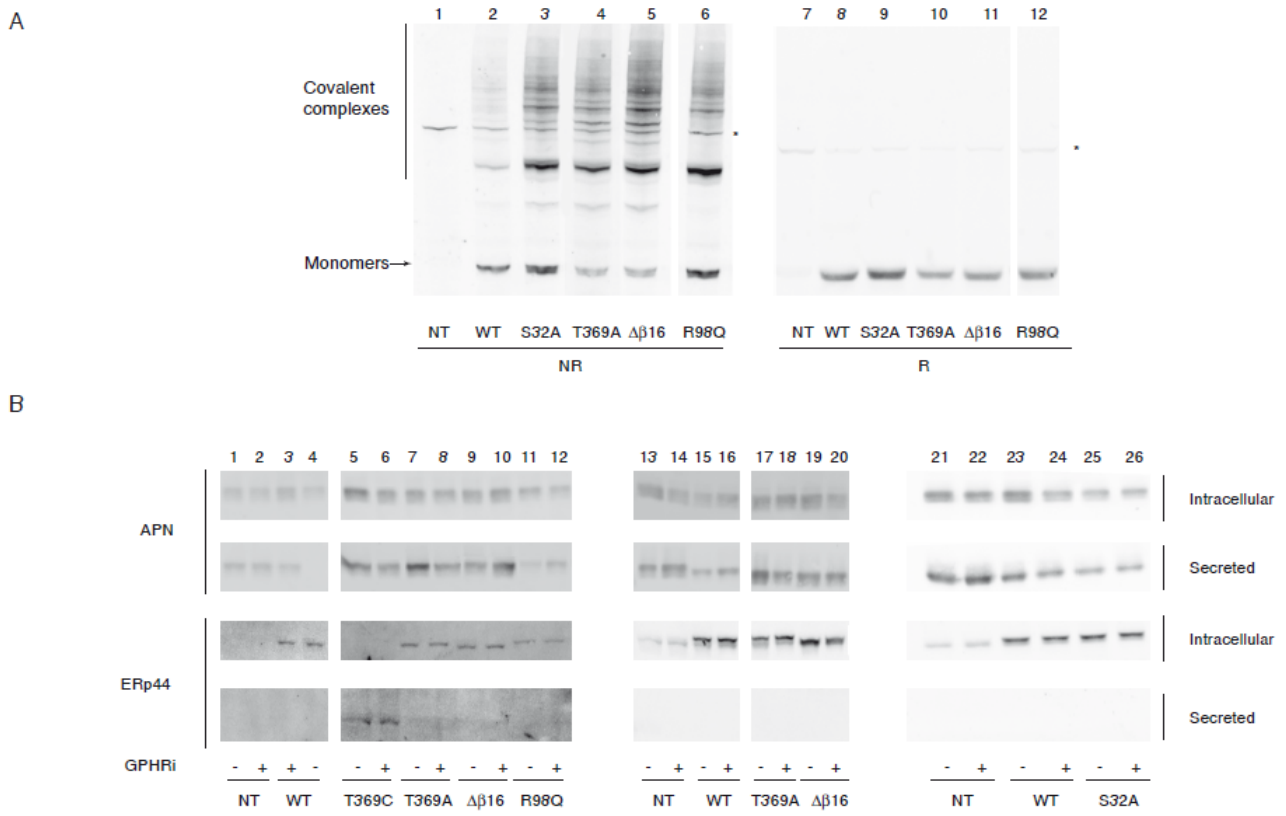

Supplemental Figure 3 (S3), related to figure 5: In vivo analysis of pH sensor mutants.

A) Aliquots of HeLa trasfectants expressing the indicated mutants were resolved under non reducing (NR) and reducing (R) conditions and decorated with anti HA antibody. Arrows indicate over-expressed monomeric ERp44. The * denotes a background band cross-reacting with our antibodies.

B) HeLa trasfectants expressing the indicated ERp44 mutants and adiponectin under GPHRi or control conditions were washed and cultured for 4 hours in fresh medium (see Fig. S2). Aliquots of the lysates (Intracellular) and culture media (Secretion) were resolved under reducing conditions and decorated with anti-adiponectin (APN), anti-HA or anti-ERp44 (36C9) antibodies, as indicated. Representative experiments are shown for different ERp44 mutants (S32A, R98Q, T369A, T369C, Δβ16).

Supplemental Experimental Procedures and Supplemental References

Molecular dynamics simulations

The X-ray structure of ERp44 (PDB code 2R2J) was used to prepare the starting configuration for molecular dynamics (MD) simulations. The Δβ16 structure was generated by deleting the coordinates of the Glu365-Arg372 segment. The missing loop in the **a** domain (Phe50-Glu53) was modelled with the ModLoop server (Fiser et al., 2000). The resulting structure was immersed in a cubic box (~ 97 x 97 x 97 $Å^3$) of ~ 29,000 TIP3P water molecules and 13 Na^+ counterions. Simulations and subsequent analyses were performed with GROMACS 3.3.3., using the ff-amber99sb porting (Sorin and Pande, 2005) of the AMBER parm99SB parameter set (Hornak et al., 2006). Periodic boundary conditions were imposed. The equations of motion were integrated using the leap-frog method with a 1-fs time step. The Berendsen algorithm was employed for temperature (T=300 K) and pressure (p=1 bar) regulation, with coupling constants of 0.1 ps. Bonds to hydrogen atoms were frozen with the LINCS method for the protein and the ligand, while SETTLE was used for water molecules. The Particle Mesh Method was used to calculate electrostatic interactions, with a 11-Å cutoff for the direct space sums, a 1.0-Å FFT grid spacing and a 6-order interpolation polynomial for the reciprocal space sums. For van der Waals interactions, a switching function was used with a double 9-10 Å cut-off. Long-range corrections to the dispersion energy were also included (Shirts et al., 2007). The system was first minimized with 2000 steps of steepest descent. Harmonic positional restraints (with a force constant of ~ 12 kcal/mol/ $Å^2$) were then imposed onto the protein heavy atoms and gradually turned off in 400 ps, while the temperature was increased from 200 to 300 K. The system was then simulated for 5 ns. To assess the reproducibility of the results, two trajectories were generated

for the wild type protein following the same protocol. The Δβ16 protein simulation was prolonged to 10 ns.

	Primers	Template	Plasmid		ERp44
Fw	GCACCCAGTGAATATAGGTATTGTCTATTGAGGGATTAACTCG	pET28 ERp44 wt	PET28	SDM	ERp44 T369C
Rv	CGAGTTAATCCCTCAATAGACAATACCTATATTCACTGGGTGC				
Fw	GTAAATTTTATGCTGACTGGGCTCGTTTCAGTCAGATGTTGC	pET28 ERp44 wt	PET28	SDM	ERp44C29A
Rv	GCAACATCTGACTGAAACGAGCCCAGTCAGCATAAAAATTTAC				
Fw	CACCCAGTGAATATAGGTATTGTCTATTGAGGGATCGAGATG	pCDNA ERp44 wt	pcDNA	SDM	ERp44T369C
Rv	CATCTCGATCCCTCAATAGACAATACCTATATTCACTGGGTG				
Fw	CCCAGCGAGTATAGGTATTGTTTATTGAGGGATCGAG	pEGFP N1	pEGFP N1	SDM	ERp44T369C Flag
Rv	CTCGATCCCTCAATAAACAATACCTATACTCGCTGGG	ERp44-Flag			
Fw	GTAAATTTTATGCTGACTGGGCTCGTTTCAGTCAGATGTTGC	pCDNA ERp44 wt	pcDNA	SDM	ERp44C29A
Rv	GCAACATCTGACTGAAACGAGCCCAGTCAGCATAAAAATTTAC				
Fw	CCTTCCAGAAACTAGCACCCAGTTAATATAGGTATACTCTATTGAGG	pCDNA ERp44 wt	pcDNA	SDM	ERp44Δβ16
Rv	CCTCAATAGAGTATACCTATATTAACTGGGTGCTAGTTTCTGGAAGG				
Fw	CAACTCGAGCGTTACCATGCATCCTGCC	pCDNA ERp44 wt	pcDNA	PCR	ERp44Δβ16
Rv	GCGCGGTACCTTAAAGCTCATCTCGACTGGGTGCTAGTTTCTGGAAG			cloning	
Fw	GAGAATACAGGGGTCAGCAGTCAGTGAAAGCATTGGC	pET28 ERp44 wt	PET28	SDM	ERp44R98Q
Rv	GCCAATGCTTTCACTGACTGCTGACCCCTGTATTCTC				
Fw	GAGAATACAGGGGTCAGCAGTCAGTGAAAGCATTGGC	pCDNA ERp44 wt	pcDNA	SDM	ERp44R98Q
Rv	GCCAATGCTTTCACTGACTGCTGACCCCTGTATTCTC				
Fw	GAAACTAGCACCCAGTGAATATCAGTATACTCTATTGAGGGATCG	pCDNA ERp44 wt	pcDNA	SDM	ERp44R367Q
Rv	CGATCCCTCAATAGAGTATACTGATATTCACTGGGTGCTAGTTTC				
Fw	GCACCCAGTGAATATCAGTATACTCTATTGAGG	pET28 ERp44 wt	PET28	SDM	ERp44R367Q
Rv	CCTCAATAGAGTATACTGATATTCACTGGGTGC				
Fw	TTTGCCAGAGTTGATGCCGATCAGCACTCTGAC	pET28 ERp44	PET28	SDM	ERp44C29A
Rv	GTCAGAGTGCTGATCGGCATCAACTCTGGCAAA	C29A			C63A
Fw	GCTGACTGGTGTCGTTTCGCTCAGATGTTGCATCCAATT	pCDNA ERp44 wt	pcDNA	SDM	ERp44S32A
Rv	AATTGGATGCAACATCTGAGCGAAACGACACCAGTCAGC				

Supplemental Table S1: List of the primers and methods (SDM, side directed mutagenesis; PCR, polymerase chain reaction) employed to generate ERp44 mutants used in all main text figures.

Supplemental References

Fiser, A., Do, R.K., and Sali, A. (2000). Modeling of loops in protein structures. Protein Sci *9*, 1753-1773.

Hornak, V., Abel, R., Okur, A., Strockbine, B., Roitberg, A., and Simmerling, C. (2006). Comparison of multiple Amber force fields and development of improved protein backbone parameters. Proteins *65*, 712-725.

Shirts, M.R., Mobley, D.L., Chodera, J.D., and Pande, V.S. (2007). Accurate and efficient corrections for missing dispersion interactions in molecular simulations. J Phys Chem B *111*, 13052-13063.

Sorin, E.J., and Pande, V.S. (2005). Empirical force-field assessment: The interplay between backbone torsions and noncovalent term scaling. J Comput Chem *26*, 682-690.

© 2014. Published by The Company of Biologists Ltd | Journal of Cell Science (2014) 127, 4260–4269 doi:10.1242/jcs.153239

RESEARCH ARTICLE

Progressive quality control of secretory proteins in the early secretory compartment by ERp44

Sara Sannino[1,2], Tiziana Anelli[1,3], Margherita Cortini[1,*], Shoji Masui[4], Massimo Degano[1,3], Claudio Fagioli[1,3], Kenji Inaba[4] and Roberto Sitia[1,3,‡]

ABSTRACT

ERp44 is a pH-regulated chaperone of the secretory pathway. In the acidic milieu of the Golgi, its C-terminal tail changes conformation, simultaneously exposing the substrate-binding site for cargo capture and the RDEL motif for ER retrieval through interactions with cognate receptors. Protonation of cysteine 29 in the active site allows tail movements *in vitro* and *in vivo*. Here, we show that conserved histidine residues in the C-terminal tail also regulate ERp44 *in vivo*. Mutants lacking these histidine residues retain substrates more efficiently. Surprisingly, they are also O-glycosylated and partially secreted. Co-expression of client proteins prevents secretion of the histidine mutants, forcing tail opening and RDEL accessibility. Client-induced RDEL exposure allows retrieval of proteins from distinct stations along the secretory pathway, as indicated by the changes in O-glycosylation patterns upon overexpression of different partners. The ensuing gradients might help to optimize folding and assembly of different cargoes. Endogenous ERp44 is O-glycosylated and secreted by human primary endometrial cells, suggesting possible pathophysiological roles of these processes.

KEY WORDS: ERp44, Golgi, O-glycosylation, Endoplasmic reticulum, Protein quality control, Protein secretion

INTRODUCTION

ERp44 is a multifunctional chaperone of the PDI-family that regulates Ca^{2+} signaling, redox homeostasis and thiol-dependent protein quality control at the endoplasmic reticulum (ER)–Golgi interface (Anelli et al., 2012; Cortini and Sitia, 2010). ERp44 is key for the retrieval of orphan subunits of disulfide-linked oligomers, like IgM and adiponectin (Anelli et al., 2003; Anelli et al., 2007; Qiang et al., 2007; Wang et al., 2007) and for the intracellular localization of Ero1 oxidases, Sumf1 and peroxiredoxin 4 (Prx4) (Fraldi et al., 2008; Kakihana et al., 2013; Otsu et al., 2006). It associates with its client proteins covalently through cysteine 29 (C29) and non-covalently, likely through the surrounding hydrophobic patches in the substrate-binding site (SBS). In the available crystal structure, the SBS is shielded by a C-terminal tail (C-tail) (Wang et al., 2008). Tail movements simultaneously expose the SBS and the C-terminal RDEL, allowing interaction with the KDEL receptors (KDELR) and, hence, the retrieval to the ER of the chaperone and its client proteins (Anelli et al., 2003; Cortini and Sitia, 2010; Vavassori et al., 2013).

We demonstrated recently that the pH gradient existing along the early secretory compartment (ESC), a term used herein to define the ER, ER–Golgi intermediate compartment (ERGIC) and Golgi complex, regulates C29 protonation and, consequently, ERp44 tail opening (Vavassori et al., 2013). In the closed state, C29 is concealed in the interface between domain-a and the C-tail, forming the hydrogen bonds with the side chains of T369 and S32 and the main chain amides of F31 and S32. At lower pH, however, the hydrogen bonds are significantly weakened, probably due to the protonation of the C29 thiol group, leading to the release of the C-tail. Such pH-dependent conformational change is advantageous in the regulated Golgi to ER transport of client proteins by ERp44. Besides C29, T369 and S32, we also noted that five histidine residues located at the border between the domain-b′ and the C-tail are highly conserved in the ERp44 family proteins (Fig. 1A). To test the possibility that these residues could also contribute in modulating ERp44 activity, we here generated deletion and replacement mutants and analyzed their activity *in vitro* and *in vivo*. Our data reveal a new mechanism controlling the binding of both clients and KDELR by ERp44 at ER–Golgi interface. We also show that O-glycosylated ERp44 can be secreted by certain cell types.

RESULTS

In the available ERp44 crystals, part of the C-tail (residues 332–350) is not resolved due to the lack of electron density (Wang et al., 2008). Two histidine residues at the beginning of this unstructured fragment (332–333) and additional ones in the upstream helices (299, 323 and 328) are highly conserved in ERp44 (Fig. 1A), as are the surrounding sequences. To investigate the potential regulatory role of this histidine-rich region, we first replaced residues 326–350 with a short spacer (SGSG) to generate the ΔHis mutant (see supplementary material Fig. S1A for details) and investigated its *in vitro* reactivity with maleimide modified with polyethylene glycol 2000 (MalPEG) (Fig. 1B) or 1-anilinonaphthalene-8-sulfonate (ANS) (Fig. 1C) as a function of pH. ERp44 contains two unpaired cysteine residues (C29 and C63) and four cysteine residues engaged in structural disulfide bonds (C160–C212 and C272–C289 in domains b and b′, respectively) (Wang et al., 2008). In a preceding study, we found that C29 was the primary residue that reacts with MalPEG, whereas C63 was also modifiable, although with much lower

[1]Divisions of Genetics and Cell Biology and Immunology, Transplantation and Infectious Diseases, IRCCS Ospedale San Raffaele, 20132 Milan, Italy. [2]Department of Bioscience, Università degli Studi di Milano, Via Celoria 26, 20133 Milan, Italy. [3]Università Vita-Salute San Raffaele, 20132 Milan, Italy. [4]Institute of Multidisciplinary Research for Advanced Materials, Tohoku University Katahira 2-1-1, Aoba-ku, Sendai 980-8577, Japan.
*Present address: Department of Life Science, Università of Modena and Reggio Emilia, 41125 Modena, Italy.

‡Author for correspondence (r.sitia@hsr.it)

Received 18 March 2014; Accepted 17 July 2014

Journal of Cell Science

Journal of Cell Science (2014) 127, 4260–4269 doi:10.1242/jcs.153239

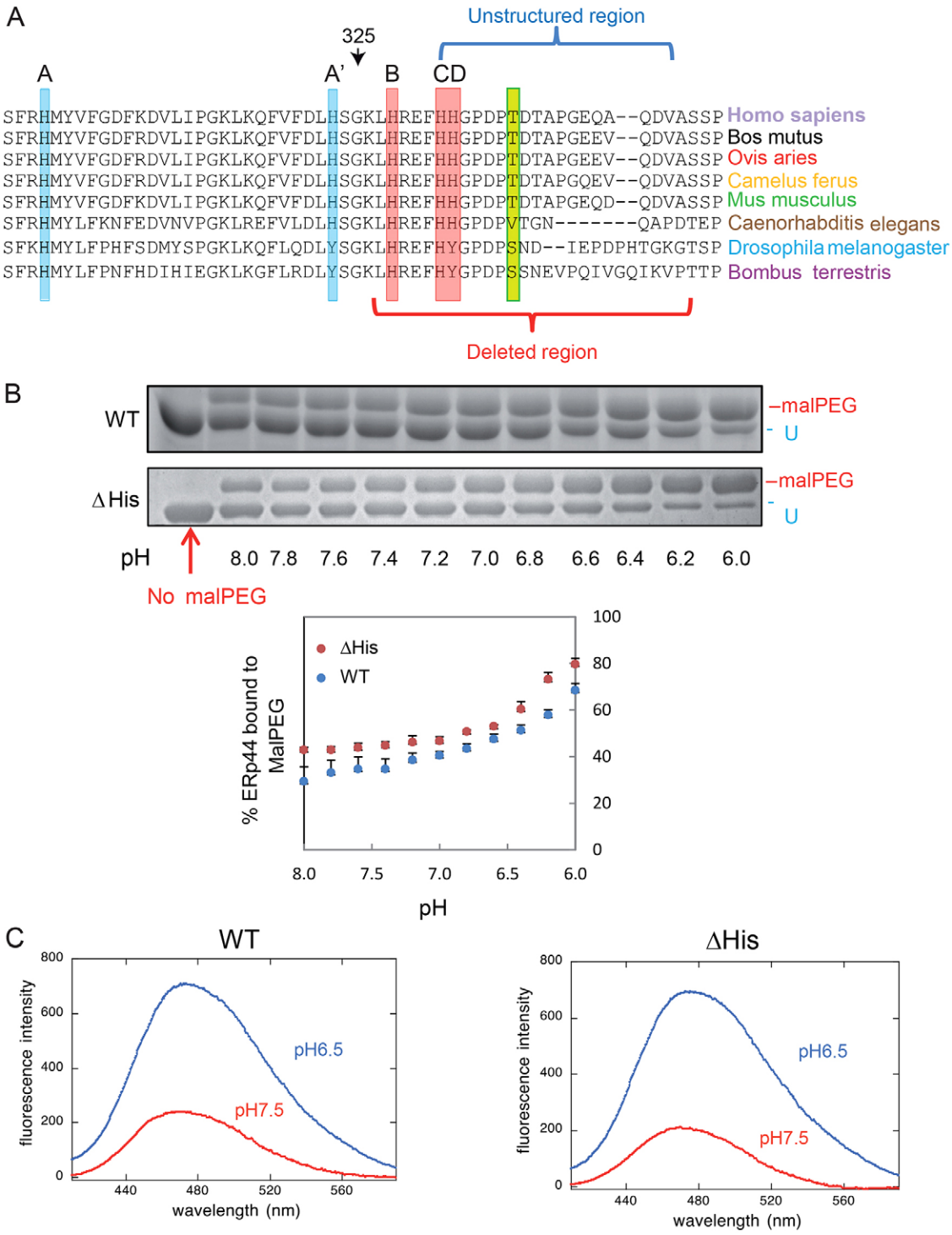

Fig. 1. pH-dependent conformational changes of ERp44 ΔHis *in vitro*. (A) Sequence conservation in the proximal part of the ERp44 C-tail. ClustalW2 alignment of the histidine-rich region and of the first part of the C-terminal tail of ERp44 reveals high sequence conservation in different organisms. Three histidine residues reside in the tail (B, C and D, highlighted here in red) and two in the domain-b′ (A and A′, in pale blue). A, B and C are the most conserved histidine residues, whereas A′ and D are absent in arthropods. The unstructured region in the crystal and the region deleted in the ΔHis mutant are indicated by blue and red brackets. (B) pH-dependent accessibility of ERp44 cysteine 29. Upon in vitro alkylation with MalPEG (10 min at room temperature), ERp44 undergoes an easily detectable mobility shift in SDS-PAGE, indicating the accessibility of C29 to MalPEG (upper two panels) (Vavassori et al., 2013). The percentage of MalPEG-bound ERp44 was plotted as a function of pH (lower panel). Clearly, lowering the pH increases the accessibility of C29 to MalPEG in the ΔHis mutant as well as in wt ERp44. (C) pH-dependent tail movements in wt and ΔHis ERp44 compared by ANS binding *in vitro*. ANS fluorescence spectra were measured for ERp44 wt or ΔHis. The exposure of hydrophobic surfaces correlates with increased and blue-shifted ANS fluorescence (Vavassori et al., 2013). In this assay, ERp44 wt and ΔHis also show similar pH-dependent changes.

Journal of Cell Science (2014) 127, 4260–4269 doi:10.1242/jcs.153239

efficiency (Vavassori et al., 2013). In the ΔHis mutant, the C-tail was still long enough to shield C29 and the surrounding hydrophobic patches at pH>7.0 (Fig. 1B,C). Even after deletion of the His-rich loop, however, more MalPEG was bound to ERp44 and the ANS fluorescence peak was blue-shifted and enhanced upon lowering the pH. These data suggested that *in vitro* C29 and the hydrophobic regions in ΔHis became exposed at pH values encountered in the Golgi (6.5), as we previously demonstrated for wild-type (wt) ERp44 (Vavassori et al., 2013).

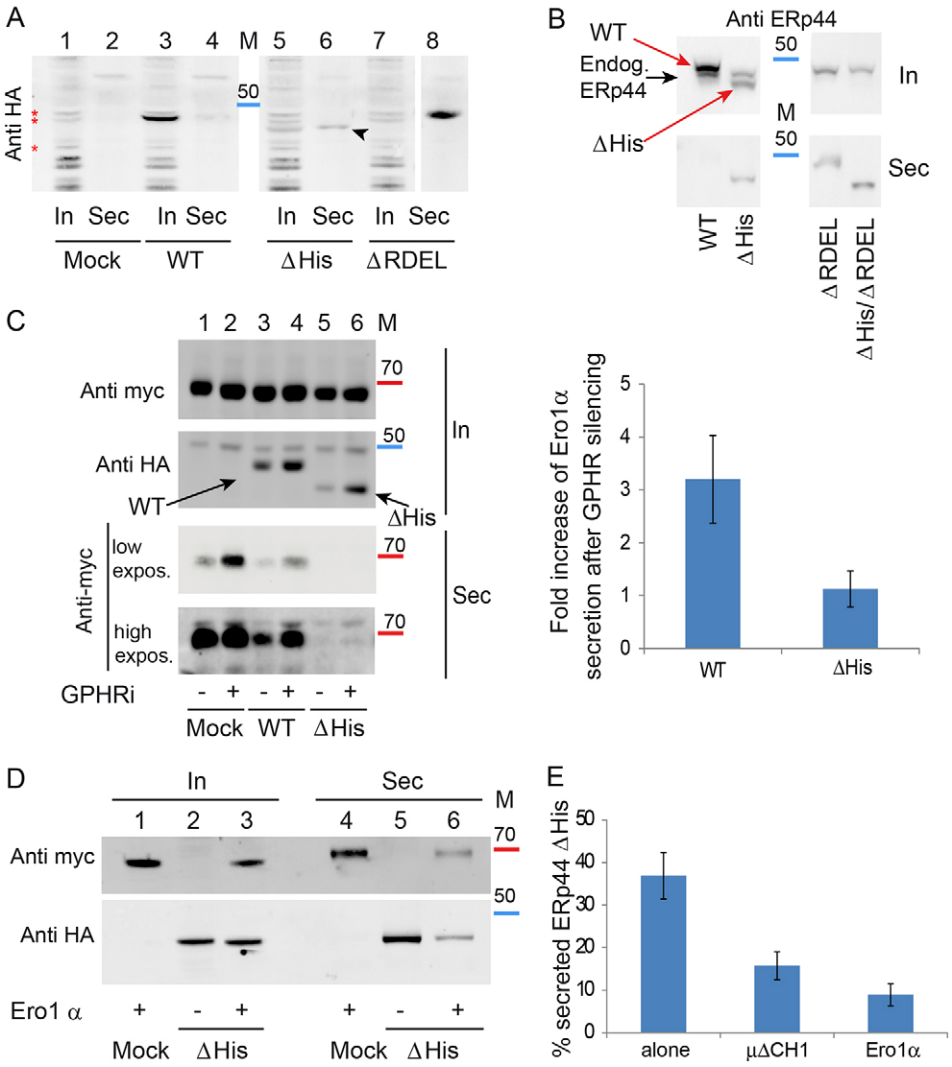

Fig. 2. The histidine-rich loop regulates accessibility of the active site and RDEL motif *in vivo*. (A) ERp44 mutants lacking the histidine-rich loop are secreted. The indicated HeLa transfectants were cultured for 4 h in fresh medium, and aliquots from lysates (In) and supernatants (Sec) analyzed under reducing conditions by western blotting with anti-HA antibodies. The first two lanes (Mock) show cells transfected with an empty plasmid. The arrowhead points at secreted ΔHis ERp44. Red asterisks point at background bands recognized by anti-HA antibodies. Albeit not elegant, these unwanted bands provide good loading controls. In all western blot analyses, molecular mass markers were used (see also Fig. 5): the red and blue bands indicate the migration of the 70- and 50-kDa markers. (B) Residual retention of ERp44 ΔHis is due to KDELR activity. Aliquots from lysates (In) and spent media (Sec) were collected from HeLa transfectants (treated as in A) and analyzed under reducing conditions by western blotting with monoclonal anti-ERp44 antibodies (36C9) that recognize also endogenous ERp44. The black and red arrows point to endogenous and HA-tagged overexpressed ERp44 molecules, respectively. Note that deletion of the C-terminal RDEL allows complete ΔHis secretion, whereas no endogenous ERp44 is detectable extracellularly. (C) ERp44 ΔHis is more efficient in retaining Ero1α in a pH-independent manner. HeLa cells were co-transfected with ERp44 variants and Ero1α as indicated and the pH gradient in the ESC was altered by GPHR silencing (– lanes show cells treated with irrelevant siRNA) as described previously (Vavassori et al., 2013). Aliquots from lysates (In) and culture media (Sec) were collected and analyzed by western blotting using sequential staining of the same filter with anti-HA and anti-Myc antibodies to detect ERp44 or Ero1α, respectively, as indicated. Note that less Ero1 is secreted out of cells expressing the ΔHis mutant, although its intracellular level is lower than that of wt ERp44. A higher exposure of the secreted samples is shown to detect the small amounts of Ero1α secreted out of cells expressing the ΔHis mutant. Intracellular and secreted proteins were quantified by densitometric analyses, and the mean fold of induction of Ero1α secretion upon GPHR silencing calculated relative to controls (right panel). Data represent the mean±s.d. of eight or more experiments like the one shown in the left panel. (D) Client-induced retention of ΔHis. Aliquots of lysates (In) and supernatants (Sec) of the indicated HeLa transfectants were analyzed as above. Note that much less ERp44 ΔHis is secreted in the presence of Ero1α, and vice versa. (E) Secretion of ERp44 ΔHis is inhibited by client proteins (Ero1α and μΔCH1). Secretion of ΔHis in the presence or absence of overexpressed Ero1α or μΔCH1 was analyzed as above. To quantify secretion, we calculated the ratios between the ΔHis bands detected extra- and intra-cellularly after 4 h cultivation in fresh medium. To facilitate the comparison amongst different transfectants, the values obtained for wt ERp44 and ΔRDEL were arbitrarily set at zero and 100, respectively. Histograms show the mean±s.d. for three or more experiments.

Journal of Cell Science (2014) 127, 4260–4269 doi:10.1242/jcs.153239

The histidine-rich loop regulates the accessibility of the active site and RDEL motif *in vivo*

Even though ERp44 ΔHis behaved similarly to wt ERp44 *in vitro*, the mutant did show evident phenotypes *in vivo*. Indeed, ΔHis was partially secreted by HeLa cells (Fig. 2A, lane 6, black arrowhead), suggesting lower RDEL accessibility. Accordingly, the double mutant ΔHis/ΔRDEL was secreted at levels similar to ERp44 ΔRDEL (Fig. 2B). Pulse-chase assays (supplementary material Fig. S2A) confirmed that the ΔHis mutant was secreted by HeLa transfectants, and not degraded to a significant extent. Taken together, these findings indicate that in the absence of the histidine loop the RDEL motif interacts less efficiently with its cognate receptors.

Next, we investigated whether the ΔHis mutant maintained the ability to prevent the secretion of Ero1α. Like Prx4, Ero1α also lacks a KDEL motif and is retained inside cells through interactions with PDI or ERp44 (Kakihana et al., 2013; Otsu et al., 2006). Secretion assays clearly demonstrated that: (i) ΔHis was in part secreted (Fig. 2A), (ii) ΔHis was more efficient than

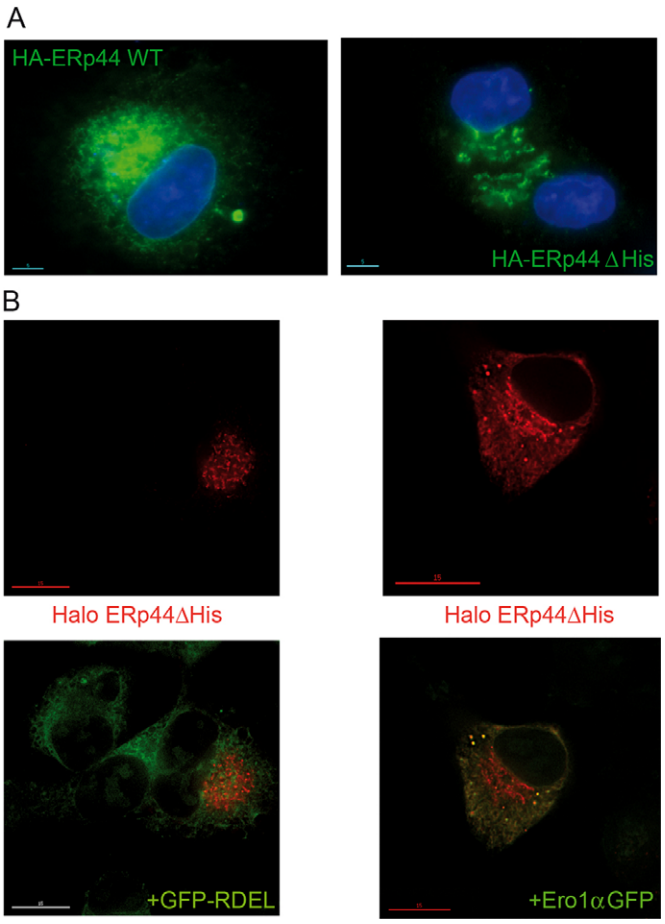

Fig. 3. Deletion of histidine-rich loop favors accumulation of ERp44 in distal ESC stations. (A) Steady-state localization. HepG2 transfectants expressing HA-tagged wt and ΔHis ERp44 were analyzed by immunofluorescence with anti-HA antibody (green). The blue staining (DAPI) was used to detect nuclei. Note that much less green staining is detected in the nuclear membrane or peripheral ER in ΔHis transfectants, as compared to cells expressing wt ERp44. (B) Client-induced relocalisation of ΔHis to the ER. Co-expressing Ero1α–GFP, but not sGFP–RDEL, causes the re-localization of ΔHis in the ER. HepG2 cells were co-transfected with Halo-tagged ERp44 ΔHis and sGFP–RDEL or Ero1α–GFP and then decorated with a Halo ligand (red signal). Clearly, no colocalization is detectable between sGFP–RDEL (green) and ERp44 ΔHis (red), whereas expression of Ero1α–GFP also causes ΔHis to localize in the ER, yielding a reticular yellow staining (bottom right panel). Scale bars: 5 μm (A); 15 μm (B).

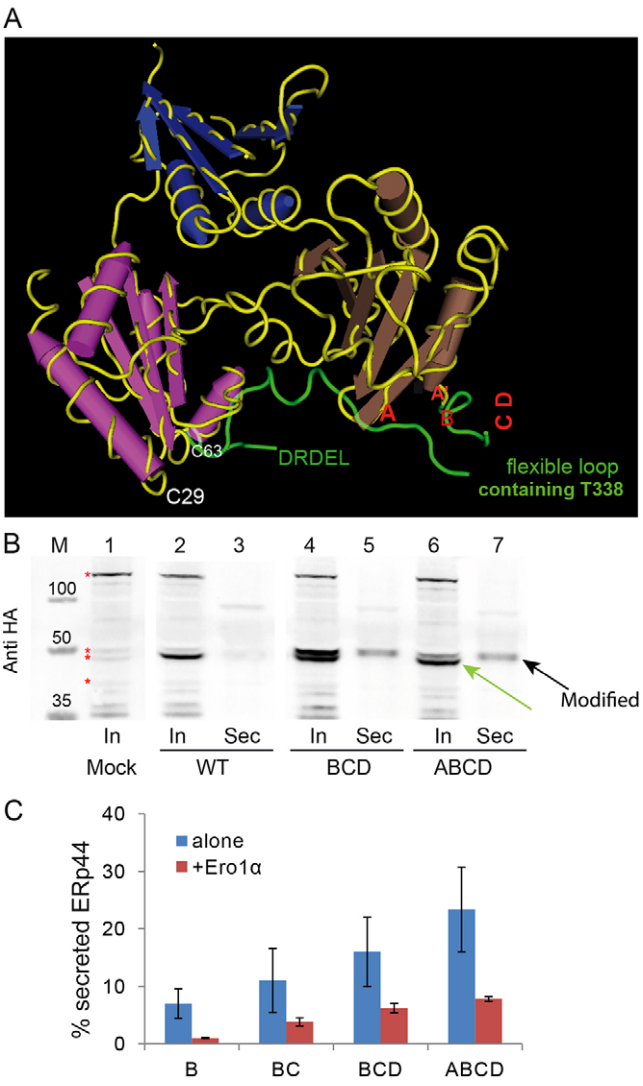

Fig. 4. Replacing conserved histidines causes O-glycosylation and secretion of ERp44. (A) 3D localization of conserved histidine residues. The panel highlights the 3D crystal structure of ERp44 with the C-tail in green. Red letters (A, A′, B, C and D) point at the position of the five histidine residues. Histidine residues C and D are located at the beginning of an unstructured histidine loop (332–350) which, as the five C-terminal DRDEL residues, is not resolved in the crystal. (B) Replacement of histidine residues induces secretion of modified ERp44. Aliquots from lysates (In) and culture media (Sec) were collected from HeLa transfectants expressing the indicated ERp44 variants and blots were stained with anti-HA antibody. Similar experiments were performed for other histidine mutants (data not shown). Note that anti-HA antibodies specifically detect two bands in the lysates of the BCD and ABCD mutants, of which only the upper one is secreted (black arrow). The green arrow points at the only intracellular band recognized in transfectants expressing wt ERp44. Red asterisks point at some background bands recognized by anti-HA antibodies, which provide useful loading controls. (C) His replacement mutants are retrieved more efficiently upon Ero1α co-expression. ERp44 secretion was quantified as described in Fig. 2E in HeLa cells expressing the indicated ERp44 mutants alone or with Ero1α. The histograms show the percentage of secreted ERp44 for the different mutants. The data represent the mean±s.d. of three or more experiments in the presence of Ero1α. Secretion efficiency was calculated as described in legend to Fig. 2E.

Journal of Cell Science (2014) 127, 4260–4269 doi:10.1242/jcs.153239

wt ERp44 in preventing Ero1α secretion (Fig. 2C, lanes 3 and 5), and (iii) paradoxically, the co-expression of a client (Ero1α) inhibited the secretion of the retainer (ΔHis, Fig. 2D, lanes 5 and 6). These findings suggest that client binding could favor RDEL exposure in ΔHis. The 'client-induced retention' of ΔHis was evident upon co-expressing not only Ero1α (Fig. 2E) but also Ig-μΔCH1, another known ERp44 substrate (Anelli et al., 2007; Ronzoni et al., 2010; Vavassori et al., 2013).

To analyze the pH dependency of ΔHis in living cells, we silenced the Golgi pH regulator [GPHR (Maeda et al., 2008)], specifically raising the pH in the Golgi (Vavassori et al., 2013). Owing to the unavailability of anti-GPHR antibodies, the efficiency of silencing was monitored by RT-PCR assays (supplementary material Fig. S2B). As previously observed (Vavassori et al., 2013), neutralizing the ER–Golgi pH gradient allowed Ero1α secretion (Fig. 2C, lanes 1 and 2), as was the case in cells overexpressing wt ERp44 (Fig. 2C, lanes 3 and 4). In contrast, basification of the cis-Golgi did not affect the capability of ΔHis to retain Ero1α (Fig. 2C, lanes 5 and 6).

Thus, deletion of histidine-rich loop allowed secretion of ERp44 unless high-affinity client proteins were co-expressed. At the same time, it increased its ability to retain Ero1α (Fig. 2C) and Ig-μΔCH1 (data not shown) and limited its pH dependency (Fig. 2C). Secreted Ero1α could be detected only upon overexposure of the Western blot, such was the efficiency of ΔHis in retaining the oxidase.

Deletion of histidine-rich loop favours accumulation of ERp44 in distal ESC stations

How could ERp44 ΔHis be so efficient in retaining Ero1α? Endogenous ERp44 is mainly localized in the ERGIC and cis-Golgi, partly owing to interactions with the lectin ERGIC-53 (Anelli et al., 2007). In contrast, overexpressed ERp44 accumulates in the ER (Anelli et al., 2002; Anelli et al., 2003). The ΔHis mutant localized more distally than wt ERp44 when expressed in the secretory HepG2 cell line (Fig. 3A). Organelle fractionation assays confirmed that ΔHis accumulated in the ERGIC and cis-Golgi, a localization that would favor capture of clients destined to be retrieved (data not shown).

Based on the earlier observation that overexpression of high-affinity client proteins prevented secretion of ΔHis, we investigated whether the presence of Ero1α–GFP could alter the subcellular localization of the ΔHis mutant. An ER-resident protein that does not bind ERp44 (sGFP–RDEL) was used as a control (Fig. 3B). Clearly, the co-expression of Ero1α–GFP, but not sGFP–RDEL, caused re-localization of ΔHis into the ER. These data reinforced the notion that interactions with high-affinity clients (e.g. Ero1α) keep the tail of ERp44 in an open conformation, favoring RDEL exposure and KDELR-dependent retrieval of the complex to the ER.

Conserved histidines regulate C-tail movements *in vivo*

Considering their conservation from *Homo sapiens* to *Caenorhabditis elegans* (Fig. 1A), we replaced histidine residues 299, 323, 328, 332 and 333 (called hereafter A, A′, B, C or D, respectively) with alanine residues, singularly or in combinations. The A and A′ residues are part of the domain-b′, whereas residues B, C and D are located in the C-tail (Wang et al., 2008). Histidine residues A, A′ and B are part of structured 3_{10} helices whereas histidine residues C and D reside in a flexible loop (Fig. 4A) and are hence most likely to be exposed to the solvent. A, B and C are conserved throughout evolution. Single mutation of each of them allowed partial secretion. In contrast, replacing the less conserved histidine residues, A′ or D, had little, if any, effect (Table 1; data not shown). Clearly, the more histidine residues were replaced, the more ERp44 was secreted (Fig. 4B,C). Deleting the entire loop had even stronger effects (Fig. 2A). Taken together, these results suggest that in living cells the flexible His-rich loop is important to favor tail movements leading to RDEL exposure in the absence of high-affinity clients. Without this loop, the RDEL motif likely remains less accessible to cognate receptors and as a consequence the mutant is secreted. By contrast, co-expression of Ero1α

Table 1. Phenotypic characterization of ERp44 histidine mutants

	Ero1α retention[a]		ERp44 secretion[b]			
ERp44 variant	Untreated	GPHRi	Alone	Ero1α	O-glyc.	Subcellular localization[c]
WT	++	+	Undetectable	Undetectable	No	ER–ERGIC
ΔRDEL	−	−	100%[c]	100%	Yes	Barely detectable
ΔHis	++++	++++	36%	9%	No	ERGIC–cis-Golgi
A	++	ND	<10%	Undetectable	Yes	ND
A′		ND	<5%	Undetectable	Yes	ND
B	++	ND	<10%	No	Yes	ER–ERGIC
C	ND	ND	<10%	ND	Yes	ER–ERGIC
D	+	ND	<5%	Undetectable	Yes	ER–ERGIC
BC	++	ND	≈10%	<5%	Yes	ERGIC
BD	+	ND	<10%	Undetectable	Yes	ND
CD	+++	++	<10%	Undetectable	Yes	ERGIC
BCD	+++	ND	15–20%	≈5%	Yes	ERGIC–cis-Golgi
A′BCD	+++	ND	≈10%	≈5%	Yes	ND
ABCD	+++	ND	20–25%	<10%	Yes	ERGIC–cis-Golgi

The data summarize the main features of the mutants described in this paper, including the capability of retaining overexpressed Ero1α, and of being secreted in different conditions, and their basal subcellular localization. GPHRi , GPHR-silenced cells; ND, not determined.

[a]Scoring is relative to the mutants with the highest (ΔHis ++++) and lowest (ΔRDEL −) efficiency. The former efficiently retains Ero1 even when expressed at rather low levels (see Fig. 2C).

[b]For ERp44 secretion, scoring is relative to a maximum (100%, ΔRDEL) and a minimum (0%, wt ERp44), which is undetectable in the spent media (4 h) of our HeLa transfectants. Precise values are given only for ΔHis, for which the experiment has been repeated over 10 times.

[c]Subcellular localization was determined by immunofluorescence, based on data like those shown in Fig. 3 and and supplementary material Fig. S3. Owing to its rapid secretion (Anelli et al., 2007), the DRDEL mutant is not easily detectable inside cells unless radioactive pulse-chase assays are utilized (see supplementary material Fig. S2).

Journal of Cell Science (2014) 127, 4260–4269 doi:10.1242/jcs.153239

strongly inhibited secretion of the mutants (Fig. 4C), as described earlier for ΔHis (Fig. 2D). Given that ERp44 is a pH-regulated chaperone, it is not surprising that the histidine residues (whose intrinsic pK_a is near neutral) contained in or immediately upstream the loop contribute to the control of RDEL exposure *in vivo*. In line with their high evolutionary conservation, histidine residues A, B and C appear to be particularly important in regulating tail movements.

Secreted ERp44 is O-glycosylated at threonine 338

Western blotting analyses revealed the presence of two bands in the lysates of the BCD and ABCD mutants, of which only the upper was secreted (Fig. 4B, see arrows). Although ERp44 has no potential N-glycosylation sites, mutants that escaped KDELR-dependent retrieval could undergo O-glycosylation in the Golgi. To ascertain whether this was indeed the case, we treated HeLa transfectants with brefeldin A (BFA), a drug known to induce the retrograde transport of Golgi enzymes to the ER (Lippincott-Schwartz et al., 1989). The electrophoretic mobility of wt and BCD ERp44, but not of ΔHis, was lower after BFA treatment (Fig. 5A, compare lanes 3, 7 and 10). Treatment with O-glycosidase restored faster migration (lane 4) and abolished the doublet observed in the BCD mutant (lane 9), demonstrating that ERp44 can undergo O-glycosylation before being secreted. In contrast, ΔHis ERp44 was not modified in the presence of BFA, indicating that either the target residue was deleted in this mutant or the replacement caused its inaccessibility to O-glycosyl transferases.

Notably, endogenous ERp44 was also modified upon BFA treatment (Fig. 5B, see black arrow). Non-reducing gels revealed that O-linked glycosylation did not prevent ERp44 from forming covalent complexes with its clients (Fig. 5B, see lanes 3 and 4). The fact that most wt ERp44 was not modified in normal conditions implied its retrieval before the modification occurs. *In silico* prediction programs (Hamby and Hirst, 2008; Steentoft et al., 2013) pointed at threonine residues 338 and 340 as possible substrates of O-glycosylation. Both are located within the loop deleted in ΔHis, which would explain why this mutant is not O-glycosylated. Replacing the most conserved one, T338, with alanine in a mutant that was in part secreted and modified (ABCD) was sufficient to prevent the processing (Fig. 5C, lanes 5 and 6). Failure to undergo O-glycosylation did not prevent secretion (Fig. 5D). Thus, ERp44 can be O-glycosylated at T338.

Despite the fact that in the experiment shown in Fig. 4B the BCD and ABCD mutants were secreted at similar levels, more O-glycosylated accumulated intracellularly in the former mutant.

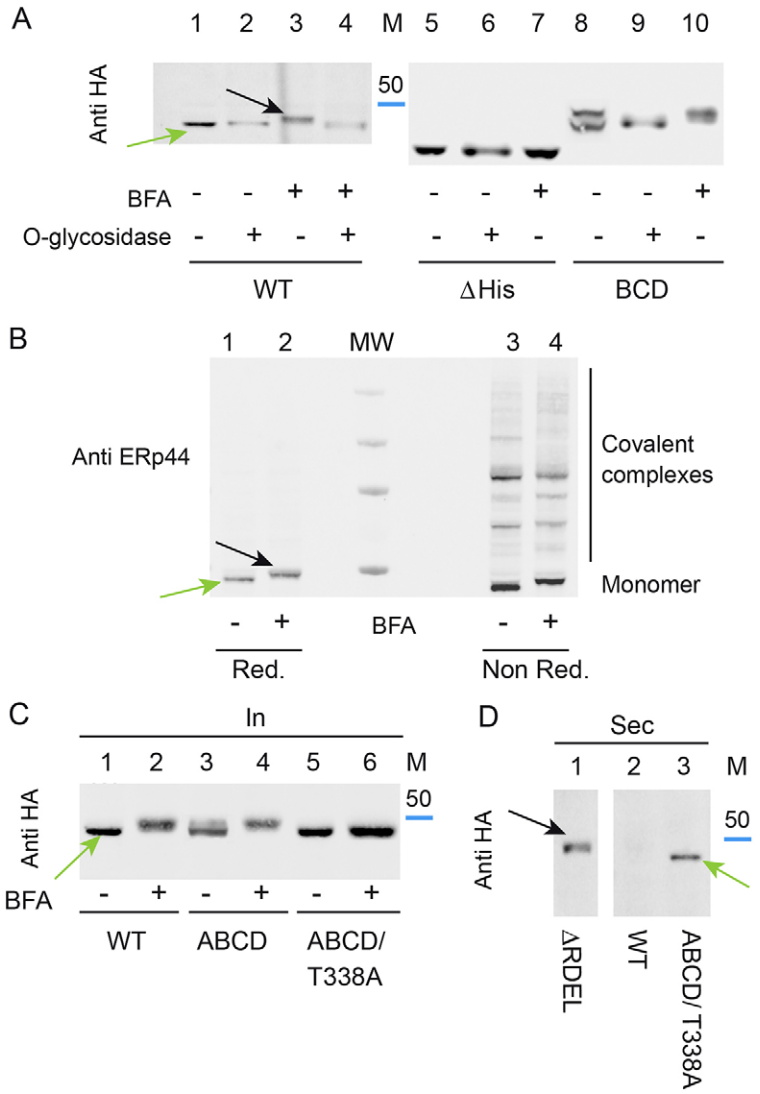

Fig. 5. Mapping client-induced retrieval of His replacement mutants with respect to O-glycosylation. (A) Secreted ERp44 is O-glycosylated. HeLa cells transfected as indicated were treated with (lanes 3, 4, 7, 10) or without brefeldin A (BFA) for 4 h to determine whether retrieval of Golgi enzymes to the ER caused processing of ERp44. Aliquots from the lysates were digested with (lanes 2, 4, 6, 9) or without O-glycosidase (see Materials and Methods), resolved by gel electrophoresis and blots stained with anti-HA antibody. The blue band indicates the migration of the 50-kDa marker. (B) Endogenous ERp44 can also be O-glycosylated and form covalent complexes with client proteins. Untransfected HeLa cells were treated with BFA as above and resolved under reducing (lanes 1–2) and non-reducing (lanes 3–4) conditions before blotting and staining with 36C9 monoclonal anti-ERp44 antibodies. Molecular mass markers (250, 130, 70 and 50 kDa) are shown in the center lane (MW). (C) ERp44 is O-glycosylated on threonine 338. Aliquots from the lysates of the indicated HeLa transfectants treated with or without BFA were analyzed by western blotting with anti-HA antibody. (D) Replacing threonine 338 does not impede secretion of the ABCD mutant. The supernatants of cells transfectants were resolved under reducing conditions and stained with anti-HA antibody. The green arrow points at the secreted product of the T338A. This mutant displays faster mobility than the O-glycosylated ΔRDEL secretory products (black arrow).

Journal of Cell Science (2014) 127, 4260–4269 doi:10.1242/jcs.153239

These findings suggest that BCD could also be more efficiently retrieved from stations downstream the compartment where O-glycosylation takes place. The lower pH of these downstream stations could increase the exposure of RDEL (Vavassori et al., 2013) and/or the activity of KDELR (Wilson et al., 1993).

Exploiting O-glycosylation to map where ERp44 binds its clients

As described in Fig. 2D and Fig. 4C, overexpression of high-affinity ERp44 clients prevented the secretion of histidine mutants, likely increasing RDEL accessibility. The notion that these histidine mutants could be O-glycosylated prompted us to determine whether the binding of different clients occurred before or after the compartment where this modification takes place. Substrates binding before encountering the glycosylating enzymes would increase the lower molecular mass band accumulating in cell lysates, whereas O-glycosylated forms would prevail if the interaction occurred in downstream stations. The ABCD mutant was hence expressed with Ero1α, Prx4, Ig-μΔCH1, adiponectin or Sumf1, and the unmodified:modified band ratios were calculated (Fig. 6A). Clearly, expression of Ero1α and Prx4 favored accumulation of the unglycosylated species. In contrast, Sumf1 induced retrieval of ABCD after it had been processed by O-glycosyl transferases. μΔCH1 and adiponectin had intermediate effects (Fig. 6B). These observations might reflect differences in the binding affinities or pH dependency of the interactions between

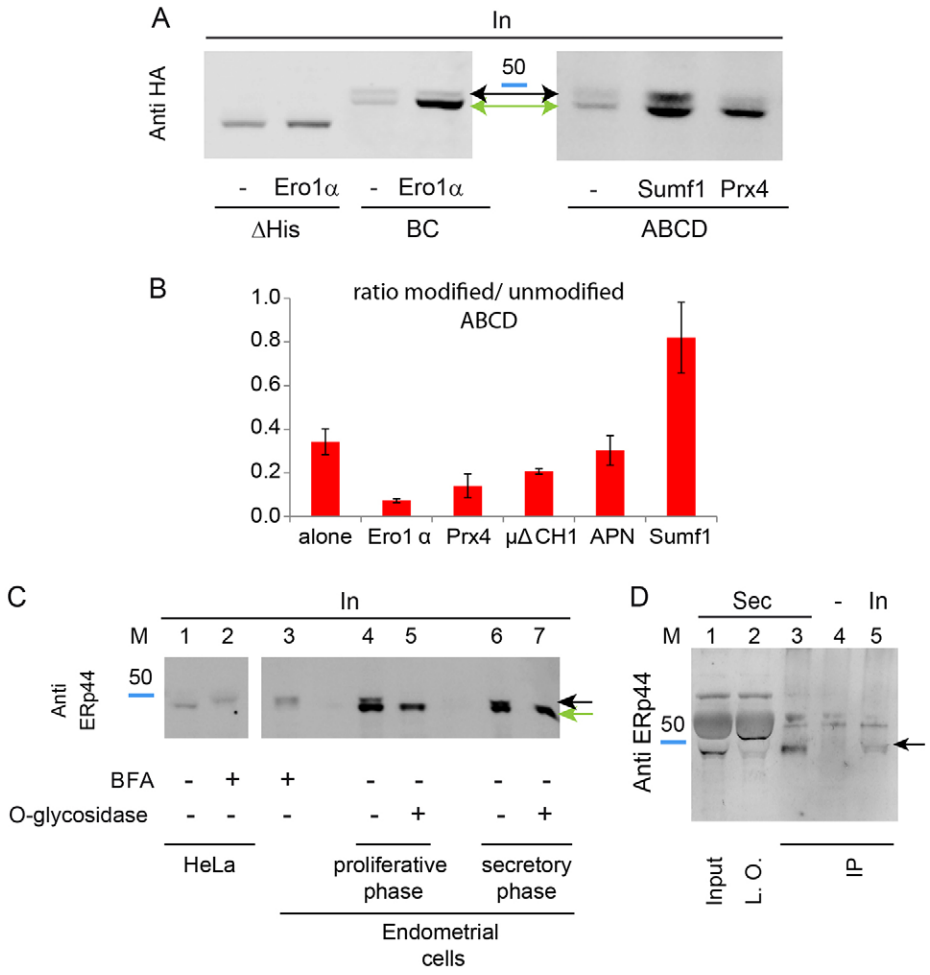

Fig. 6. Client-induced retrieval of ERp44. (A) Sumf1 can also bind ERp44 after O-glycosylation. HeLa cells were co-transfected as indicated. Aliquots from the lysates were then resolved by SDS-PAGE and blots stained with anti-HA. Note the accumulation of non-glycosylated histidine mutants in the lysates of cells co-expressing Ero1α or Prx4. Instead, Sumf1 expression allows significant accumulation of O-glycosylated ABCD ERp44. (B) Sequential client-induced retrieval of ERp44 histidine mutants. The histograms show the ratio between modified and unmodified ABCD ERp44 in the presence of Ero1α, Prx4, Sumf1, Ig-μΔCH1 or adiponectin (APN). Data represent the mean±s.d. of three or more experiments. (C) Endogenous ERp44 is O-glycosylated in primary endometrial cells. Aliquots of the lysates obtained from endometrial cells in their proliferative (lanes 4–5) or secretory (lanes 3, 6–7) phase (Di Blasio et al., 1995) were digested with (lanes 5, 7) or without (lanes 3, 4, 6) O-glycosidase and resolved by gel electrophoresis under reducing conditions. Note that upon digestion, the doublet visible in untreated samples collapses into a single higher mobility band, which comprises un-glycosylated and de-glycosylated ERp44 (green arrow). The black arrow points at the O-glycosylated species, the main form accumulating in HeLa (lane 2) or endometrial (lane 3) cells after treatment with BFA. (D) Endogenous ERp44 is secreted by endometrial stromal cells. Aliquots from the lysates or spent media (48 h) corresponding to 8×10^4 or 7×10^5 endometrial cells in their secretory phase were immunoprecipitated (IP) with the 36C9 monoclonal anti-ERp44 antibody, resolved under reducing conditions and stained with rabbit anti-ERp44 antibody (JDA1). Lanes 1 and 2 show one-third of the spent medium before (Input) or after (L.O., left over) immunoprecipitation. The band migrating above the 50-kDa marker is BSA, which is highly abundant in fetal calf serum. Cross-linked beads were used as a negative control (lane 4). Endogenous ERp44 is clearly detectable in the culture medium and migrates with a molecular mass similar to the O-glycosylated ERp44 species present intracellularly (black arrow).

Journal of Cell Science (2014) 127, 4260–4269 doi:10.1242/jcs.153239

ERp44 and its clients. In addition, other factors, including molecules binding to the histidine-rich region, could regulate the strength and location of the interactions between ERp44 and its clients.

The above data demonstrated that certain ERp44 mutants could be O-glycosylated. To verify the physiological relevance of ERp44 processing, we screened a wide panel of cell lines and tissues (E. Yoboue, T.A., S.S. and R.S., data not shown). ERp44 yielded a doublet band in primary endometrial cells obtained from normal volunteers (Fig. 6C, lanes 4 and 6). The mobility of the upper band (highlighted by a black arrow) is comparable to the one accumulating upon treatment with BFA (lanes 2 and 3). Treatment with O-glycosidase collapsed the doublet into a single band (lanes 5–7, see green arrow), confirming that endogenous ERp44 can undergo O-glycosylation. Notably, the relative abundance of O-glycosylated ERp44 was higher in endometrial cells in the secretory phase than in the proliferative phase (Di Blasio et al., 1995). Processed ERp44 was detected in the spent medium of secretory endometrial cells (Fig. 6D, lanes 1 and 3).

DISCUSSION

To promote productive folding, chaperones must bind and release their clients. Some are regulated by ATP and others by the redox state, whereas ERp44 exploits the pH gradient existing between the ER and the Golgi (Vavassori et al., 2013, and references therein). How does ERp44 sense pH? We show here that highly conserved histidine residues in the ERp44 C-tail provide a second sensing device that acts coordinately with the C29 protonation mechanism previously shown to regulate ERp44 cycling and activity within the ESC (Vavassori et al., 2013).

Deletion or replacement of the key conserved ERp44 histidine residues had notable consequences *in vivo*. In fact, it caused secretion of the histidine mutants by the cells, likely owing to a reduced accessibility of the RDEL motif to KDELR in the Golgi. Accordingly, co-expression of clients that would bind to the SBS and force RDEL exposure restored their retrieval (see Fig. 7). In contrast, deletion or mutation of the conserved histidine residues had marginal effects *in vitro* (Fig. 1A, and our unpublished results), indicating that additional 'histidine-region-binding factors' regulate ERp44 *in vivo* (Fig. 7). Such factors could bind ERp44 in the ER and limit its forward transport, accounting for the enrichment of the histidine mutants in post-ER compartments (Fig. 3). Alternatively, the mutants might be present and/or be activated in distal compartments to assist in tail opening (and consequent RDEL exposure) in the absence of clients. Thus, whereas the C29-based tail regulation is intrinsic to ERp44 and can be revealed *in vitro*, the histidine-dependent mechanisms are evident only *in vivo* as they require additional regulatory elements.

Histidine mutants are more efficient than wt ERp44 in preventing Ero1α secretion. This feature was rather unexpected because they are partly secreted, and might reflect their increased specificity towards Ero1α. Some clients would be more effective than others in competing with the C-tail for the substrate-binding site in the histidine mutants, which likely have a higher kinetic barrier for tail opening. In this context, Ero1 and Prx4 bind to ERp44 mainly before it undergoes O-glycosylation, whereas Sumf1 can also interact afterwards (Fig. 6A,B). These observations suggest that different proteins could be deposited sequentially in the exocytic pathway, depending on their affinity for ERp44 or on the pH dependency of the chaperone–client interaction. Along these lines, it is interesting that most ERp44

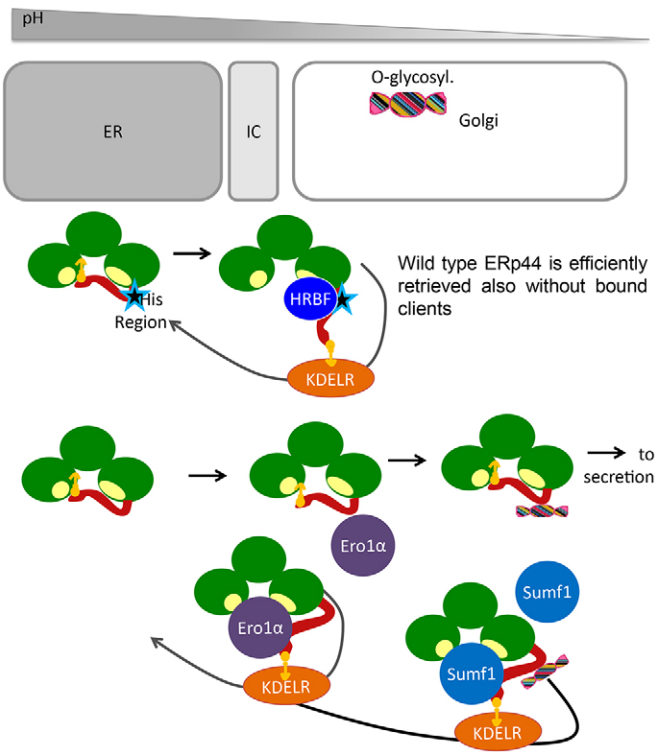

Fig. 7. Schematic model of ERp44 regulation. The lower pH encountered by ERp44 as it proceeds along the early secretory pathway, favors opening of the C-tail and KDELR binding regardless of the presence or absence of high-affinity client proteins. Accordingly, ERp44 mutants that bind few, if any, substrates in cells (e.g. ERp44C29S; Anelli et al., 2003) are not secreted. By contrast, mutants lacking key conserved histidine residues or a loop at the border between the domain-b′ and the tail (star) bind poorly to KDELRs, proceed towards the extracellular space and are O-glycosylated. Client binding induces KDELR-dependent retrieval of histidine mutants before (Ero1, Prx4) or after (Sumf1) O-glycosylation takes place. Given that histidine mutants remain pH sensitive *in vitro*, we hypothesize that histidine-region binding factor(s) (HRBF) favor tail movements *in vivo*, allowing efficient RDEL exposure.

substrates and/or partners that are ER-resident enzymes (Ero1α, Prx4 and Sumf1) lack a C-terminal KDEL sequence and rely on protein–protein interactions for their intracellular localization. Thus, the relative abundance of ERp44 is likely to regulate their localization and activity in and between different cells (Pagani et al., 2001; Swiatkowska et al., 2010; Zito et al., 2007).

Consistent with its many intracellular functions (Cortini and Sitia, 2010), ERp44 is efficiently retained by most of the cell types analyzed. Notably, however, endometrial cells secrete O-glycosylated ERp44 and do so more efficiently in the secretory phase of the menstrual cycle (Fig. 6C,D). These findings also suggest possible role(s) for ERp44 in intercellular dialogues. Accordingly, ERp44 can be released by platelets following activation (Holbrook et al., 2010). It is thus possible that other mechanisms, including pH regulation, regulate the localization of ERp44 and in turn of many of its clients and interactors. Controlling the release of ERp44 might have relevant pathophysiological implications.

MATERIAL AND METHODS

Reagents and cell cultures

Chemicals were from Sigma, unless otherwise indicated. Monoclonal and polyclonal anti-ERp44 antibodies (36C9 and JDA1 respectively),

anti-Myc (9E10) and anti-GM130 were as previously described (Anelli et al., 2002; Anelli et al., 2007). Polyclonal anti-PDI was a kind gift of Ineke Braakman (Utrecht, The Netherlands). Unconjugated goat anti-mouse-Ig antibodies were from Southern Biotechnology Associates, Inc. (Birmingham, AL), and horseradish peroxidase (HRP)-bound goat anti-mouse-Ig and anti-rabbit-Ig were from Jackson ImmunoResearch Laboratories, Inc. Fluorescent goat anti-mouse- and anti-rabbit-IgG (H^+L) conjugated to Alexa Fluor 700, 647, 546 and 488 were from Invitrogen Molecular Probes (Eugene, Oregon, USA).

HeLa and HepG2 cell lines were purchased from the ATCC. Tissue culture, transfection, and silencing were performed as described previously (Anelli et al., 2007). HepG2 cells were transfected by FugeneHD (Promega Corporation, Madison, USA) following the manufacturer's instructions. Primary endometrial cells were collected from healthy donors and cultured as described by Di Blasio at al. (Di Blasio at al., 1995). All women provided informed consent for their clinical data and samples to be used for research purposes. The San Raffaele Hospital Ethical Committee approved the study protocol.

Plasmids and vectors

The cDNA encoding human ERp44 without the signal sequence from pGEX-4T-1-ERp44 and the vector for sGFP–RDEL expression were as previous described (Vavassori et al., 2013). Vectors driving the expression of human ERp44 were as previously described (Anelli et al., 2002). Mutants were obtained by PCR or by site-directed mutagenesis (SDM) using the primers listed in supplementary material Table S1. All the primers were purchased from PRIMM srl (Milano, Italy). Plasmids encoding mutated secretory Ig-μ chains (μΔCH1) were as previously described (Cenci et al., 2006; Mattioli et al., 2006).

Halo ERp44 vector construction

A Halo tag was inserted after the ERp44 leader sequence cleavage site as follows: ERp44 without tags was cleaved from the pcDNA3.1 (−) vector by XhoI and KpnI and inserted in pBlueScript II KS (+). A SgfI site was inserted after the leader sequence cleavage site by PCR (p44sgfI Fw, 5′-CCTGTAACAACTGAAATAGCGATCGCTGAAATAACAAGT-3′ and p44sgfI Rv, 5′-ACTTGTTATTTCAGCGATCGCTATTTCAGTTGTT-ACAGG-3′). The PCR product was then re-inserted into pcDNA 3.1 (−) vector following XhoI and KpnI digestion. In pHTN-HaloTagCMV-neoVector® (Promega Corporation), HaloTag was mutagenized inserting a SgfI site at the N-terminal extremity by PCR (pHTN SgfI Fw, 5′-GCCGCGATCGCTGAAGCAGAAATCGGTAACTGGCTTTCCATTC-3′ and pHTN SgfI Rv: 5′-GGAAGCGATCGCGTTATCGCTCTG-3′). Halo-ERp44 was obtained by ligating SgfI fragments overnight at 16℃, which were then screened by SmaI digestion and validated by sequencing.

Western blotting, densitometric quantifications and biochemical techniques

Fluorograms or western blot images were acquired with the Chemidoc-it Imaging System (UVP, Upland, CA) or with FLA-900 Starion (Fujifilm Life Science, USA) and quantified with Image J as described previously (Anelli et al., 2007).

To assess O-glycosylation, aliquots from HeLa cell lysates were denatured at 95℃ for 10 min in glycoprotein denaturing buffer (New England BioLabs Inc.), digested with neuraminidase and O-glycosidase overnight at 37℃ and analyzed by western blotting with specific antibodies.

As loading controls for western blotting assays, we used Ponceau and/or anti-tubulin antibody staining. In some experiments, some nonspecific bands were present in blots stained with anti-HA antibody (see for instance red asterisks in Figs 2 and 4). Signal intensity was quantified with Image J. The loading of the lanes rarely, if ever, differed more than 5%, with the exception for O-glycosidase treatment where the protein levels were about 20% lower with respect to BFA or untreated samples.

Immunoprecipitation of endogenous ERp44 from primary endometrial cell lysates and spent medium was performed with Sepharose-immobilized 36C9 as previously described (Anelli et al., 2012).

Wild-type and mutant ERp44 were purified and analyzed as described previously (Masui et al., 2011; Vavassori et al., 2013). Briefly, ANS fluorescence spectra were recorded in 1-cm cuvettes on a Hitachi F-2500 spectrofluorometer. ERp44 and mutants (5 μM) were mixed with 100 μM ANS in 20 mM Tris-HCl (pH 7.5) or MES (pH 6.5) containing 150 mM NaCl and incubated at 20℃ for 10 min before measurement.

For maleimidyl PEG-2K modification of ERp44 C29, each ERp44 derivative (5 μM) was incubated on ice for 30 min in various pH buffers containing 100 mM sodium phosphate and 150 mM NaCl, followed by incubation with maleimidyl PEG2K (300 μM) for 10 min at room temperature. The reaction was stopped by the addition of 5% trichloroacetic acid, and the protein pellet was washed with acetone and dissolved in buffer containing 50 mM Tris-HCl (pH 7.0) and 1% SDS before loading onto a reducing SDS gel (10%).

Radioactive pulse-chase assays

Cells were starved for 5 min in cysteine- and methionine-free DMEM (GIBCO, Invitrogen), pulsed for 10 min with [^{35}S]cysteine and [^{35}S]methionine (Easy Tag, Perkin-Elmer), washed twice and chased in complete medium. After the indicated chase times, cells were treated with 10 mM NEM and lysed in RIPA buffer as described previously (Vavassori et al., 2013). Immunoprecipitates were resolved by SDS-PAGE under reducing conditions, transferred onto nitrocellulose and filters visualized by autoradiography with FLA900 Starion (Fujifilm Life Science, Tokyo, Japan).

Immunofluorescence

HepG2 cells were plated on 15-mm glass coverslips and transfected. After 48 h of transfection, cells were fixed in 4% PFA, permeabilized with 0.2% Triton X-100 and stained with different antibodies. For Halo-tagged proteins, cells were incubated overnight with 10 nM TMR Halo ligand (Promega Corporation). Samples were analyzed on an Olympus inverted fluorescence microscope (model IX70) with DeltaVision RT Deconvolution System (Alembic, HSR, Milano). After deconvolution, images were processed with Adobe Photoshop CS4 (Adobe Systems Inc.).

GPHR silencing

Total RNA from untreated and GPHR silenced (GPHRi) HeLa transfectants was extracted with Tryzol from Thermo Fisher Scientific (Waltham, USA) following the manufacturer instructions and its quality was checked by OD_{260}:OD_{280} readings and electrophoresis. An aliquot of each sample was retro-transcribed by Super-Script II kit (Invitrogen, USA). Real-time PCR was performed with Syber green Master Mix in 25 μl of volume by ABI7900 (Applied Biosystem, Foster City, CA). Finally data were analyzed by SDS 2.1 software (Applied Biosystem).

Acknowledgements

We thank Stefano Vavassori (Université de Lausanne, CH-1066 Epalinges, Switzerland) for his contribution in designing and producing the ΔHis mutant, and for many stimulating discussions. We are indebted to Maria Francesca Mossuto, Anna Rubartelli, Eelco van Anken, Edgar Yoboue and other members of our laboratories for suggestions, criticisms and reagents, the Alembic facility for help in imaging and Roberta Colzani for secretarial assistance. We specially thank Paola Panina and Federica Quattrone (Division of Genetics and Cell Biology, IRCCS Ospedale San Raffaele) for kindly providing primary endometrial cells and for most helpful discussions.

Competing interests

The authors declare no competing interests.

Author contributions

S.S. performed most of the *in vivo* experiments, with the continuous help of T.A. M.C. analyzed the efficiency of substrate retrieval by the different mutants. S.M. and K.I. performed the *in vitro* experiments. C.F. was responsible for the pulse-chase assays and reagent optimization. With the fundamental help of K.I., T.A., M.D. and S.S., R.S. designed the strategy and coordinated the work described herein.

Funding

This work was supported by grants from Telethon [grant number GGP11077]; Associazione Italiana Ricerca sul Cancro (AIRC) [grant number IG 10721 and 5×1000 Special Project 9965 to R.S.]; the Japan Society for the Promotion of Science (JSPS) to S.M.; and the Next Generation World-Leading Researchers program (MEXT) to K.I.

Supplementary material

Supplementary material available online at
http://jcs.biologists.org/lookup/suppl/doi:10.1242/jcs.153239/-/DC1

References

Anelli, T., Alessio, M., Mezghrani, A., Simmen, T., Talamo, F., Bachi, A. and Sitia, R. (2002). ERp44, a novel endoplasmic reticulum folding assistant of the thioredoxin family. *EMBO J.* **21**, 835-844.

Anelli, T., Alessio, M., Bachi, A., Bergamelli, L., Bertoli, G., Camerini, S., Mezghrani, A., Ruffato, E., Simmen, T. and Sitia, R. (2003). Thiol-mediated protein retention in the endoplasmic reticulum: the role of ERp44. *EMBO J.* **22**, 5015-5022.

Anelli, T., Ceppi, S., Bergamelli, L., Cortini, M., Masciarelli, S., Valetti, C. and Sitia, R. (2007). Sequential steps and checkpoints in the early exocytic compartment during secretory IgM biogenesis. *EMBO J.* **26**, 4177-4188.

Anelli, T., Bergamelli, L., Margittai, E., Rimessi, A., Fagioli, C., Malgaroli, A., Pinton, P., Ripamonti, M., Rizzuto, R. and Sitia, R. (2012). Ero1α regulates Ca(2+) fluxes at the endoplasmic reticulum-mitochondria interface (MAM). *Antioxid. Redox Signal.* **16**, 1077-1087.

Cenci, S., Mezghrani, A., Cascio, P., Bianchi, G., Cerruti, F., Fra, A., Lelouard, H., Masciarelli, S., Mattioli, L., Oliva, L. et al. (2006). Progressively impaired proteasomal capacity during terminal plasma cell differentiation. *EMBO J.* **25**, 1104-1113.

Cortini, M. and Sitia, R. (2010). ERp44 and ERGIC-53 synergize in coupling efficiency and fidelity of IgM polymerization and secretion. *Traffic* **11**, 651-659.

Di Blasio, A. M., Centinaio, G., Carniti, C., Somigliana, E., Viganò, P. and Vignali, M. (1995). Basic fibroblast growth factor messenger ribonucleic acid levels in eutopic and ectopic human endometrial stromal cells as assessed by competitive polymerase chain reaction amplification. *Mol. Cell. Endocrinol.* **115**, 169-175.

Fraldi, A., Zito, E., Annunziata, F., Lombardi, A., Cozzolino, M., Monti, M., Spampanato, C., Ballabio, A., Pucci, P., Sitia, R. et al. (2008). Multistep, sequential control of the trafficking and function of the multiple sulfatase deficiency gene product, SUMF1 by PDI, ERGIC-53 and ERp44. *Hum. Mol. Genet.* **17**, 2610-2621.

Hamby, S. E. and Hirst, J. D. (2008). Prediction of glycosylation sites using random forests. *BMC Bioinformatics* **9**, 500.

Holbrook, L. M., Watkins, N. A., Simmonds, A. D., Jones, C. I., Ouwehand, W. H. and Gibbins, J. M. (2010). Platelets release novel thiol isomerase enzymes which are recruited to the cell surface following activation. *Br. J. Haematol.* **148**, 627-637.

Kakihana, T., Araki, K., Vavassori, S., Iemura, S., Cortini, M., Fagioli, C., Natsume, T., Sitia, R. and Nagata, K. (2013). Dynamic regulation of Ero1α and peroxiredoxin 4 localization in the secretory pathway. *J. Biol. Chem.* **288**, 29586-29594.

Lippincott-Schwartz, J., Yuan, L. C., Bonifacino, J. S. and Klausner, R. D. (1989). Rapid redistribution of Golgi proteins into the ER in cells treated with brefeldin A: evidence for membrane cycling from Golgi to ER. *Cell* **56**, 801-813.

Maeda, Y., Ide, T., Koike, M., Uchiyama, Y. and Kinoshita, T. (2008). GPHR is a novel anion channel critical for acidification and functions of the Golgi apparatus. *Nat. Cell Biol.* **10**, 1135-1145.

Masui, S., Vavassori, S., Fagioli, C., Sitia, R. and Inaba, K. (2011). Molecular bases of cyclic and specific disulfide interchange between human ERO1alpha protein and protein-disulfide isomerase (PDI). *J. Biol. Chem.* **286**, 16261-16271.

Mattioli, L., Anelli, T., Fagioli, C., Tacchetti, C., Sitia, R. and Valetti, C. (2006). ER storage diseases: a role for ERGIC-53 in controlling the formation and shape of Russell bodies. *J. Cell Sci.* **119**, 2532-2541.

Otsu, M., Bertoli, G., Fagioli, C., Guerini-Rocco, E., Nerini-Molteni, S., Ruffato, E. and Sitia, R. (2006). Dynamic retention of Ero1alpha and Ero1β in the endoplasmic reticulum by interactions with PDI and ERp44. *Antioxid. Redox Signal.* **8**, 274-282.

Pagani, M., Pilati, S., Bertoli, G., Valsasina, B. and Sitia, R. (2001). The C-terminal domain of yeast Ero1p mediates membrane localization and is essential for function. *FEBS Lett.* **508**, 117-120.

Qiang, L., Wang, H. and Farmer, S. R. (2007). Adiponectin secretion is regulated by SIRT1 and the endoplasmic reticulum oxidoreductase Ero1-L alpha. *Mol. Cell. Biol.* **27**, 4698-4707.

Ronzoni, R., Anelli, T., Brunati, M., Cortini, M., Fagioli, C. and Sitia, R. (2010). Pathogenesis of ER storage disorders: modulating Russell body biogenesis by altering proximal and distal quality control. *Traffic* **11**, 947-957.

Steentoft, C., Vakhrushev, S. Y., Joshi, H. J., Kong, Y., Vester-Christensen, M. B., Schjoldager, K. T.-G., Lavrsen, K., Dabelsteen, S., Pedersen, N. B., Marcos-Silva, L. et al. (2013). Precision mapping of the human O-GalNAc glycoproteome through SimpleCell technology. *EMBO J.* **32**, 1478-1488.

Swiatkowska, M., Padula, G., Michalec, L., Stasiak, M., Skurzynski, S. and Cierniewski, C. S. (2010). Ero1alpha is expressed on blood platelets in association with protein-disulfide isomerase and contributes to redox-controlled remodeling of alphaIIbbeta3. *J. Biol. Chem.* **285**, 29874-29883.

Vavassori, S., Cortini, M., Masui, S., Sannino, S., Anelli, T., Caserta, I. R., Fagioli, C., Mossuto, M. F., Fornili, A., van Anken, E. et al. (2013). A pH-regulated quality control cycle for surveillance of secretory protein assembly. *Mol. Cell* **50**, 783-792.

Wang, L., Wang, L., Vavassori, S., Li, S., Ke, H., Anelli, T., Degano, M., Ronzoni, R., Sitia, R., Sun, F. et al. (2008). Crystal structure of human ERp44 shows a dynamic functional modulation by its carboxy-terminal tail. *EMBO Rep.* **9**, 642-647.

Wang, Z. V., Schraw, T. D., Kim, J. Y., Khan, T., Rajala, M. W., Follenzi, A. and Scherer, P. E. (2007). Secretion of the adipocyte-specific secretory protein adiponectin critically depends on thiol-mediated protein retention. *Mol. Cell Biol.* **27**, 3716-3731.

Wilson, D. W., Lewis, M. J. and Pelham, H. R. B. (1993). pH-dependent binding of KDEL to its receptor in vitro. *J. Biol. Chem.* **268**, 7465-7468.

Zito, E., Buono, M., Pepe, S., Settembre, C., Annunziata, I., Surace, E. M., Dierks, T., Monti, M., Cozzolino, M., Pucci, P. et al. (2007). Sulfatase modifying factor 1 trafficking through the cells: from endoplasmic reticulum to the endoplasmic reticulum. *EMBO J.* **26**, 2443-2453.

Schematic representation of the ERp44 mutants used in this study

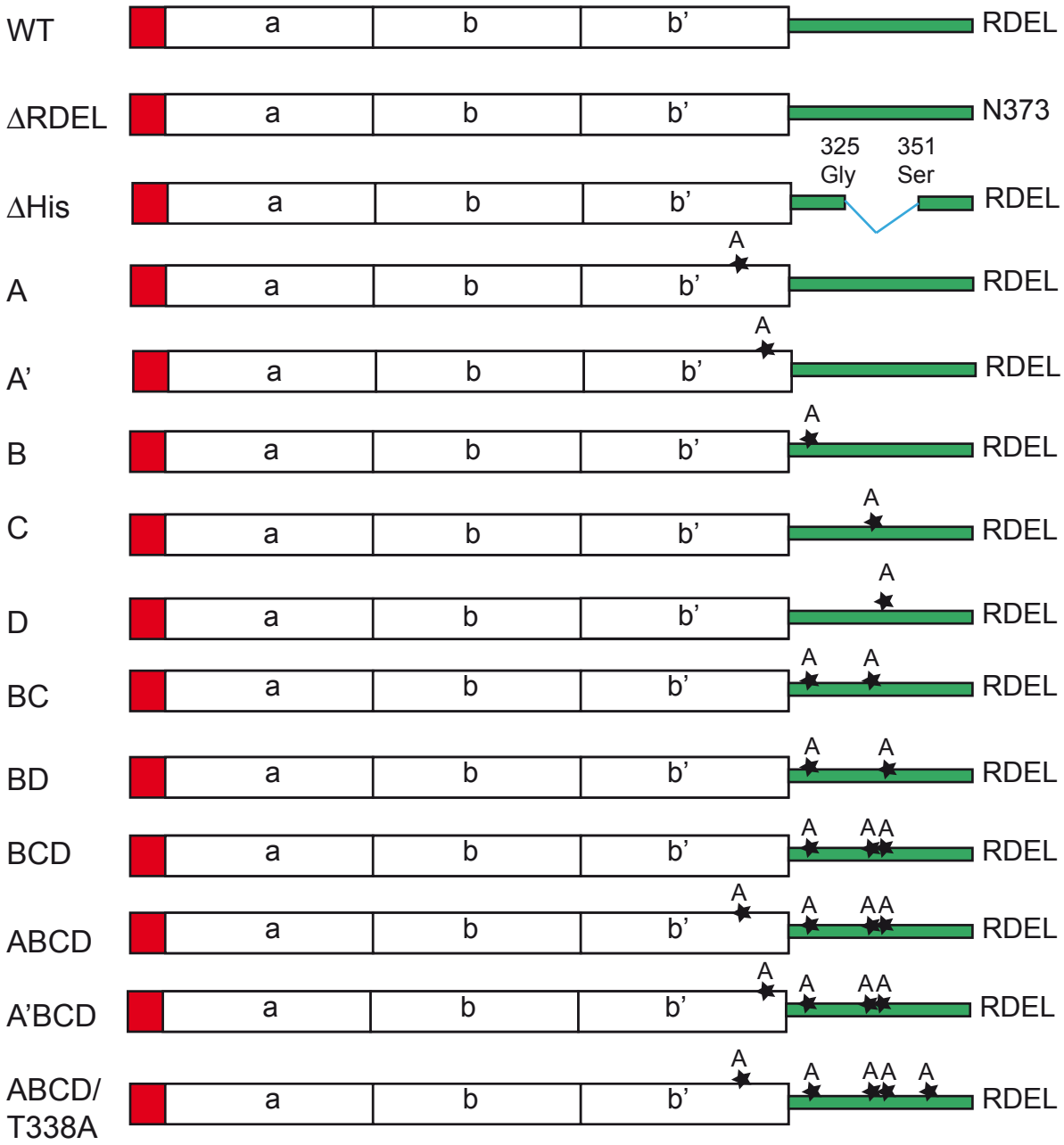

The red rectangle at N-terminus represents the tag (HA or Halo), placed immediately after the signal sequence. The signal sequence, tag and RDEL motif are absent in the vectors used for E.coli expression. Black stars indicate point mutations. The ΔHis mutant was generated by replacingthe 25 residues of the His loop (326-350) with a short spacer (SGSG, light blue rectangle).

Supplementary Figure 1

A

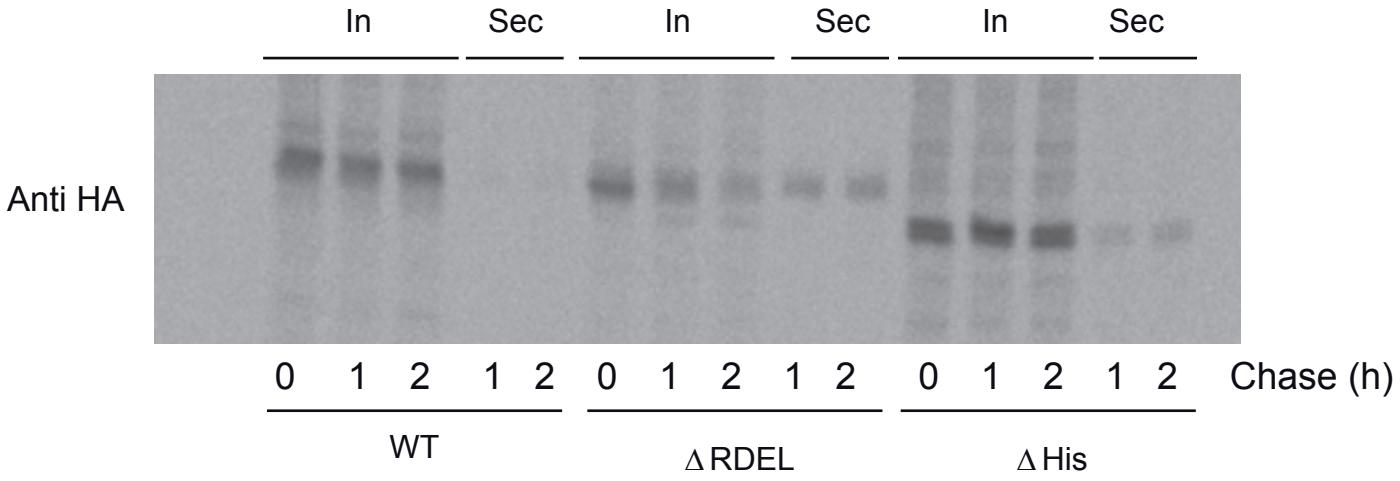

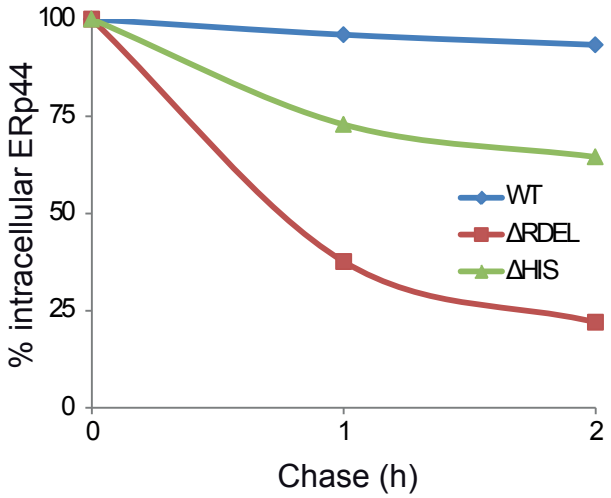

B

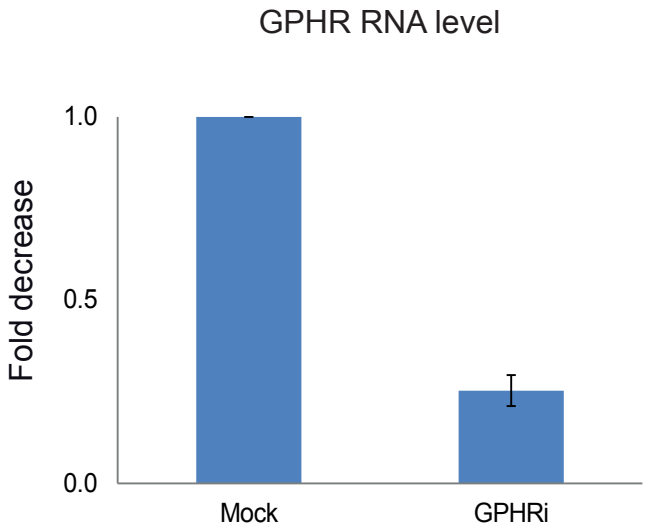

A. *ERp44 ΔHis is secreted.* HeLa transfectants were pulsed with radiolabeled amino acids and chased in cold medium. At the indicated times, aliquots from the lysates (In) and supernatants (Sec) were immunoprecipitated with anti-HA antibody and analyzed by gel electrophoresis. Intracellular ERp44 levels were quantified and the values depicted in the graph shown on the right. While the intracellular pool of ΔHis decreases, the total HA signal (In plus Sec) remain rather constant, indicating that the mutant is not degraded to a significant extent.

B. *GPHR silencing.* The efficiency of silencing was verified by RealTime PCR. The average of five experiments are represented in the graph with SEM .

Supplementary Figure2

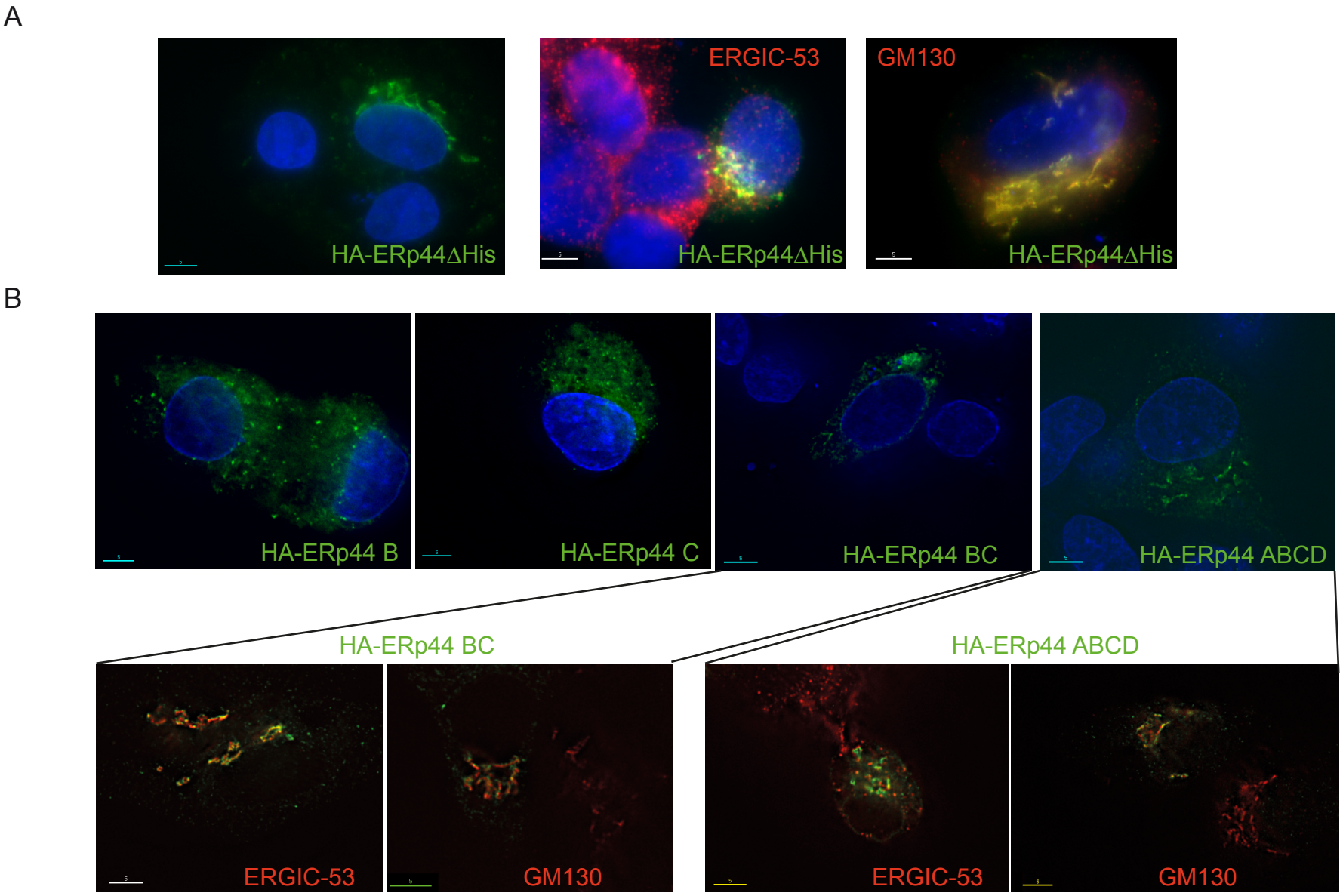

Localization of HA-tagged ERp44 mutants. HepG2 transfectans expressing HA-ERp44 ΔHis (A) or different histidine mutants (B) were decorated with anti-HA (green signal) and with different ESC markers (in red, either ERGIC-53 or GM130). ΔHis and ABCD colocalize mainly with GM130 and partially with ERGIC-53, whilst BC colocalizes preferentially with ERGIC-53.

Supplementary Figure3

	primers	Template		ERp44
FW	CACCGCTAGCGAAATAACAAGTCTTGATACAGAGAAT		PCR	
RV	GCGCCTCGAGTTAATCCCTCAATAGAGTATACCTATAT	pET28	cloning	ERp44 ΔHis
FW	GCGCGCGGATCCGGTAGTCCTGAGAGAGCTCCTTC			
RV	GCGCGGATCCAGAATGTAAGTCAAATACGAA			
FW_1	CAACTCGAGCGTTACCATGCATCCTGCC		cut and	
RV_1	GCGGCGGTACCTTAAAGCTCATCTCGATCCCTC	pcDNA ERp44 wt	paste	ERp44 ΔHis
FW	ATCGCTATTGACAGCTTTAGAGCTATGTATGTGTTTGGAG			
RV	CTCCAAACACATACATAGCTCTAAAGCTGTCAATAGCGAT	pcDNA ERp44 wt	SDM	ERp44 A (H299A)
FW	GACTTACATTCTGGAAAACTGGCCAGAGAATTCCATCATGGAC			
RV	GTCCATGATGGAATTCTCTGGCCAGTTTTCCAGAATGTAAGTC	pcDNA ERp44 wt	SDM	ERp44 B (H328A)
FW	CACAGAGAATTCGCTCATGGACCTGAC			
RV	GTCAGGTCCATGAGCGAATTCTCTGTG	pcDNA ERp44 wt	SDM	ERp44 C (H332)
FW	CTGCACAGAGAATTCCATGCTGGACCTGACCCAACTGAT			
RV	ATCAGTTGGGTCAGGTCCAGCATGGAATTCTCTGTGCAG	pcDNA ERp44 wt	SDM	ERp44 D (H333A)
FW	AAACTGGCCAGAGAATTCGCTCATGGACCTGACCCAACT			ERp44 BC
RV	AGTTGGGTCAGGTCCATGAGCGAATTCTCTGGCCAGTTT	pcDNA ERp44 B	SDM	(H328-332A)
FW	CTGGAAAACTGCACAGAGAATTCGCTGCTGGACCTGACCCAACTGATACAG			ERp44 CD
RV	CTGTATCAGTTGGGTCAGGTCCAGCAGCGAATTCTCTGTGCAGTTTTCCAG	pcDNA ERp44 wt	SDM	(H332-333A)
FW	CTGGCCAGAGAATTCCATGCTGGACCTGACCCAACTGAT			ERp44 BD
RV	ATCAGTTGGGTCAGGTCCAGCATGGAATTCTCTGGCCAG	pcDNA ERp44 B	SDM	(H328-333A)
FW	GACTTACATTCTGGAAAACTGGCCAGAGAATTCCATCATGGAC			ERp44 BCD
RV	GTCCATGATGGAATTCTCTGGCCAGTTTTCCAGAATGTAAGTC	pcDNA ERp44 CD	SDM	(H328-332-333A)
FW	ATCGCTATTGACAGCTTTAGAGCTATGTATGTGTTTGGAG			ERp44 ABCD (H299
RV	CTCCAAACACATACATAGCTCTAAAGCTGTCAATAGCGAT	pcDNA ERp44 BCD	SDM	328-332-333A)
FW	GCTGCTGGACCTGACCCAGCTGATACAGCCCCAGGAGAG	pcDNA ERp44		ERp44
RV	CTCTCCTGGGGCTGTATCAGCTGGGTCAGGTCCAGCAGC	ABCD	SDM	ABCD/T338A

Supplementary Table 1 List of the primers and methods (SDM, side directed mutagenesis; PCR, polymerase chain reaction) employed to generate the ERp44 mutants used in this study.

OPEN ACCESS Freely available online

PLOS ONE

A Dynamic Study of Protein Secretion and Aggregation in the Secretory Pathway

Maria Francesca Mossuto[1], Sara Sannino[1,2], Davide Mazza[3,4], Claudio Fagioli[1], Milena Vitale[1,3], Edgar Djaha Yoboue[1], Roberto Sitia[1,3¶], Tiziana Anelli[1,3*¶]

1 Division of Genetics and Cell Biology, IRCCS Ospedale San Raffaele, Milan, IT, **2** Department of Biosciences, Università degli Studi di Milano, Milan, IT, **3** Università Vita-Salute San Raffaele, Milan, IT, **4** Experimental Imaging Center, IRCCS Ospedale San Raffaele, Milan, IT

Abstract

Precise coordination of protein biogenesis, traffic and homeostasis within the early secretory compartment (ESC) is key for cell physiology. As a consequence, disturbances in these processes underlie many genetic and chronic diseases. Dynamic imaging methods are needed to follow the fate of cargo proteins and their interactions with resident enzymes and folding assistants. Here we applied the Halotag labelling system to study the behavior of proteins with different fates and roles in ESC: a chaperone, an ERAD substrate and an aggregation-prone molecule. Exploiting the Halo property of binding covalently ligands labelled with different fluorochromes, we developed and performed non-radioactive pulse and chase assays to follow sequential waves of proteins in ESC, discriminating between young and old molecules at the single cell level. In this way, we could monitor secretion and degradation of ER proteins in living cells. We can also follow the biogenesis, growth, accumulation and movements of protein aggregates in the ESC. Our data show that protein deposits within ESC grow by sequential apposition of molecules up to a given size, after which novel seeds are detected. The possibility of using ligands with distinct optical and physical properties offers a novel possibility to dynamically follow the fate of proteins in the ESC.

Citation: Mossuto MF, Sannino S, Mazza D, Fagioli C, Vitale M, et al. (2014) A Dynamic Study of Protein Secretion and Aggregation in the Secretory Pathway. PLoS ONE 9(10): e108496. doi:10.1371/journal.pone.0108496

Editor: Jeffrey L. Brodsky, University of Pittsburgh, United States of America

Received June 12, 2014; **Accepted** August 21, 2014; **Published** October 3, 2014

Data Availability: The authors confirm that all data underlying the findings are fully available without restriction. All relevant data are within the paper.

Funding: This work was supported by Telethon (GGP11077), AIRC (IG and 5×1000 Special Project) to RS. MFM was supported by a FEBS Long-Term Fellowship. The funders had no role in study design, data collection and analysis, decision to publish, or preparation of the manuscript.

Competing Interests: The authors have declared that no competing interests exist.

* Email: anelli.tiziana@hsr.it

¶ These authors are joint last authors on this work.

Introduction

To achieve their native structure, secretory and membrane proteins exploit the vast array of chaperones and enzymes that reside in the endoplasmic reticulum (ER), the port of entry into the secretory compartment. Here, they undergo stringent quality control [1,2]: only properly folded and assembled proteins are given the green light and proceed along the secretory pathway. Proteins that fail to attain their native state are eventually retro-translocated to the cytosol for proteasomal degradation. Not all proteins entering the ER are secreted or directed to the plasma membrane. Even if in some conditions the flux of cargo can become intense, resident proteins stop at the desired stations to maintain organelle identity and guarantee function. For instance, soluble ER residents are retrieved from downstream stations via KDEL-Receptors [3].

The sophisticated systems deployed by cells to regulate this intense traffic and prevent dangerous jams in ESC are unfortunately not fully reliable. Sometimes, an overzealous quality control can cause systemic loss of function diseases preventing the transport of mutants that are nonetheless active. Unless promptly degraded, moreover, these can condense in ESC and cause gain of function diseases [4].

Secretory IgM are complex polymers [5] whose biogenesis occurs stepwise in ESC [6]. Like other unassembled Ig-H chains, secretory μ (μ_s) interact with BiP via their first constant domain (C_H1). Assembly with Ig-L displaces BiP, and μ2L2 complexes are then slowly polymerized [7]. When C_H1 is lacking, $\mu\Delta C_H1$ accumulate in a detergent insoluble form within dilated ESC cisternae, also called Russell Bodies (RB) [8,9] providing a suitable model system for Heavy Chain Disease (HCD [10] and references therein) and ER storage disorders (ERSD [11]). We recently identified some of the factors that modulate $\mu\Delta C_H1$ condensation in living cells. For instance, over-expression of ERp44, a multifunctional chaperone that mediates thiol-dependent quality control of IgM subunits and other clients [12,13], stimulated the accumulation of $\mu\Delta C_H1$ in RB [14].

To learn more about how cells handle different proteins in ESC, we generated different chimeric proteins containing a Halotag (Halo) derived from a *Rhodococcus rhodochrous* Haloalkane dehalogenase whose active site has been engineered to covalently bind fluorescently-labelled chloro-alkane derivatives [15,16]. With respect to more conventional live-cell labelling based on fluorescent proteins the Halotag post-translational labelling system has several advantages. First, it allows to using organic dyes such as TMR (tetramethyl-rhodamine) or R110, that are brighter and more photostable than fluorescent proteins [17] and whose

fluorescence is relatively pH-insensitive [18]. By selecting suitable ligands the same tag can be used for live cell microscopy, immunofluorescence, Western Blotting, protein purification and co-precipitation assays [16,17,19–26]. Moreover, the Halotag allows following the accumulation and/or the degradation of the protein of interest by two-color pulse/chase experiments with high temporal resolution [27]. Lastly, the Halotag has the advantage of not possessing glycosylation sites, that could affect folding and transport of the chimeric proteins in the secretory compartment.

Another hybrid system, based on small molecules able to covalently bind genetically specified proteins, is the tetracysteine biarsenical system [28]. Unfortunately, due to the oxidative environment of the ER, this system cannot be applied to the study of secretory proteins.

In this work, after confirming that Halo folds and maintains its activity in ESC without grossly perturbing the fate of the target protein, we followed the condensation of Halo-$\mu\Delta C_H1$ in ESC and analysed the growth and mobility of the resulting RB *in vivo* exploiting the property of covalently binding ligands coupled to different fluorochromes. Moreover, by appending the Halotag to short- and long-lived ER residents and to transport competent molecules, we show that it is possible to follow protein degradation and secretion bypassing classic radioactive pulse and chase techniques. Thus, Halo is a versatile non-invasive tool to follow key events in the secretory pathway.

Results and Discussion

Following protein aggregation in the ER at single cell level

When deleted of the C_H1, Ig-μ chains display a strong tendency to become detergent insoluble and form RB [9]. To follow the biogenesis of RB *in vivo*, we inserted the Halo tag between the variable and the second constant domain of $\mu\Delta C_H1$. Halo-$\mu\Delta C_H1$ oligomerized and displayed detergent solubility similar to its untagged counterpart (Figure 1, inset). This behaviour suggests that even in the oxidising ER environment the Halotag, which contains two free cysteines, does not form aberrant intra- or inter-chain disulphide bonds, as confirmed also by the electrophoretic mobility of an ER-located Halotag alone under reducing and non-reducing conditions (Figure S1). We thus investigated how Halo-$\mu\Delta C_H1$ aggregates grow in living cells by designing fluorescent pulse-chase experiments. The rationale of these assays is to use sequentially differently coloured ligands (TMR and R110) to differentially label pre-existing 'old' molecules and newly made 'young' ones. HeLa cells expressing Halo-$\mu\Delta C_H1$ were labelled 24 hours with the red ligand (TMR) and washed before addition of the green ligand (R110). After different time intervals, cells were fixed and analysed by confocal microscopy. As the incubation time with the R110 ligand increases, green staining becomes progressively more intense (Figure 1). When protein synthesis was blocked by the addition of cycloheximide 2 hours before and 4 hours during the treatment with the second ligand, no green staining was detectable. This confirmed that all the pre-existing molecules were labelled with the red ligand and that no ligand exchange between molecules occurs in living cells. Hence, our labelling protocol can be used to discriminate between pre-existing and newly synthesized molecules. After 4 hours, green staining almost completely co-localized with the pre-existing RB. As synthesis continued, bigger yellowish dots became evident, consistent with the accumulation of newly made molecules next to pre-existing aggregates, which progressively grew in size. At later times, a green circle could be observed around most pre-existing red aggregates: these onion-like structures imply that roundish deposits of pre-existing molecules grow by sequential addition of layers containing newly made proteins. Together with the old growing aggregates, new green small dots can be observed at later times, probably representing new seeds of protein condensation. Very few red-only aggregates can be seen, indicating that most pre-existing structures act as seeds. We measured the increase in size of the aggregates after 24 hours of growth in the presence of the green ligand: we observed a relative diameter increase of about 16% (Figure 2A, upper panel). As a control, no difference in the diameter of the aggregates was observed when cells were incubated simultaneously with both red and green ligands (Figure 2A, lower panel). The possibility of detecting RB by Immunofluorescence correlates with the accumulation of $\mu\Delta C_H1$ chains in the detergent insoluble fractions. These derive from the condensation of proteins that fail to be degraded by ERAD [9,14]. Interestingly, young molecules distribute into soluble and insoluble fraction as the old ones, indicating that independently on the aggregation-step the Halo-$\mu\Delta C_H1$ molecule reaches equilibrium between soluble and insoluble species (Fig. 2B). Hence also the smaller green dots observed in fluorescence contain insoluble molecules.

Next, we analysed the movement of Halo-$\mu\Delta C_H1$ aggregates by tracking the individual RB in living cells by confocal live-cell microscopy (Figure 3A–B). For each of the 115 tracks extracted from 8 movies we measured the mean-square displacements (MSD) as function of time (Figure 3C) and we fitted the first 20 points of the MSD curves with a model for anomalous diffusion, $MSD = 4Dt^{\alpha}$ to obtain estimates for the short-term diffusion coefficient D and for the anomalous diffusion exponent α. In general, the tracks displayed anomalous subdiffusion, representative of constrained motion, with an average anomalous exponent $\alpha = 0.74 \pm 0.02$ and average diffusion coefficient $D = 0.0045 \pm 0.0005\ \mu m^2/s$. This value is significantly lower than the diffusion coefficients of soluble ER proteins [29–32], further confirming that Halo-$\mu\Delta C_H1$ clusters display constrained mobility. Interestingly, RB diffuse with a similar anomalous exponent independently of their size, while as expected larger (and potentially older) clusters displayed a reduced diffusion coefficient (Figure 3D). We also observed a few small clusters moving directionally (blue arrowed in Figure 3B), suggesting that the microtubule network might play a role in the dynamic behaviour of the clusters. We therefore quantified the mobility of the clusters following the depolymerization of microtubules. Upon treatment with Nocodazole the Halo-$\mu\Delta C_H1$ clusters displayed comparable size to the untreated samples, but their diffusion coefficients were 0.5x smaller on average (Figure 3E), confirming that the motion of the clusters is at least partially associated to the microtubule network.

Following the degradation of an ER resident protein

In the absence of Ig-L, orphan μ_s are retained in the ER via interactions with BiP [7]. After a lag that varies amongst different substrates and/or cell types, they are retro-translocated into the cytosol and eventually degraded by proteasomes [33–35]. Like its untagged counterpart, Halo-μ_s is also retained in the ER, as indicated by its co-localization with the ER chaperone PDI (Figure 4A). Also in this case, the Halotag does not interfere with oligomer formation or solubility of the tagged protein (Figure 1, inset).

The standard approach to study protein degradation is based on radioactive pulse and chase experiments [36], limited by the restrictions of using radioactive isotopes and the difficulties in analysing the phenomenon at the single cell level. The use of cycloheximide chases [37] is restricted to short-lived proteins, since

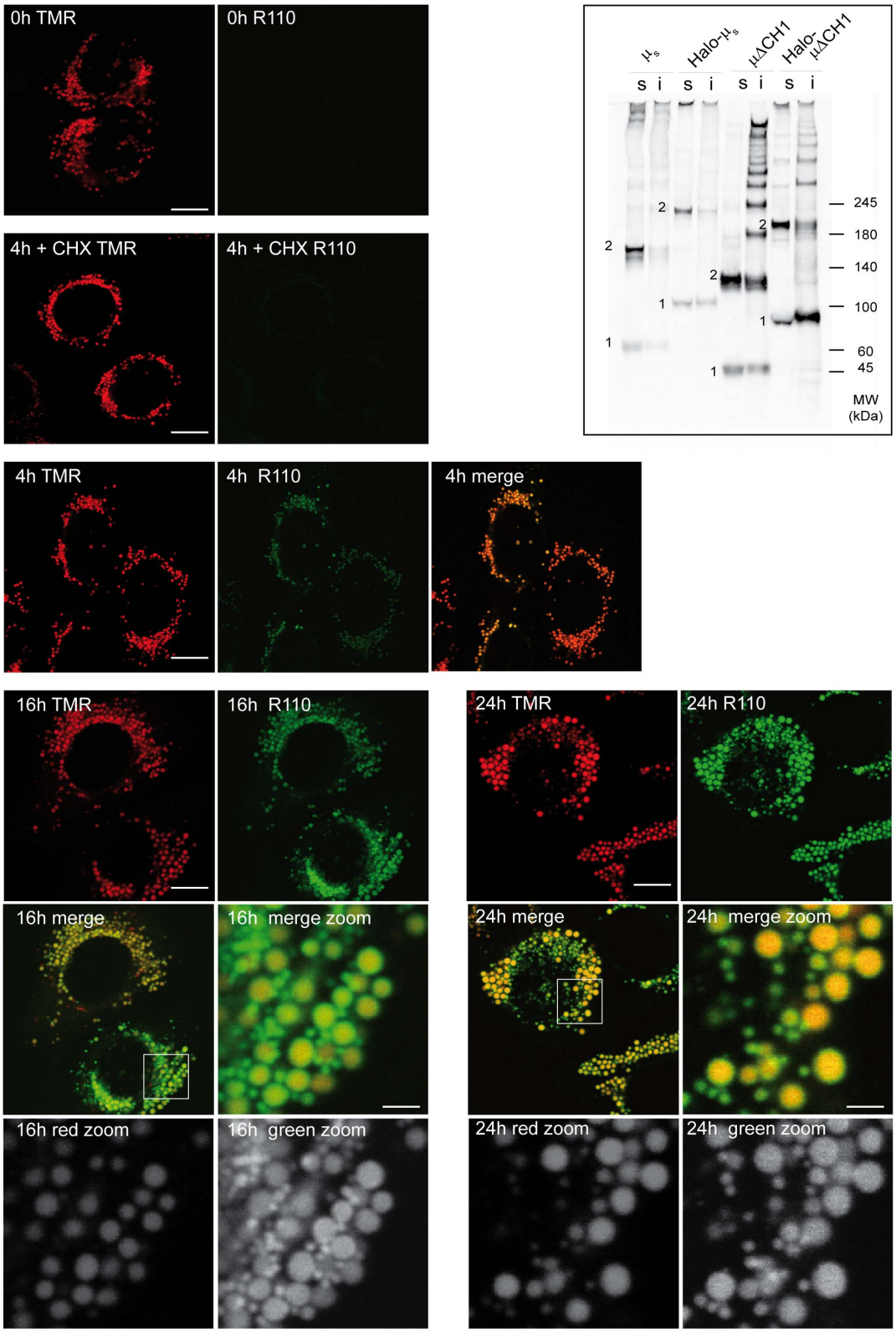

Figure 1. Halotag can be used to follow the aggregation/condensation of a protein in the ER. HeLa cells expressing Halo-μΔCH1 were labelled for 24 hours with the red TMR ligand (5 μM) in complete medium. After extensive washings, cells were incubated with the green ligand R110 (5 μM) for the indicated times. To control saturation, cells were treated with cycloheximide (0.5 mM) for the last 2 hours of the first TMR incubation, and then during the incubation with R110 for 4 hours. Cells were then fixed in paraformaldheyde and analyzed by confocal microscopy. Images are shown as confocal slices. With the progression of the chase, the green signal co-localizes with the pre-existing red signal and newly formed aggregates (only green) can be visible. Pre-existing red aggregates grow by apposition of newly synthetized proteins which can be labeled in green. (Bar: 5 μm). Single channel signals in gray scale are shown for the thumbnails (Bar: 1 μm). **Inset**: HeLa cells transiently expressing Halo-μΔC_H1 or Halo-

μ_s were lysed, and aliquots from soluble (s) and insoluble (i) fractions resolved under non-reducing conditions on a 3–8% polyacrylamide gradient gel. Nitrocellulose membranes were decorated with anti-μ. Bands indicated with 1 represent monomeric proteins, while bands indicated with 2 represent homodimers.
doi:10.1371/journal.pone.0108496.g001

prolonged inhibition of protein synthesis can affect cell proteostasis [38]. For ERAD substrates retrotranslocation and degradation are often monitored by cell fractionation, deglycosylation or ubiquitination, and more recently exploiting split GFP- or Venus-based dislocation assay [39,40]. Here we propose the use of Halotag to follow ER proteins degradation.

We first analysed whether the presence of a Halotag with or without a covalently bound ligand influenced μ_s degradation in HeLa transfectants (Figure 4B). To this aim, cells transfected with μ_s or Halo-μ_s were pulsed for 10 min with ^{35}S. Where indicated, cells were treated with TMR before (16 hours) and during the radioactive pulse. Cells were then chased for different time points in a medium without TMR or radioactive amino acids and lysed

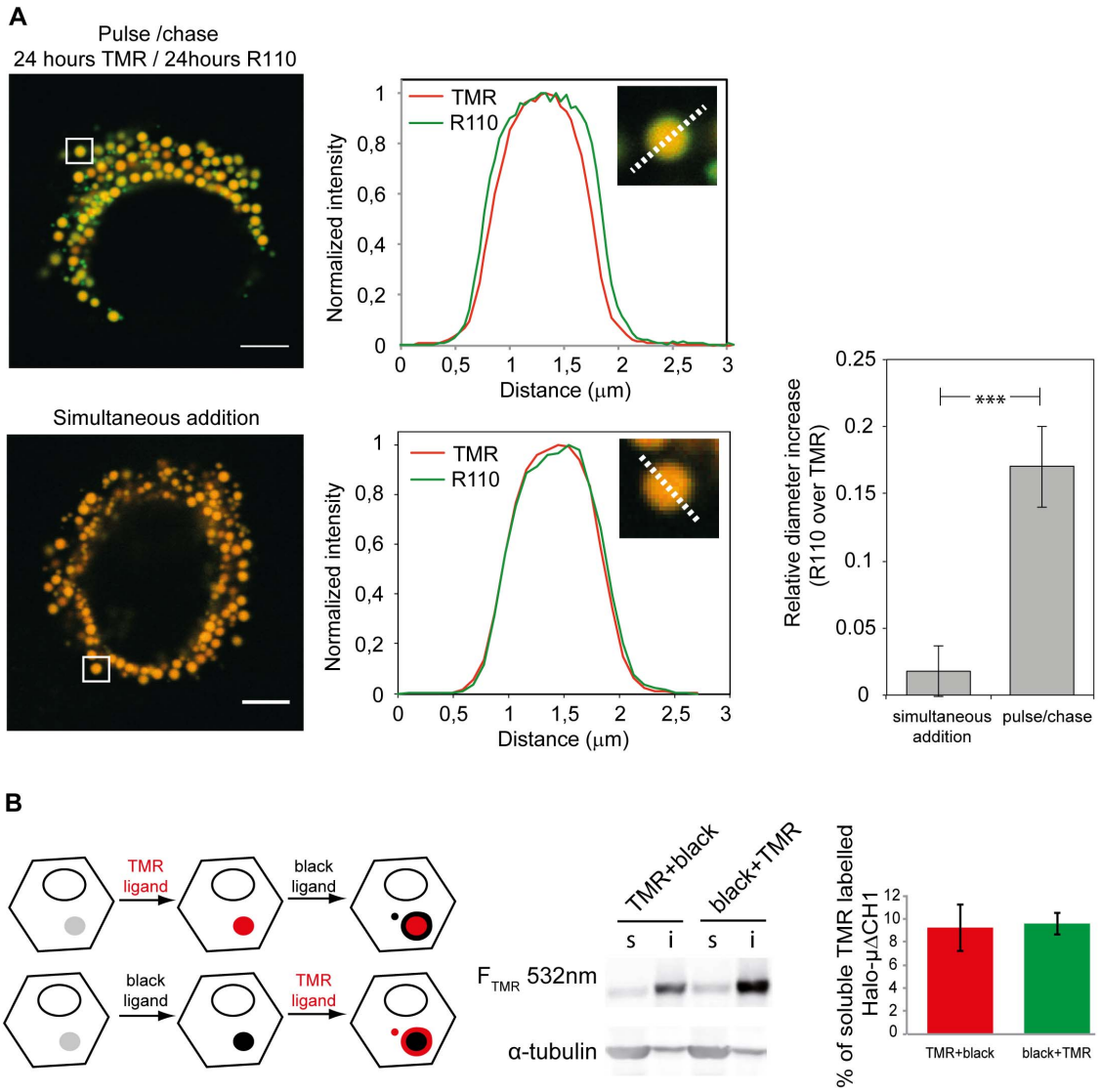

Figure 2. Visualising the growth of RB. A *Quantification of cluster growth by pulse-chase.* Images were acquired as described above and analyzed with custom-written Matlab routines to quantify the size of the clusters in the two channels. When the two ligands are added in sequence (with a 24 hours chase) an average 16%+/−3% (SEM) increase in the cluster size is observed, while no difference in size can be measured when the two ligands are added simultaneously. For the pulse and chase experiment 9 cells and 99 clusters were examined. For the simultaneous addition of the two ligands 9 cells and 101 clusters were analyzed. Bar: 5 μm. **B** *Distribution of old and young Halo-μΔC_H1 molecules*. HeLa cells transiently expressing Halo-μΔC_H1 were subjected to fluorescent pulse-chase assays: 24 hours with the TMR ligand and 24 h with the non-labelled ligand (TMR+black) or 24 hours with non-labelled ligand and 24 hours with the TMR ligand (black+TMR). Halo-ligands were used at 5 μM. Aliquots of soluble (s) and insoluble (i) material were then resolved under reducing conditions on a 10% polyacrylamide gel. After transferring to nitrocellulose, the signal of the TMR ligand was collected using fluorescence technology by FLA900 Starion. Densitometric quantifications are shown on the right. Average of 3 independent experiments +/− standard deviation.
doi:10.1371/journal.pone.0108496.g002

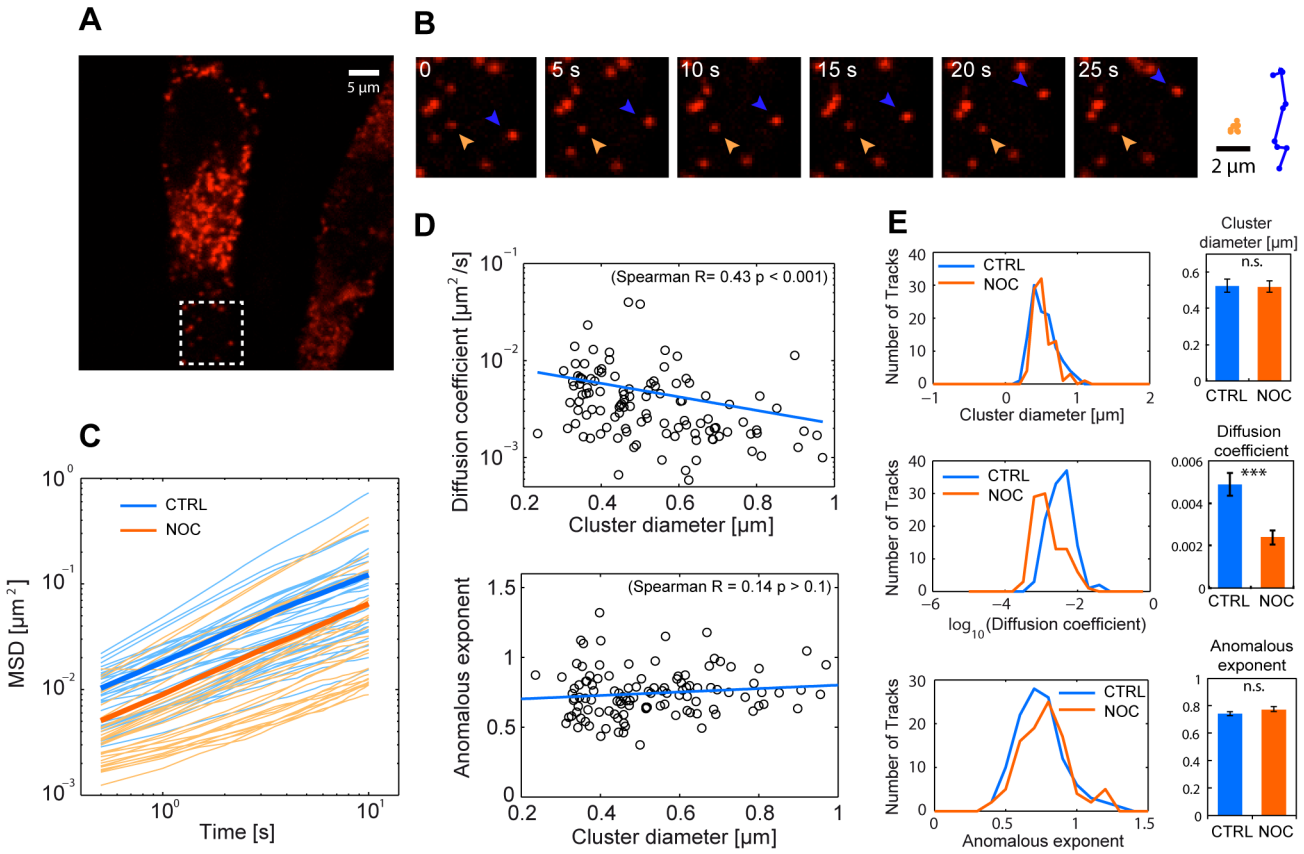

Figure 3. Live-imaging of ER protein aggregation. A HeLa cells expressing Halo-µΔC_H1 were labeled for 24 h with 5 µM TMR. Living cells were then imaged by confocal microscopy at a frame rate of 2 images/s. **B** Aggregates display a heterogeneous dynamic behavior with some clusters moving directionally (orange arrowhead) and others showing confined diffusion (blue arrowhead). **C** We tracked individual clusters in 8 cells and we selected tracks that were longer than 150 frames (115 tracks) and we plotted individual MSD curves (orange thin lines) and their average (thick line). Treatment of cells with 0.3 µg/ml Nocodazole for 15 hours (blue lines) decreased of the mobility of the aggregates. **D** The diffusion coefficient D and the anomalous exponent α were calculated from the MSD curves obtained from the untreated samples and plotted against the estimated diameter of the clusters. On average we measured $\alpha = 0.74 \pm 0.02$ and average diffusion coefficient $D = 0.0045 \pm 0.0005$ µm²/s. A value of $\alpha < 1$ is representative of anomalous subdiffusion, probably due to obstacles constraining the mobility of the clusters. While the anomalous exponent did not seem to depend on the cluster size, the diffusion coefficient was found to inversely correlate with the particle diameter. **E** We compared the distribution of measured particle sizes, diffusion coefficients and anomalous exponents for the untreated and the Nocodazole treated samples: the diffusion coefficient was the only parameter significantly affected by the disruption of the cytoskeleton (error bars: Mean ± SEM).
doi:10.1371/journal.pone.0108496.g003

in detergent. The anti-µ immunoprecipitates were resolved by SDS-PAGE under reducing conditions and transferred to nitrocellulose. Gels were first developed for autoradiography and then for TMR signal. As shown in Figure 4B, the degradation patterns of μ_s and Halo-μ_s are very similar, almost one third of radioactive μ_s present at time 0 being degraded after 4 hours of chase. Importantly, the presence of the ligand itself did not interfere with Halo-μ_s degradation. This is an important observation, since in all likelihood ERAD substrates are at least partially unfolded before being retro-translocated across the ER membrane and entirely before entry into the proteasomal cavity. The presence of a folded domain with covalently linked ligand could have impacted either one or both steps in the disposal of an ER luminal substrate. No other fragment containing the ligand can be seen in the blot (not shown), making very unlikely the possibility that endoproteases clipped the Halotag with the bound ligand off [41]. The degradation of the protein can also be seen directly by following the disappearance of the TMR fluorescence on the gel (red line in the graph). The decay observed in fluorescence is more rapid than the disappearance of the radioactive signal because in the 16 hours of staining with the Halo ligand also older molecules (closer to the dislocation-degradation steps) have been stained.

Taken together, these data show that the degradation of ERAD substrates can also be followed directly monitoring the disappearance of the TMR fluorescence.

The Halo tag can be used to follow protein secretion

ERp44 cycles between the ER and cisGolgi and plays key roles in thiol-mediated protein quality control, redox homeostasis and calcium signalling [13,42]. When expressed in mammalian cells, ERp44 prevents secretion of Ero1 flavoproteins and Peroxiredoxin 4, ER resident proteins which lack KDEL or other known localization motifs [12,43,44]. We inserted a Halotag between the cleavable ERp44 leader sequence and its first active sequence. Halo-ERp44 retained the subcellular distribution previously described for HA-tagged or untagged ERp44 [6], co-localizing mostly with the ERGIC marker ERGIC-53 and much less with GM130, a cisGolgi resident (Figure 5A). Halo-ERp44 can be easily visualized *in vivo*, staining cells with TMR (Figure 5A) or R110 (not shown). Moreover, Halo-ERp44 was as active as HA-ERp44 in retaining excess Ero1α (Figure 5B). Note how Western

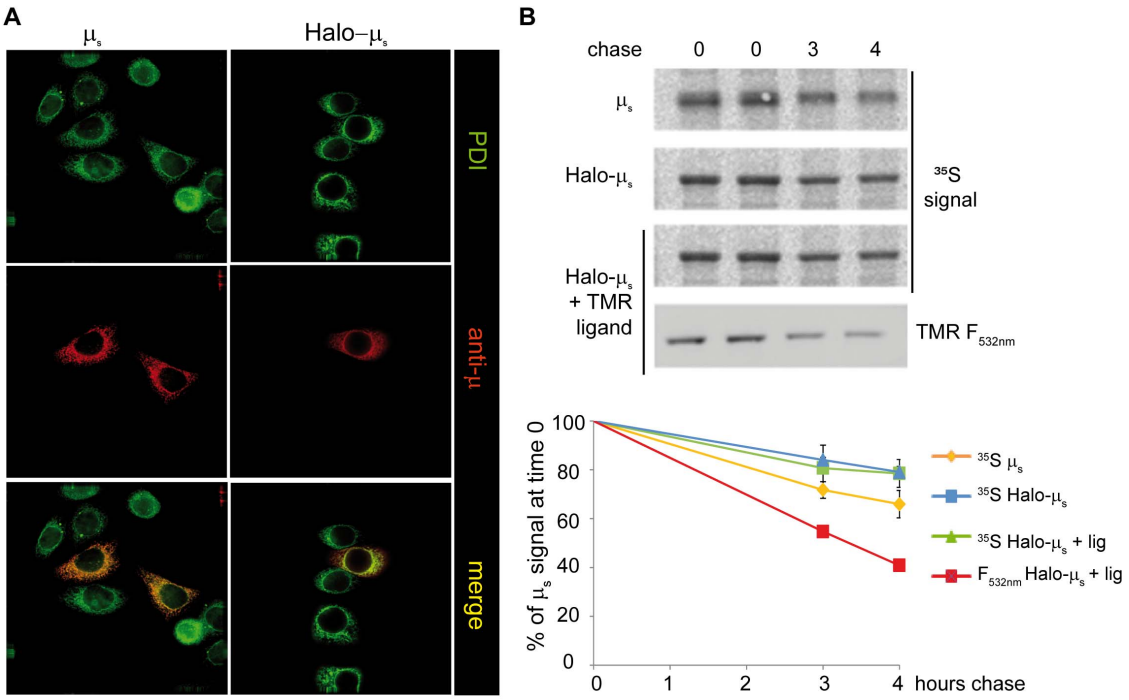

Figure 4. Exploting Halotag to study ERAD. A *Halo-tagging does not alter the localization of unassembled Ig-μ_s.* HeLa cells were transiently transfected with μ_s or Halo-μ_s as indicated, fixed with PFA and stained with antibodies specific for PDI or Ig-μ. In this experiment, transfection efficiency was about 25%. Bar: 5 μm. **B** *The Halotag with or without bound ligand does not interfere with μ_s degradation.* 48 hours after transfection, HeLa cells expressing μ_s or Halo-μ_s cells were pulsed for 10 minutes with ^{35}S aminoacids and chased in the presence of 5 mM DTT for the indicated time points, to accelerate degradation [35]. One sample (Halo-μ_s+ligand) was pre-treated with TMR (2.5 μM) before and during the radioactive pulse. Aliquots from the lysates corresponding to 10^6 cells for each time point were precipitated with anti-μ, resolved under reducing conditions and transferred to nitrocellulose membranes which were first developed for the ^{35}S signal and then for TMR fluorescence (532 nm). Densitometric quantification was performed by ImageJ. The graph shown in the bottom panel represents the percentage of the total μ present at time 0 remaining at individual times.
doi:10.1371/journal.pone.0108496.g004

blots can be simultaneously stained with ligands and different antibodies emitting at different wavelengths, providing high quality, elegant images. The intracellular retention of ERp44 relies on its C-terminal RDEL motif [6]. We previously showed, using ^{35}S radiolabeling [6], that deletion of the RDEL motif leads to rapid ERp44 secretion. As expected, also Halo-tagged ERp44ΔRDEL is massively secreted (Figure 5C), indicating that tagging does not interfere with folding or trafficking of the protein. The small molecular weight shift between intra- and extra-cellular Halo-ERp44ΔRDEL is due to O-glycosylation [45]. The velocity of secretion can be studied by using a protocol that resembles the ^{35}S pulse and chase technique. HeLa cells transiently transfected with Halo-ERp44ΔRDEL were labelled with R110 ligand overnight. After several washes, the cells were incubated with a fresh medium without the ligand and the secreted material was then collected at different time points and analysed by SDS-PAGE. Consistently with our previous data, the pool of labelled Halo-ERp44ΔRDEL is completely secreted after 2 hours of chase, the curve reaching a plateau. On the contrary, the signal detected with anti-Halo antibodies (and hence representing labelled and non-labelled secreted ERp44ΔRDEL) kept steadily increasing, due to the addition to the release new molecules that are synthetized during the chase. Thus, the Halotag labelling is a valid alternative to the use of radioisotopes or cycloheximide treatment for studying protein secretion. Altogether our data indicate that the Halotag can be safely used to tag and follow an ER chaperone without disturbing its regulatory properties.

Concluding Remarks

A significant advantage of the Halo domain is its ability to covalently bind ligands with tailored features. In this study, we exploited this property to visualise and quantify the traffic, condensation and degradation of different proteins within the early secretory pathway. First, we showed that the Halo moiety can correctly fold also in the oxidizing environment of the ER without forming aberrant intra- or inter-chain disulphide bonds. Moreover, no significant differences have been observed between ER-localized and cytosolic Halo for what concerns binding to its ligands (not shown). Our data also demonstrated that appending a Halo domain to different proteins had minor if any effects on the degradation, secretion or localisation of the resulting chimeras. Therefore, we could follow the fate of different proteins in the secretory pathway, without utilising radioactive isotopes or cycloheximide.

The most novel aspect of our work is the use of the Halotag technology to determine how potentially harmful protein deposits form and grow in the secretory pathway. We show here that aggregates formation over time proceeds as deposition of newly made proteins on a pre-existing condensation core, resulting in a progressive increase of the clusters size. In this external shell of the aggregates, no mixing between new and old material is observed, suggesting that μΔC_H1 clusters are therefore rather "viscous" and grow mostly on the surface. However, given the limited resolution of confocal microscopy (200 nm laterally and 700 nm axially), we

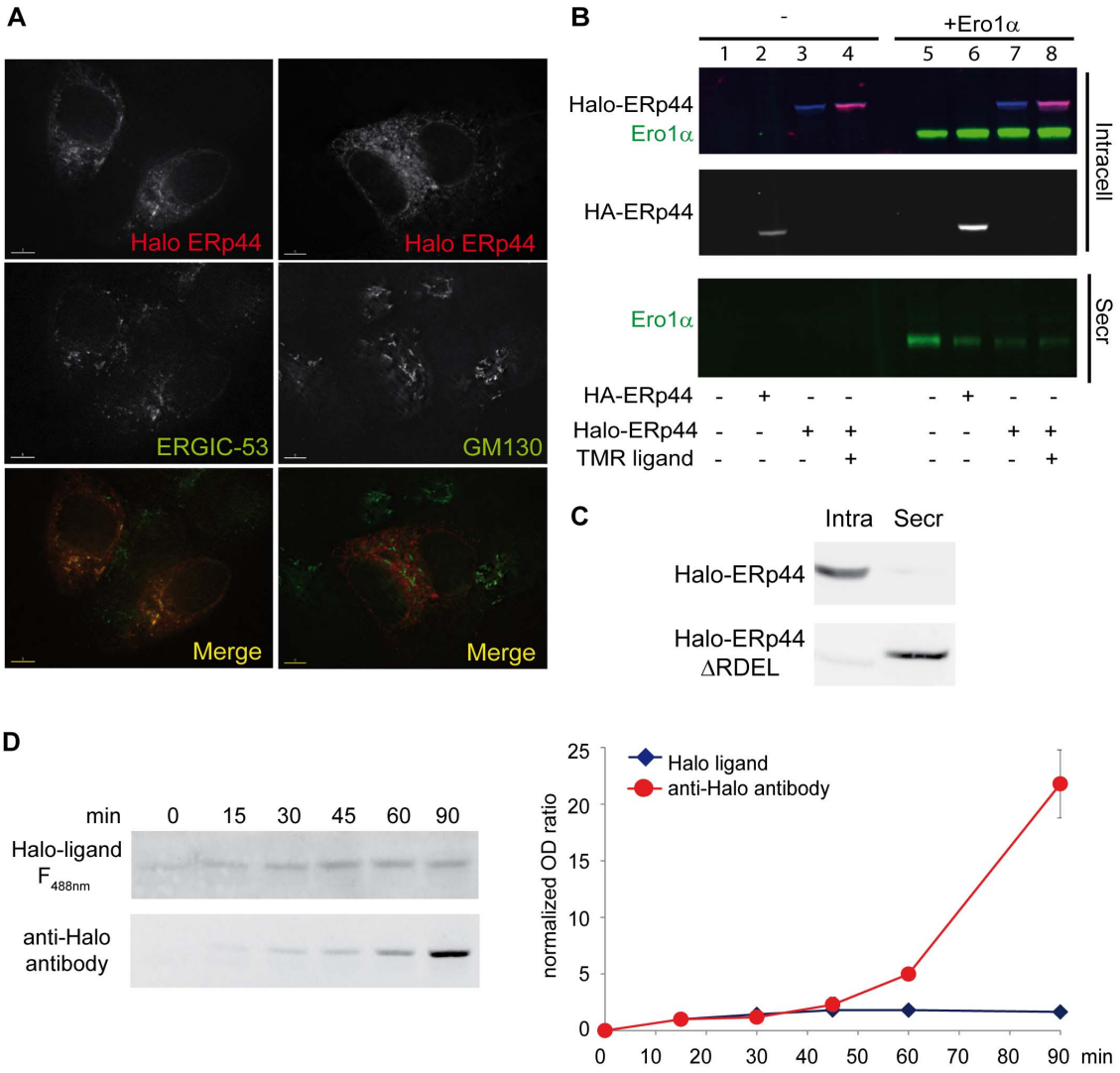

Figure 5. Halotag does not influence the function or localization of ERp44. A *Halo-tagging does not alter the localization of ERp44.* HepG2 cells were transiently transfected with Halo-ERp44 and pre-treated with TMR ligand (10 nM O/N) before fixation and staining with antibodies specific for ERGIC-53 or GM130 as markers of ERGIC or Golgi). Images were acquired with a 60X objective on an Olympus inverted fluorescence microscope and subjected to deconvolution. Single channel images and the merge are shown. Bar: 5 μm. **B** *Halo-ERp44 retains Ero1α efficiently.* Hela cells were transiently transfected with Halo-ERp44 and HA-ERp44 (alone or in combinations with Ero1α as indicated) 48 hours after transfection cells were washed and incubated for 4 hours in OPTIMEM. One sample was treated with TMR before and during the secretion. The spent media and cells were collected. The lysates corresponding to 10^5 cells (lanes 1–4) and the TCA precipitated supernatants of 5 times as many cells (5×10^5, lanes 5–8) were resolved under reducing conditions. Membranes were decorated with anti-Halo (blue signal), anti-HA (white signal), anti-Ero1α (green signal) and TMR fluorescence (red). Halo-ERp44 can be expressed and visualized by TMR staining. No significant differences were detected between Halo-ERp44 and HA-ERp44 in terms of function (Ero1α retention). **C** *Secretion of ERp44ΔRDEL is not impaired by appending a Halotag.* HeLa transfectants expressing Halo-ERp44 or Halo-ERp44ΔRDEL were incubated with OPTIMEM. After 4 hours, aliquots of lysates and supernatants (corresponding to 10^5 cells) were resolved under reducing conditions and the blots decorated with anti-ERp44. As HA-ERp44 ΔRDEL [6], Halo-ERp44 ΔRDEL is massively secreted implying that the tag does not interfere with folding/secretion. **D** Hela cells transiently expressing Halo-ERp44ΔRDEL were incubated overnight with the R110 ligand (35 nM), washed and incubated in OPTIMEM (without the Halo-ligand) for the indicated time points. Supernatants corresponding to $5*10^6$ cells were concentrated by TCA precipitation, resolved under reducing conditions and the TMR signal collected using a fluorescent analyzer. The nitrocellulose filters were then decorated with anti-Halo antibodies. The intensities of the R110 fluorescent ligand and anti-Halo signals were quantified by densitometry using the ImageJ software and normalized to the value after 15 minutes of secretion. The graph shows the average of 2 independent experiments +/− standard deviation.
doi:10.1371/journal.pone.0108496.g005

cannot determine if the newly deposited material can penetrate in the nucleation core of the RB.

By using live-cell imaging we also shed light on the mobility of Halo-μΔC_H1 clusters. Our data indicate that, as expected, RB have on average a diffusion coefficient much lower than soluble ER proteins. Moreover, the mobility of big clusters is lower than that of small ones. A subset of RB shows a directional movement, likely due to microtubule transport. Accordingly, inhibiting microtubules decreased RB diffusion coefficient, indicating a partial role of microtubules in determining RB movements. Very interestingly, both small and big clusters displayed constrained mobility, which was not affected by Nocodazole. This observation suggests that an important constraining factor could be the ER membrane itself.

Numerous questions remain to be answered: do different seeds coalesce together? What determines their size? What is the structural organization of these clusters? If their content is viscous, how does it distribute concentrically? How do cells dispose of RB? Extending the techniques described herein to super-resolution fluorescence microscopy could allow answering many of these relevant issues.

Given the importance of protein aggregates, granules and clusters in storage diseases and also other regulatory processes [46,47] our results describe a powerful tool for better visualizing and describing *in vivo* these events, being able to discriminate between old and young molecules in the same aggregate. Thus, this strategy is useful in order to reveal important mechanistic insights in the pathophysiology of ERSD and other disorders caused by proteotoxicity.

Materials and Methods

Reagents

Chemicals were from Sigma (St Louis, MO), unless otherwise indicated. Monoclonal anti-myc (9E10 clone) and anti-GM130 were used previously as described [48]. Polyclonal anti-PDI was a kind gift of Dr. Ineke Braakman (Utrecht, NL); goat anti-mouse IgG and IgM and anti-rabbit IgG (H+L) Alexa Fluor 700, 647, 546 and 488 were from Invitrogen Molecular Probes (Eugene, Oregon, USA); rabbit polyclonal anti-μ chain was from Zymed (San Francisco, CA). Cell permeant "no wash" TMRDirect and R110Direct ligands, and HaloTag Amine O4 ligand were from Promega (Promega Medison, WI).

Plasmids construction

Vectors for the expression of HA-ERp44 and ERp44 no tag were previous described [48]. To obtain Halo-ERp44, ERp44 no tag was cleaved form pcDNA3.1(-) vector by XhoI and KpnI and inserted in pBlueScript II KS (+). A SgfI (GCG AT▼CGC) (Promega Madison, WI) site was inserted after the leader sequence cutting site by PCR (p44sgfI Fw and p44sgfI Rv primers). The PCR product was re-inserted in pcDNA 3.1 (-) vector by XhoI and KpnI. In pHTN HaloTag CMV-neo Vector, Halotag was mutagenized inserting a Sgf I site at the N terminal extremity by PCR (pHTN SgfI Fw and pHTN SgfI Rv primers) (Promega Medison, WI). Both the mutated constructs were digested by SgfI and purified by Wizard SV Gel and PCR Clean-Up System (Promega Medison, WI). Halo-ERp44 tagged was obtained by digestion by SgfI and ligation at 16°C over night from the sequence previously purified from agarose gel. The direction of the Halotag insertion was ascertained by SmaI digestion and the construct was sequenced (Primm s.r.l., Milan, Italy).

Halo-ERp44 ΔRDEL was obtained with digestion and ligation from the sequences of Halo-ERp44 and HA-ERp44 ΔRDEL: the 1007 Kbp fragment obtained by digestion of the plasmid HA-ERp44 ΔRDEL pcDNA3.1(-) with HindIII was exchanged with the one obtained from Halo-ERp44 pcDNA3.1(-) and checked by sequencing.

HaloRDRDEL was obtained by two sequential PCR starting from HaloERp44 construct. The first PCR was done to amplify Halo tag fragment (primers FW: ACGACTCACTATAGGGAGAC; RV: TTTTTTGGGGTACCTTATGCGGCCGCACCGGTGTTATCGCTCTGAAAGTAC). The PCR product was inserted into pcDNA3.1- vector by XbaI, KpnI digestion. The obtained construct was then processed by PCR to insert RDRDEL ER retention motif (primers FW: AGCGATAACACCGGTAGGGATCGAGATGAGCTTTAAGGTACCAAGCTT; RV: AAGCTTGGTACCTTAAAGCTCATCTCGATCCCTACCGGTGTTATCGCT). The construct was fully sequenced by Primm s.r.l.

Vectors for the expression of μ_S and $\mu\Delta C_H1$ were previously described [8]. In pHTN HaloTag CMV-neo Vector, Halotag was mutagenized inserting Nru site at N terminal extremity and NotI site at C-terminal extremity by PCR. A pRS316 vector [49] $\mu\Delta C_H1$ with cherry positioned after the V_H and the pHTN HaloTag PCR product were digested by Nru and NotI, purified by Wizard SV Gel (Promega Medison, WI) and ligated to obtain pRS316 vectors carrying V_H-Halo-C_H2 etc construct. This plasmid and pcDNA3.1(+) vectors carrying μ_S and $\mu\Delta C_H1$ were digested by EcoRI and NotI to obtain respectively the V_H-Halo and the C_H1-C_H4 and the C_H2-C_H4 moieties, purified by Wizard SV Gel (Promega Medison, WI) and ligated to obtain pcDNA3.1 (-) vectors carrying μ_S-Halo and $\mu\Delta C_H1$-Halo. Halo Tag insertion direction was screened by EcoRI and XhoI digestion and checked by sequencing.

Oligonucleotides

The following oligonucleotides were obtained from Primm s.r.l. Milano, Italy):

p44SgfI Fw, CCTGTAACAACTGAAATAGCGATCGCTGAAATAACAAGT;

p44SgfI Rv, ACTTGTTATTTCAGCGATCGCTATTTCAGTTGTTACAGG;

pHTN SgfI Fw, GCCGCGATCGCTGAAGCAGAAATCGGTAACTGGCTTTCCATTC;

pHTN SgfI Rv, GGAAGCGATCGCGTTATCGCTCTG.

Cell culture, transfection and immunofluorescence

All the cell lines were obtained from ATCC and cultured and transfected by PEI (Polyethyleneimene, Polysciences inc. Warrington, PA) as previously described [50]. HepG2 cells were transfected by Fugene HD transfection reagent from Promega Corporation (Promega Medison, WI) following the manufacturer instructions.

For immunofluorescence analyses, cells were plated on 15 mm glasses and transfected. 48 hours after transfection cells were fixed with 4% PFA and processed as previously described [6]. For visualization with Halo-ligands, cells were treated O/N with the membrane permeable ligands TMR or R110 (both used at 10 nM). Samples were analyzed with a 60X objective on an Olympus inverted fluorescence microscope (model IX70) equipped with a quadriband dicroic filter (Sedat Quad, Chroma) with DeltaVision RT Deconvolution System (Alembic, HSR, Milano). After deconvolution, images were processed with Adobe Photoshop CS4 (Adobe Systems Inc.).

Western blot

For Western blot assays, HeLa cells were detached by trypsinization and washed once in ice-cold phosphate buffered saline (PBS) and once in PBS with 10 mM N-ethylmaleimide (NEM) to block disulfide interchange [6]. Cells were then lysed in 150 mM NaCl, 1% NP-40, 0.1% SDS, 50 mM Tris HCl pH 8.0 (RIPA) containing 10 mM NEM and protease inhibitors for 20 min on ice. Aliquots of the postnuclear supernatants were analyzed by SDS PAGE and western blotting with monoclonal anti-ERp44 [6], anti-HA or polyclonal anti Halo (Promega). Signals were detected by infrared technology by FujiFilm (FLA 9000) (FujiFilm Life Science, Tokyo, Japan).

Lysates of HeLa cells transiently transfected with Halo-μ_s or Halo-$\mu\Delta H1$ were produced as described [8].

Radioactive pulse and chase

Cells were incubated for 30 min in DMEM without methionine and cysteine supplemented with 1% dialysed FCS, pulsed with ^{35}S-labeled amino acids (200 mCi/9*10^6 cells) (Easy Tag, Perkin Elmer), washed and chased in complete medium for the indicated times. After different times, cells were treated with 10 mM NEM and lysed in RIPA as described [48]. Immunoprecipitates were resolved on SDS–PAGE under reducing conditions, transferred to nitrocellulose and membranes visualized by autoradiography with FLA900 Starion (FujiFilm Life Science, Tokyo, Japan). Subsequently, the red signal form TMR was visualized with infrared technology. Densitometric quantifications of the signals were performed with ImageJ.

Confocal microscopy analysis: fluorescent pulse chase

For fluorescent pulse and chase experiments, Hela cells were seeded on 25 mm glasses before transfection with Halo-μΔC_H1. The minimum incubation time necessary to have a signal in IF in our system with the "no-wash" TMRDirect ligand (5 μM) was 1 hour. However, in order to be sure to have completely saturated all the pre-existing molecules in the cells, 24 hours after transfection cells were stained for 24 hours with TMR (5 μM) in complete medium, extensively washed with PBS and then incubated with R110 (5 μM) in complete pre-warmed medium. After different chase times, cells were fixed in PFA, glasses mounted in glycerol and analyzed with a 60X objective with a Leica TCS SP2 Laser Scanning Confocal equipped with a spectral detector (Alembic, Ospedale San Raffaele, Milano, Italy). The green channel was excited with a 488 nm laser and, in order to avoid overlapping of the red channel, only the green emission spectra from 495 to 535 was acquired. The red channel was instead excited with a 543 laser and the emission spectra acquired was from 570 to 640 nm of wavelength. A single optical section, centered on the focal plane corresponding to the maximum size and brightness of the RB clusters was acquired for the quantification of the growth of the clusters. The size of the clusters was evaluated from the confocal images with a custom-written routine in Matlab, which allows the user to select the isolated clusters and plot the fluorescence intensity profile along the diameter of each cluster for both the green and the red channel. The diameter of the clusters is then measured as the full width at half maximum of the intensity profile and the relative cluster size increase is calculated as $(d_g–d_r)/d_r$ where d_g and d_g are the cluster diameters measured in the green and in the red channel respectively.

Confocal microscopy analysis: Live cell tracking of individual clusters

For live-imaging experiments, HeLa cells were seeded and transfected as above. 24 hours after transfection cells were labeled with 5 μM TMR ligand for 24 hrs. For Nocodazole treatment cells were incubated 9 hours with the TMR ligand 5 μM and 15 hours with 5 μM TMR ligand and 0.3 μg/ml Nocodazole. Cells were subsequently visualized with a Leica TCS SP5 Laser Scanning Confocal Microscope in phenol-free DMEM at 37°C and 5% CO2. A 543 nm laser was used for the excitation and the fluorescent light emitted from the sample was acquired with a 63x NA 1.4 oil immersion objective in the spectral window ranging from 560 nm to 644 nm. Time-lapse imaging was performed on individual cells by acquiring an image every 0.5 s seconds for 300 frames. We verified that no excessive photobleaching would perturb single particle tracking, by repetitive imaging of fixed samples using the same conditions as above: individual TMR molecules undergo photobleaching after more than 1000 frames on average, longer than our total acquisition time (data not shown).

To obtain tracking data on individual clusters, the time-lapse experiments were analyzed with the TrackMate plugin in Fiji [51]. Briefly, approximately 15 randomly chosen clusters were selected for each cell and tracked using the semi-automatic tracking tool in TrackMate. Tracks were then analyzed with custom-written routines in Matlab to quantify the MSD plot of each cluster. The first twenty time-points of the MSD curves were then fit by $MSD = 4Dt^{\alpha}$, to obtain estimates for the short-term diffusivity D and for the anomalous diffusion exponent α. The Matlab routines are available at: https://github.com/shiner80/TM_export-ClustTrack.

Supporting Information

Figure S1 The Halotag can fold properly in the ER. A HeLa cells were transfected with a cytosolic or an ER localized Halotag. Cells were stained O/N with the TMR ligand 5 μM and images acquired with an inverted microscope. Bar: 5 μm. **B** Lysates of HeLa cells expressing the ER-localized Halotag were loaded under reducing (R) and non-reducing (NR) conditions on a 3–8% polyacrylamide gradient gel. The Halo tag was detected with a polyclonal anti-Halo antibody. Note that no mobility shift is visible between the reducing and the non-reducing samples, indicating that the ER-localized Halo tag does not contain intra-chain or inter-chain disulfide bonds. **C** HeLa cells were transfected with a cytosolic or an ER localized Halotag and stained O/N with the TMR ligand 5 μM before lysis in RIPA buffer. Increasing amounts of lysates were loaded on reducing SDS-PAGE. First the signal of the TMR ligand was acquired; the filters were then decorated with a rabbit anti-Halo antibody and the signal of the secondary anti-Rabbit IgG antibody (Alexa 700) was then acquired. Densitometric quantifications are shown in the graph. Note that the signal of the TMR is much more linear and quantitative than the signal of the anti-Halo antibody.
(TIF)

Acknowledgments

We thank Andrea Orsi, Bruno Sterlini, Carlo Tacchetti, Eelco van Anken, Caterina Valetti and other members of our laboratories for helpful suggestions, criticisms and reagents, the Alembic staff for help with confocal and live microscopy, Marco E. Bianchi for the use of the Leica SP-5 confocal microscope and Roberta Colzani for secretarial assistance.

Author Contributions

Conceived and designed the experiments: MFM TA RS SS. Performed the experiments: MFM TA SS EY CF MV DM. Analyzed the data: MFM TA RS DM SS EY. Contributed reagents/materials/analysis tools: MFM TA SS CF DM MV EY. Wrote the paper: MFM TA SS DM RS.

References

1. Anelli T, Sitia R (2008) Protein quality control in the early secretory pathway. Embo J 27: 315–327.
2. Gidalevitz T, Stevens F, Argon Y (2013) Orchestration of secretory protein folding by ER chaperones. Biochim Biophys Acta 1833: 2410–2424.
3. Munro S, Pelham HR (1987) A C-terminal signal prevents secretion of luminal ER proteins. Cell 48: 899–907.
4. Calamini B, Morimoto RI (2012) Protein homeostasis as a therapeutic target for diseases of protein conformation. Curr Top Med Chem 12: 2623–2640.
5. Hendershot L, Sitia R (2005) Molecular Biology of B cells.

6. Anelli T, Ceppi S, Bergamelli L, Cortini M, Masciarelli S, et al. (2007) Sequential steps and checkpoints in the early exocytic compartment during secretory IgM biogenesis. Embo J.
7. Hendershot L, Bole D, Kohler G, Kearney JF (1987) Assembly and secretion of heavy chains that do not associate posttranslationally with immunoglobulin heavy chain-binding protein. J Cell Biol 104: 761–767.
8. Mattioli L, Anelli T, Fagioli C, Tacchetti C, Sitia R, et al. (2006) ER storage diseases: a role for ERGIC-53 in controlling the formation and shape of Russell bodies. J Cell Sci 119: 2532–2541.
9. Valetti C, Grossi CE, Milstein C, Sitia R (1991) Russell bodies: a general response of secretory cells to synthesis of a mutant immunoglobulin which can neither exit from, nor be degraded in, the endoplasmic reticulum. J Cell Biol 115: 983–994.
10. Bianchi G, Anderson KC, Harris LN, Sohani AR (2014) The Heavy Chain Diseases: Clinical and Pathologic Features. Oncology Journal, Hematologic Malignancies January 15.
11. Anelli T, Sitia R (2010) Physiology and pathology of proteostasis in the early secretory compartment. Semin Cell Dev Biol 21: 520–525.
12. Anelli T, Alessio M, Bachi A, Bergamelli L, Bertoli G, et al. (2003) Thiol-mediated protein retention in the endoplasmic reticulum: the role of ERp44. Embo J 22: 5015–5022.
13. Cortini M, Sitia R (2010) From antibodies to adiponectin: role of ERp44 in sizing and timing protein secretion. Diabetes Obes Metab 12 Suppl 2: 39–47.
14. Ronzoni R, Anelli T, Brunati M, Cortini M, Fagioli C, et al. (2010) Pathogenesis of ER storage disorders: modulating Russell body biogenesis by altering proximal and distal quality control. Traffic 11: 947–957.
15. Leippe DM, Zhao KQ, Hsiao K, Slater MR (2010) Cell-free expression of protein kinase a for rapid activity assays. Anal Chem Insights 5: 25–36.
16. Los GV, Encell LP, McDougall MG, Hartzell DD, Karassina N, et al. (2008) HaloTag: a novel protein labeling technology for cell imaging and protein analysis. ACS Chem Biol 3: 373–382.
17. Mazza D, Abernathy A, Golob N, Morisaki T, McNally JG (2012) A benchmark for chromatin binding measurements in live cells. Nucleic Acids Res 40: e119.
18. Seki T, Yoshino KI, Tanaka S, Dohi E, Onji T, et al. (2012) Establishment of a novel fluorescence-based method to evaluate chaperone-mediated autophagy in a single neuron. PLoS One 7: e31232.
19. Chen J, Zhang Z, Li L, Chen BC, Revyakin A, et al. (2014) Single-molecule dynamics of enhanceosome assembly in embryonic stem cells. Cell 156: 1274–1285.
20. Emborg ME, Ebert AD, Moirano J, Peng S, Suzuki M, et al. (2008) GDNF-secreting human neural progenitor cells increase tyrosine hydroxylase and VMAT2 expression in MPTP-treated cynomolgus monkeys. Cell Transplant 17: 383–395.
21. Fujita-Yoshigaki J, Matsuki-Fukushima M, Yokoyama M, Katsumata-Kato O (2013) Sorting of a HaloTag protein that has only a signal peptide sequence into exocrine secretory granules without protein aggregation. Am J Physiol Gastrointest Liver Physiol 305: G685–696.
22. Gallo S, Beugnet A, Biffo S (2011) Tagging of functional ribosomes in living cells by HaloTag(R) technology. In Vitro Cell Dev Biol Anim 47: 132–138.
23. Martincova E, Voleman L, Najdrova V, De Napoli M, Eshar S, et al. (2012) Live imaging of mitosomes and hydrogenosomes by HaloTag technology. PLoS One 7: e36314.
24. Ohana RF, Hurst R, Vidugiriene J, Slater MR, Wood KV, et al. (2011) HaloTag-based purification of functional human kinases from mammalian cells. Protein Expr Purif 76: 154–164.
25. Stagge F, Mitronova GY, Belov VN, Wurm CA, Jakobs S (2013) SNAP-, CLIP- and Halo-tag labelling of budding yeast cells. PLoS One 8: e78745.
26. Tukachinsky H, Kuzmickas RP, Jao CY, Liu J, Salic A (2012) Dispatched and scube mediate the efficient secretion of the cholesterol-modified hedgehog ligand. Cell Rep 2: 308–320.
27. Svendsen S, Zimprich C, McDougall MG, Klaubert DH, Los GV (2008) Spatial separation and bidirectional trafficking of proteins using a multi-functional reporter. BMC Cell Biol 9: 17.
28. Griffin BA, Adams SR, Tsien RY (1998) Specific covalent labeling of recombinant protein molecules inside live cells. Science 281: 269–272.
29. Ordonez A, Snapp EL, Tan L, Miranda E, Marciniak SJ, et al. (2013) Endoplasmic reticulum polymers impair luminal protein mobility and sensitize to cellular stress in alpha1-antitrypsin deficiency. Hepatology 57: 2049–2060.
30. Snapp EL, Sharma A, Lippincott-Schwartz J, Hegde RS (2006) Monitoring chaperone engagement of substrates in the endoplasmic reticulum of live cells. Proc Natl Acad Sci U S A 103: 6536–6541.
31. Wei D, Zheng H, Su N, Deng M, Lai L (2010) Binding energy landscape analysis helps to discriminate true hits from high-scoring decoys in virtual screening. J Chem Inf Model 50: 1855–1864.
32. Dayel MJ, Hom EF, Verkman AS (1999) Diffusion of green fluorescent protein in the aqueous-phase lumen of endoplasmic reticulum. Biophys J 76: 2843–2851.
33. Fagioli C, Mezghrani A, Sitia R (2001) Reduction of interchain disulfide bonds precedes the dislocation of Ig-mu chains from the endoplasmic reticulum to the cytosol for proteasomal degradation. J Biol Chem 276: 40962–40967.
34. Mancini R, Fagioli C, Fra AM, Maggioni C, Sitia R (2000) Degradation of unassembled soluble Ig subunits by cytosolic proteasomes: evidence that retrotranslocation and degradation are coupled events. Faseb J 14: 769–778.
35. Medrano-Fernandez I, Fagioli C, Mezghrani A, Otsu M, Sitia R (2014) Different redox sensitivity of endoplasmic reticulum associated degradation clients suggests a novel role for disulphide bonds in secretory proteins. Biochem Cell Biol 92: 113–118.
36. Zhou P (2004) Determining protein half-lives. Methods Mol Biol 284: 67–77.
37. Baliga BS, Pronczuk AW, Munro HN (1969) Mechanism of cycloheximide inhibition of protein synthesis in a cell-free system prepared from rat liver. J Biol Chem 244: 4480–4489.
38. Alvarez-Castelao B, Ruiz-Rivas C, Castano JG (2012) A critical appraisal of quantitative studies of protein degradation in the framework of cellular proteostasis. Biochem Res Int 2012: 823597.
39. Zhong Y, Fang S (2012) Live cell imaging of protein dislocation from the endoplasmic reticulum. J Biol Chem 287: 28057–28066.
40. Grotzke JE, Lu Q, Cresswell P (2013) Deglycosylation-dependent fluorescent proteins provide unique tools for the study of ER-associated degradation. Proc Natl Acad Sci U S A 110: 3393–3398.
41. Bhamidipati A, Denic V, Quan EM, Weissman JS (2005) Exploration of the topological requirements of ERAD identifies Yos9p as a lectin sensor of misfolded glycoproteins in the ER lumen. Mol Cell 19: 741–751.
42. Anelli T, Bergamelli L, Margittai E, Rimessi A, Fagioli C, et al. (2012) Ero1alpha regulates Ca(2+) fluxes at the endoplasmic reticulum-mitochondria interface (MAM). Antioxid Redox Signal 16: 1077–1087.
43. Kakihana T, Araki K, Vavassori S, Iemura S, Cortini M, et al. (2013) Dynamic regulation of Ero1alpha and peroxiredoxin 4 localization in the secretory pathway. J Biol Chem 288: 29586–29594.
44. Otsu M, Bertoli G, Fagioli C, Guerini-Rocco E, Nerini-Molteni S, et al. (2006) Dynamic retention of Ero1alpha and Ero1beta in the endoplasmic reticulum by interactions with PDI and ERp44. Antioxid Redox Signal 8: 274–282.
45. Sannino S, Anelli T, Cortini M, Masui S, Degano M, et al. (2014) Progressive quality control of secretory proteins throughout the Golgi by ERp44. J Cell Sci in press.
46. Gooptu B, Dickens JA, Lomas DA (2014) The molecular and cellular pathology of alpha(1)-antitrypsin deficiency. Trends Mol Med 20: 116–127.
47. Maji SK, Wang L, Greenwald J, Riek R (2009) Structure-activity relationship of amyloid fibrils. FEBS Lett 583: 2610–2617.
48. Anelli T, Alessio M, Mezghrani A, Simmen T, Talamo F, et al. (2002) ERp44, a novel endoplasmic reticulum folding assistant of the thioredoxin family. Embo J 21: 835–844.
49. Sikorski RS, Hieter P (1989) A system of shuttle vectors and yeast host strains designed for efficient manipulation of DNA in Saccharomyces cerevisiae. Genetics 122: 19–27.
50. Vavassori S, Cortini M, Masui S, Sannino S, Anelli T, et al. (2013) A pH-regulated quality control cycle for surveillance of secretory protein assembly. Mol Cell 50: 783–792.
51. Schindelin J, Arganda-Carreras I, Frise E, Kaynig V, Longair M, et al. (2012) Fiji: an open-source platform for biological-image analysis. Nat Methods 9: 676–682.